Thermal Analysis of Double Effect Absorption System Cascaded with Ejector and Enhanced Vapor Compression Refrigeration Cycle

Submitted By

Sefat Mahmud Siddique

190011125

Md. Muhtasim Uzzaman

190011106

Supervised By

Dr. Mohammad Monjurul Ehsan

A Thesis submitted in partial fulfillment of the requirement for the degree of Bachelor of Science in Mechanical Engineering

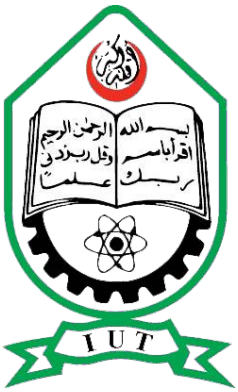

Department of Mechanical and Production Engineering (MPE)

Islamic University of Technology (IUT)

July, 2024

DECLARATION

*I hereby declare that this thesis entitled "**Thermal Analysis of Double Effect Absorption System Cascaded with Ejector and Enhanced Vapor Compression Refrigeration Cycle**" is an authentic report of study carried out as requirement for the award of degree B.Sc. (Mechanical Engineering) at Islamic University of Technology, Gazipur, Dhaka, under the supervision of Dr. Mohammad Monjurul Ehsan, Professor, MPE, IUT in the year 2024.*

The matter embodied in this thesis has not been submitted in part or full to any other institute for award of any degree.

Sefat Mahmud Siddique
190011125

Md. Muhtasim Uzzaman
190011106

Recommendation of the Thesis Supervisors

The thesis titled "**Thermal Analysis of Double Effect Absorption System Cascaded with Ejector and Enhanced Vapor Compression Refrigeration Cycle**" submitted by Sefat Mahmud Siddique, Student No: 190011125 and Md. Muhtasim Uzzaman, Student No: 1900111106 has been accepted as satisfactory in partial fulfillment of the requirements for the degree of B Sc. in Mechanical Engineering **on 5th July, 2024.**

1. ----------
   Dr. Mohammad Monjurul Ehsan (Supervisor)
   Professor
   MPE Dept., IUT, Board Bazar, Gazipur-1704, Bangladesh.

CO-PO Mapping of ME 4800 -Theis and Project

COs	Course Outcomes (CO) Statement	(PO)	Addressed by	
CO1	Discover and Locate research problems and illustrate them via figures/tables or projections/ideas through field visit and literature review and determine/Setting aim and objectives of the project/work/research in specific, measurable, achievable, realistic and timeframe manner.	**PO2**	Thesis Book	
			Performance by research	
			Presentation and soft skill	
CO2	Design research solutions of the problems towards achieving the objectives and its application. Design systems, components or processes that meets related needs in the field of mechanical engineering	**PO3**	Thesis Book	
			Performance by research	
			Presentation and soft skill	
CO3	Review, debate, compare and contrast the relevant literature contents. Relevance of this research/study. Methods, tools, and techniques used by past researchers and justification of use of them in this work.	**PO4**	Thesis Book	
			Performance by research	
			Presentation and soft skill	
CO4	Analyse data and exhibit results using tables, diagrams, graphs with their interpretation. Investigate the designed solutions to solve the problems through case study/survey study/experimentation/simulation using modern tools and techniques.	**PO5**	Thesis Book	
			Performance by research	
			Presentation and soft skill	
CO5	Apply outcome of the study to assess societal, health, safety, legal and cultural issue and consequent possibilities relevant to mechanical engineering practice.	**PO6**	Thesis Book	
			Performance by research	
			Presentation and soft skill	
CO6	Relate the solution/s to objectives of the research/work for improving desired performances including economic, social and environmental benefits.	**PO7**	Thesis Book	
			Performance by research	
			Presentation and soft skill	
CO7	Apply moral values and research/professional ethics throughout the work, and justify to genuine referencing on sources, and demonstration of own contribution.	**PO8**	Thesis Book	
			Performance by research	
			Presentation and soft skill	
CO8	Perform own self and manage group activities from the beginning to the end of the research/work as a quality work.	**PO9**	Thesis Book	
			Performance by research	
			Presentation and soft skill	
CO9	Compile and arrange the work outputs, write the report/thesis, a sample journal paper, and present the work to wider audience using modern communication tools and techniques.	**PO10**	Thesis Book	
			Performance by research	
			Presentation and soft skill	
CO10	Organize and control cost and time of the work/project/research and coordinate them until the end of it.	**PO11**	Thesis Book	
			Performance by research	
			Presentation and soft skill	
CO11	Recognize the necessity of life-long learning in career development in dynamic real-world situations from the experience of completing this project.	**PO12**	Thesis Book	
			Performance by research	
			Presentation and soft skill	

Student Name /ID:

1……..

2. ……..

Signature of the Supervisor:

……

Name of the Supervisor:

……..

K-P-A Mapping of ME 4800 -Theis and Project

COs	POs	Related Ks								Related Ps							Related As				
		K1	K2	K3	K4	K5	K6	K7	K8	P1	P2	P3	P4	P5	P6	P7	A1	A2	A3	A4	A5
CO1	PO2																				
CO2	PO3																				
CO3	PO4																				
CO4	PO5																				
CO5	PO6																				
CO6	PO6																				
CO7	PO8																				
CO8	PO9																				
CO9	PO10																				
CO10	PO11																				
CO11	PO12																				

Student Name /ID:

1……..

2. ……..

Signature of the Supervisor:

……

Name of the Supervisor:

……..

Acknowledgment

We are deeply appreciative of the unwavering support and consistent guidance that our supervisor, Dr. Mohammad Monjurul Ehsan, has provided to our work. His insightful feedback and suggestions have significantly influenced our research, and his dedication to our endeavor has been a source of inspiration. We were kept motivated and focused by his encouragement during difficult periods. Furthermore, we would like to express our gratitude to Yasin Khan, our co-supervisor, for his guidance and counsel at all times. His willingness to assist and his expertise have been instrumental in surmounting a variety of challenges. His practical insights and timely interventions provided the clarity necessary to progress.

Abstract

The traditional Double Effect Absorption Refrigeration Cycle (DE-ARC) series and parallel configuration cascaded with the conventional Vapor Compression Refrigeration (VCR) technology solves the limitations faced with these standalone respected cycles. Although these systems (Compression Double Effect Absorption Cycle (C-DAC (Series), C-DAC (Parallel))) have difficulties in utilizing high waste heat recovery and consume high compressor power. Regarding these limitations, in our present study, a modified DE-ARC (Series and Parallel) with a Refrigerant Heat Exchanger (RHX) is combined with an improved vapor compression refrigeration (VCR) system that includes an ejector, resulting in the development of the proficient Ejector Double Effect Absorption Cycle. (E-DAC (Series), E-DAC (Parallel)) and Ejector Injection Double Effect Absorption Cycle (EI-DAC (Series), EI-DAC (Parallel)) using $LiBr/H_2O$ and R41 as the working fluid. The Engineering Equation Solver (EES) is employed to generate a numerical model for the purpose of conducting a thorough analysis based on the concepts of energy, mass, and exergy conservation, encompassing both the first and second laws of thermodynamics. The results indicate that the four suggested systems outperform the traditional cascaded cycles. Among these four combinations, the EI-DAC (Parallel) configuration shows the highest performance, with an improvement of approximately 16.5% and 14% compared to the C-DAC (Series) and C-DAC (Parallel) configurations, respectively. Further analysis reveals that the coefficient of performance (COP) of our proposed systems exhibits a linear relationship with the evaporator temperature. Furthermore, the systems exhibit improved performance at higher generator temperatures, making them well-suited for utilizing larger quantities of waste heat while still being able to operate at lower evaporator temperatures. Output of this comprehensive theoretical thermodynamic study yield a thorough comprehension of the performance of E-DAC (Series and Parallel) and EI-DAC (Series and Parallel) systems and provide useful suggestions for future enhancement and optimization.

Table of Contents

List of Figures

List of Tables

Nomenclatures

Abbreviation	
VCR	Vapor compression Refrigeration cycle
ER	Entrainment Ratio
ARC	Absorption refrigeration cycle
C-DAC	Compression double effect absorption cycle
DE-ARC	Double effect absorption refrigeration cycle
CARC	Compression absorption refrigeration cycle
E-DAC	Ejector double effect absorption cycle
EI-DAC	Ejector injection double effect absorption cycle
LTC	Low-temperature circuit
CHX	Cascade heat exchanger
RHX	Refrigerant heat exchanger
HTC	High-temperature circuit
LPG	Low Pressure Generator
HPG	High Pressure Generator
TV	Throttle valve
COP	Coefficient of performance
Ex_{eff}	Exergy efficiency
$LiBr/H_2O$	Lithium bromide water solution
NH_3/H_2O	Ammonia water solution
FT	Flash tank
Symbols	
h	Enthalpy [kJ kg^{-1}]
s	Entropy [kJ kg^{-1} K^{-1}]
P	Pressure [kPa]
T	Temperature [°C]
$\dot{W}_{comp}$	Compressor load [kW]
$\dot{W}$	Rate of work [kW]
ex_i	Point exergy [kW]
$\dot{E}_D$	Exergy destruction rate [kW]
η_{II}	Exergetic efficiency [dimensionless]
η_{is}	Isentropic efficiency [dimensionless]
ΔT	Temperature difference
ΔP	Pressure drop
mot-noz	Ejector's motive nozzle
suc-noz	Ejector's suction nozzle
Mix	Ejector's mixing chamber
Diff	Ejector's diffuser
E	heat exchanger effectiveness
Subscript	
1,2,3,4….	State points
I	inlet
E	exit
0	Dead state point
gen	Generator
cond	Condenser

abs	Absorber
evp	Evaporator
comp	Compressor
HPG	High Pressure Generator
LPG	Low Pressure Generator

Chapter 1: Introduction

The exponential growth in population of the world has resulted in demand of more efficient and effective refrigeration and cooling technologies. Energy recovery and conversion have become increasingly important in recent years due to the limited availability of fossil fuels and the rising impact of the greenhouse effect [1]. One of the major aims in this sector of research is the enhancement of refrigeration cycles that can operate in ultra-low temperature proficiently considering all the environmental factors with the reduction of cost providing the most optimal performance [2]. Cooling systems have widespread range of usages in our life. Refrigeration plays an essential role in thermal comfort considering both heating and cooling applications, in commercial food freezing and conservations, electrical component cooling, industrial activities like liquefaction processes of natural gasses and so on[3][4][5]. However, all these processes mostly require electricity to function. And the rising surge of power globally is a real phenomenon to deal with. Studies show that systems like VCR that are extensively employed in various settings such as residential and business buildings, supermarkets to deliver cooling or freezing capabilities- consume approximately 15% of the world's electricity [6]. Hence, thermodynamic cycles with competent use of electric energy are the modern-day solution to the problem. This research takes a deep dive to find better alternatives to conventional refrigeration systems by the integration of various configurations of improved thermodynamic cycles that will be able to provide cooling at very low temperature with most efficient use of electrical energy. Analysis is performed from both energy and exergy perspectives, showing a vivid representation of contemporary cooling methods.

Chapter 2: Literature Review

2.1 Characteristics of conventional VCR systems and integrated VCR systems

The Vapor Compression Refrigeration Cycle is widely employed in the Air conditioning and cooling industry. This approach is the most fundamental and uncomplicated one. Water boiling, space cooling and heating, and refrigeration are primarily reliant on vapor compression refrigeration (VCR) in energy systems. In the United States, these activities account for 76% of the total energy consumption in residential houses [7]. Vapor compression refrigeration system’s thermodynamic actions produce enormous amounts of heat that is released the environment. It is evident that the highest amount of energy and exergy loses takes place in compressor among all the VCR components. Aikins et al. [8] wrote about the problems of single staged VCRs when the requirements are high condensing temperature, low evaporating temperature and also leading to higher compression ratios. All of these conditions will

ultimately produce very low COP which is highly undesirable. To overcome this problem, multistage cascade refrigeration system has been introduced as a solution. Z. Sun & Wang [9] experimented about the cascade refrigeration system with two-stage compression using R1150/R717 as the refrigerant group to enhance the efficiency of the industrial refrigeration model in the − 120◦C to − 80◦C temperature range. Jain et al. [10] shown in his study that the cascaded VCR in aspect of electric power consumption is reduced by 61% and compression side's COP is improved by 155% with respect to the same values of conventional VCR. A cascade between single effect absorption cycle using LiBr-H_2O as fluid a subcritical CO2 vapor-compression cycle was tested, and shown very high COP in various performing conditions and was measured to have a reduction up to 31% of electricity demand than that of standard VCR, according to Garimella et al.[11].

2.2 Exploration on the advancement of VCR systems

Vapor compression refrigeration cycle can be improved in numerous ways to make it more compact, efficient and useful. Subcooling is one of the most fundamental ways to improve the COP of the system. Some of the used subcooling methods are liquid to suction heat exchanger (LSHX) sub-cooling), integrated mechanical sub-cooling (IMS), condensate assisted sub-cooling and dedicated mechanical sub-cooling (DMS)[12]. This study also narrates that the sub-cooling technologies provide a moderate COP improvement.

The flash tank is an additional component incorporated into the VCR system to enhance its performance. It segregates the gaseous phase from the liquid phase in the substance to enhance efficiency. According to a study by Sirwan et al. [13] , inserting a flash tank between the condenser and evaporator can increase the entrainment ratio of the ejector. This configuration significantly improves the cooling capacity of the modified system when operated under various conditions by reducing the amount of flash gas that reaches the evaporator.

The ejector-based VCR has been recognized as a significant advancement in VCR technology. The ejector has a crucial function in the low temperature circuit as it directs the low-pressure vapor into a mixture with the high-pressure vapor in the convergent-divergent section of the nozzle. In a study conducted by Megdouli et al.,[14] it was discovered that the modified VCR system, which includes ejector displays, exhibited a 25% increase in COP and a notable reduction of 20% in mechanical power consumption when compared to the regular VCR cycle. By employing a basic liquid-vapor ejector refrigeration cycle, there was an improvement of 18% in the coefficient of performance (COP), a 25% increase in exergy efficiency, and a reduction of 31% in power consumption were found by Sanaye et al. [15]. **Table 1** displays a

detailed overview of the mention worthy researches performed on the advancement and modifications of the VCR cycle. It is mention-worthy that the most significant development in performance is noticed with the employment of the ejector enhanced system in the cycle, allowing to pre-compress the low-pressure vapor which significantly reduces the compressor load and thus ultimately leads to better efficiency of the system.

Table 1: A thorough investigation of researches carried out on the progress of VCR technology.

Suggested Modification	Year	Salient Features	Temperature range	Remarks	Reference
Incorporation of Heat Exchanger (HX)	2013	• An experimental investigation to analyse the impact of internal heat exchanger (IHX) on the operational efficiency of a VCR technology. • R1234yf refrigerant used as a replacement for R134a.	--13°C to 7°C	• The usages of IHX shows the enhancement of both cooling capacity and COP, being comparatively higher in the case of R1234yf. • The substitution of R134a with the fluid R1234yf result in decreases in cooling capacity and COP of 6% to 13%, but the inclusion of an IHX can mitigate these losses to a lesser extent of 2% to 6%.	J. Navarro-Esbrí et al. [16]
	2020	• Theoretical assessment of implementing the liquid-suction heat exchanger. (SLHX) • Refrigerant used- R22, R600a, R134a	--40°C to 70°C	• The COP of R134a is 7% greater than that of R600a and 12% higher than that of R22. • The coefficient of performance (COP) can be increased by up to 20% depending on the kind of refrigerant and the condition of operation of the liquid-suction heat exchanger.	R. A. Mahmood [17]
	2018	• Two-stage vapor compression	-30 °C to 15 °C	• The cycle presents an optimum COP for a specific displacement ratio, and	F. M. Tello-Oquendo et al.

		cycles with vapor-injection technology. • Two configurations are proposed using flash tank & economizer.		economizer size plays significant role in controlling the parameters.	[18]
Usages of sub-cooler cycles	2021	• Experimental investigation of vapor injection based on flash-tank and intermediate heat exchanger. • 3°C of superheating in the outlet of the evaporator and 5°C of subcooling at the outlet of the condenser is implemented	-20°C to 7°C	• The heating capacity and is found 3.2%-13.0% and 0.1%-2.2% higher in the FT based system compared to IHX based system. • The introduction of vapor enhances the pace and uniformity of the flow of the working fluid, while simultaneously reducing the exhaust entropy.	J. Wang et al. [19]
	2016	• Use of ejector in compression-refrigeration cycle to improve the efficiency. • Constant-pressure mixing model • Refrigerant used- R141b	-5°C to 10°C	• Using an ejector instead of an expansion valve in a vapor-compression system has been demonstrated to enhance performance improvement ratio by 5.29% to 9.62% under varying operating conditions. • There is an optimal value for the mixing pressure that results in the highest values for the entrainment ratio, exit pressure of the ejector, and overall system performance.	F. Wang et al. [20]
	2022	• Ejector-implemented	9.5°C to 55°C	• COP of the proposed system is 12.1% greater	X. Cao et al. [21]

Ejector based modification in VCR		double-stage evaporation cycle • Refrigerant- Transcritical CO_2		than that of the ejector cycle, 6.9% greater than that of the two-stage evaporation cycle, and 22.0% greater than that of the fundamental refrigeration system. • the novel system may decrease the exergy loss of the expansion step by 49.6% and the exergy reduction of the heat transfer method in evaporators by 21.5%.	
	2024	• Introduces a two-ejector enhanced dual-stage auto-cascade refrigeration cycle (ETARC) • Working fluid - R600a/R41/R 1150	-30°C to 55°C	• Utilizing the two ejectors efficiently enhances the performance of the system. Shows a 16.07% improvement in COP. • When comparing the cycle at an evaporation temperature of -85°C and a condensation temperature of 45°C, a 29.43% gain in volumetric refrigeration capacity, and a 17.17% reduction in the total exergy destruction rate is noticed.	R. Shi et al. [22]
Injection based ejector enhancement technology	2015	• A proposal for a CO_2 transcritical heat pump cycle with an ejector and increased vapor injection, together with a sub-cooler. • Refrigerant- Transcritical CO2	-25°C to -5°C	• The enhancements in the maximum system COP and volumetric heating capacity might potentially achieve an increase of up to 7.7% and 9.5% respectively. • The exergy analysis shows the sequence of biggest ratio of exergy destruction starts with compressor, followed by the evaporator and gas cooler	T. Bai et al. [23]
	2023	• An examination of the energy and exergy of an ejector-	-30°C to 33°C	• At an evaporator temperature of -60◦C, the suggested system demonstrates an 8.571% enhancement in the	M. Walid Faruque et al. [24]

	injection refrigeration system. • Improving effectiveness by combining an electronic expansion valve with a changeable intercooling fluid temperature.		coefficient of performance (COP) and a 7.241% enhancement in exergy efficiency. • The ejector pressure-drop and condensation temperature in the lower temperature circuit of the cascaded cycle plays an important role in the efficiency of the system.	
2024	• Ejector-enhanced vapor injection cycle with dual evaporators. • Refrigerant used- R1234yf	5°C to 25°C	• COP and volumetric heating capacity shows improvement of 18.88% and 66.99% respectively. • demonstrates superior exergy efficiency due to a 75.98% reduction in exergy degradation caused by expansion valves in conventional systems compared to proposed novel model.	S. Jing et al. [25]

2.3 Absorption system and its possibilities

Absorption system uses low grade waste heat as its heat source, which gives this cycle an edge over other thermodynamic cycles. The deduction of compressor makes the system more flexible, resulting in minimum electricity consumption. In addition, solar energy is a very dependable input source for absorption systems, effectively advancing the technology of renewable and sustainable energy sources [26]. ARC provides several advantages over traditional systems, including the use of environmentally friendly refrigerants, the efficient utilization of wasted power through heat recuperation from different sources, and the reduction of system losses. These features enhance the system's versatility.

Although ARC comes with a lot of perks, it has some major drawbacks as well. The identified limitations include crystallization, corrosion, and the need for vacuum operating pressures in H_2O/LiBr systems. Additionally, the rectification of the refrigerant vapor exiting the desorber and the requirement for high activation temperatures are challenges in NH_3/H_2O systems [27]. For any LiBr salt concentration, there exists a particular minimum temperature at which the salt starts to crystallize out of the solution. LiBr solution undergoes crystallization when the

concentration ratio is increased or when the solution temperature is decreased below the crystallization limit [28]. Consequently, if may lead to the formation of slush that can potentially cause complete flow blockage if it solidifies [29].

The simplest configuration is single effect absorption system and the improved cycle is the double effect absorption cycle. Nikbakhti et al. [30] conducted a thorough study on the different configuration with different pair of refrigerants in double effect absorption cycle. Multi-effect absorption cycle has been proved more efficient in the optimal operating conditions in that research. In a study of Chahartaghi et al. [31] for the comparison between series and parallel configuration of the double effect absorption system, it is measured that in optimum operating conditions the series configuration can generate higher COP when the generator temperature is provided below 150 degrees; otherwise, the parallel configuration is suitable for temperature higher than 150 degrees. For the refrigerant choice, the H_2O-NH_3 and LiBr-H_2O pair has been the most useful and popular choice [32]. **Table 2** provides a comprehensive analysis of the important research carried out on the advancement of absorption refrigeration system.

Among all the new innovations introduced for the ARS system, double effect and triple effect absorption system is statistically more promising. Triple-effect ARS systems are equipped with an extra high-temperature generator and condenser, in contrast to double-effect ARS systems. The number of heat exchanging components, such as generators, condensers, heat exchangers, and pumps, will increase with the increase in the number of effects. This will depict the intricacy, dissipation of heat, expenses, and susceptibility to corrosion of the system [33]. Investigating among the two configurations of the double effect absorption system, it is already established that the parallel flow system performs comparatively better operating at a higher generator temperature. The split of the stream of the solution before entering into the high-pressure generator reduces the load into the HPG, ultimately resulting in the reduction of Q_{HPG} and thus the enhancement of COP [34]. Also, the simultaneous operation of both the generators makes this system more efficient compared to the series configuration. From the literature, it is pretty evident that the parallel flow double effect absorption cycle is a fairly superior system compared to others when considering all criteria.

Table 2: A detailed study of research undertaken on the progress of AR system.

Suggested Modification	Year	Salient Features	Refrigerants	Remarks	Reference
	2010	• Compressor incorporated between evaporator	NH_3-$LiNO_3$	• Operates at lower driving temperature compared to the single	R. Ventas et al. [35]

Compressor booster in absorption cycle .		and absorber. • based on UA-ΔT_{lm} models, specifically designed for different sections of plate-type heat exchangers.		effect cycle, thus consuming less electricity. • The COP was determined to be greater than that of an ammonia vapor compression cycle for a wide range of operating circumstances.	
	2017	• The compression booster is positioned intermediate to the absorber and the evaporator. • Both a mechanical compressor and a thermal compressor (vapor-ejector) are employed to enhance compression.	NH_3-H_2O	• provides exceptional capability with varying the compression ratio in response to changes in heat source and heat rejection temperatures. • By incorporating a vapor ejector into the cycle, the cooling capacity can be enhanced by approximately 42% while operating at a driving heat source temperature ranging from 105°C to 130°C.	D. S. Ayou et al. [36]
Incorporation of ejector	2014	• Introduces ejector to replace the solution expansion valve to recover pressure for single effect absorption cycle. • Numerical computational model	NH_3-NaSCN	• It is demonstrated that combined cycles outperform single effect cycles when generator temperatures are low. • Both COP and exergy efficiency are much higher compared to the conventional cycle	L. Garousi Farshi et al. [37]
	2018	• Solar Assisted Combined Power and Refrigeration System. • The energetic and exergetic performance were evaluated.	NH_3-$LiNO_3$	• Out of the many fluids used in the ORC circuit, the R141b fluid had the highest efficiency (14.6%) in converting solar energy intake into usable energy output. • An increase in the turbine inlet pressure	A. Khaliq et al. [38]

				resulted in a significant increase in both the exergetic and energetic output of the cycle.	
Double effect absorption system	2009	• Numerical analysis to compare the absorption systems of single and double effects. • Based on first law and second law analysis.	LiBr-H_2O	• The COP of a double effect system is roughly twice that of a single effect system. • Under varying conditions, the double effect refrigeration systems exhibit maximum COP values ranging from 1.22 to 1.42, while the maximum exergetic efficiency values vary from 14.3% to 25.1%.	R. Gomri et al. [39]
	2015	• energy and exergy analysis on a double effect series flow absorption refrigeration system utilizing various heat sources such as hot water, hot air and steam through High Pressure Generator.	LiBr-H_2O	• An increase in the operating temperatures of the HPG leads to a reduction in the exergy destruction of the HPG. • Similarly, an increase in the operating temperatures of the LPG leads to a reduction in the exergy degradation of the HPG. The reduction is 41.5% for hot air, 41.8% for steam, and approximately 42.2% for hot water at the lowest source temperature.	O. Kaynakli et al. [40]
	2019	• Study of the comparison between series and parallel flow configurations. • The Genetic Algorithm (GA) method has been employed to optimize the	LiBr-H_2O	• The series configuration yielded a higher COP for T_{hpg} values below 150°C, but the parallel configuration resulted in a stronger COP for T_{hpg} values over 150°C. • The parallel cycle has a	M. Chahartaghi et al. [31]

		Coefficient of Performance (COP) of the system in both series and parallel cycles.		greater operational range compared to the series cycle since it has a narrower range of crystal formation. • Furthermore, while employing a flow splitter in the parallel cycle, the concentration of the inlet solution to the absorber is decreased, effectively preventing crystallization in the absorber.	
Triple effect absorption system	2014	• This study provides a performance comparison of five distinct configurations of absorption cooling systems. • Analyses of single-effect, half-effect, double-effect in series, double-effect inverse and triple-effect.	NH_3-$LiNO_3$	• Triple-effect systems offer the best coefficients of performance, but also necessitate the highest generator temperatures (beginning from 150°C). • Additionally, they are the most intricate and are mostly suitable for air conditioning purposes.	L.A. Domínguez-Inzunza et al. [41]

2.4 Research on VCR-ARC cascade refrigeration system

Based on the studies stated above, it is clear that the VCR or ARC, when used as a standalone system, does not meet all the necessary requirements. Vapor compression cycles have a greater power consumption, while it is challenging to improve the lower coefficient of performance in an absorption refrigeration cycle. However, the cascade of compression-absorption system (CARC) enables the utilization of both cycles based on their respective strengths. The distinguishing feature of the vapor compression-absorption integration system lies in its ability to utilize a wide range of fluids and its adaptability. The VCR's capacity to function at lower temperatures and the ARC's ability to be combined with low-quality energy input can lead to a sustainable and efficient system with various possibilities. [42][43]

When the compression-absorption cascade refrigeration cycles and the standard vapor compression refrigeration cycles are weighed at the uniform conditions applying the exact similar cooling capacity for both cases, relying on absorption fluid pairs such as LiBr-H_2O and

NH_3-H_2O, 48-51% less electric energy is wasted in the integrated cycles [44]. Yu et al. [45] conducted thorough research on cascade compression absorption cycle utilizing low-grade waste heat as energy source, it was found that the developed system can optimize 24.44% of the exergy destruction compared to the standard system, with a lower cost. A study carried out about the compression-absorption incorporated refrigeration system by J. Fernandez-Seara et al. [46] shows that with the performed computer simulation optimization [47], the enhancement in COP and exergy efficiency was 7.3% and 3.3% consecutively. A theoretical study conducted by Sun et al. [48] that proposes two-stage CO_2 compression refrigeration system with parallel compression and solar absorption partial cascade refrigeration system (CTRS + PC + PCRS) was contrasted with the basic CO_2 two-stage compression refrigeration system (BCTRS), the research shows that depending on the different regions and climates, the CTRS + PC + PCRS system shows enhancement of the COP up to 47.28% compared to the BCTRS. Moreover, Razmi et al. [49] investigated about the combined heating and cooling power proposing a hybrid compression absorption refrigeration system. The outcome displays that the novel system can generate 2280kW electrical energy and 416.7kW cooling simultaneously, enhancing the exergy efficiency with the reduction of adverse impact on environment. Furthermore, incorporation of flash tank and reheater in compression-absorption system can boost the COP and exergy efficiency up to 18.49% compared to the conventional cascade cycle, shows the study of Faruque et al. [50]. Xu et al. [51] performed both experimental and simulation validation for novel compression absorption cascaded system employed for ultra-low temperature. The proposed system could achieve evaporating temperature of up to -170°C. It is evident that the cascaded compression-absorption technology has advanced enormously in recent years, with more opportunities of investigations and researches to be conducted for widespread usages.

2.5 Formulating research scope and problems

The cascaded compression absorption system has been proven to be a prominent solution that integrates VCR in the LTC to achieve efficient cooling at lower temperatures, and ARS in the HTC to minimize power consumption effectively. Nevertheless, the typical Compression absorption refrigeration cycle exhibits numerous limitations. Significant energy losses occur as a result of the isenthalpic throttling process in the expansion valve, and excessive power is required by the single stage compressor in the VCR [52]. Furthermore, the simple VCAR system has a significant deficiency in heat dissipation [10] leading to an inadequate level of output.

The primary objective of this research is to discover improved solutions for the aforementioned issues by integrating two separate setups of a modified double effect absorption system into the HTC that will be combined with an ejector and an injection-enhanced vapor compression refrigeration cycle in the LTC. The double effect absorption refrigeration system (ARS) is enhanced by incorporating a RHX, which improves the heat removal capacity and thus increases the COP. Utilizing two generators in the absorption refrigeration system aids in decreasing the mass flow rate, hence reducing the load and achieving optimal efficiency. Utilizing the ejector assists in diminishing the workload on the compressor, resulting in a decrease in electricity usage. The two sophisticated VCR systems utilize both parallel and series flow models to create four innovative cascaded compression-absorption systems, namely E-DAC (series and parallel) and EI-DAC (series and parallel). These integrations enable the circuits to function at low evaporation temperatures, resulting in efficient cooling at very low temperatures. Furthermore, this minimizes losses during the throttling process and also reduces power consumption, leading to superior overall performance.

In order to thoroughly examine the effectiveness of the new systems, both first law and second law analyses are undertaken. These analyses allow us to analyze five key performance parameters, that are COP, generator load, compressor load, exergy efficiency, and exergy destruction. The parameters of the novel systems were compared to those of the standard cascaded systems in order to validate the improvements. This research work stands apart since it investigates cascade compression absorption devices, specifically examining their practicality and limitations. The study introduces the advanced novel systems, E-DAC (series and parallel) and EI-DAC (series and parallel), as unique solutions. It conducts a thorough analysis from various perspectives to ensure a full comprehension.

Chapter 3: Description of the System

3.1 Conventional compression-absorption refrigeration

Absorption refrigeration cycles have been proven to be a system of great potential in the refrigeration field. It's ability to use low-grade heat energy as input makes it a standout, facilitating the exclusion of any compressor in the system using the generator-absorber duo. Various kinds of solution-refrigerant pair can be implemented in this system, LiBr-H_2O and NH_3- H_2O being most used among them. The absorption system comparatively has a low COP in comparison to the VCR cycle due to its usage of poor-grade thermal energy, in contrast to the better-quality electrical input that is employed in VCR cycles. The most basic absorption cycle is the single effect absorption system, but its thermal efficiency is not the most promising. The double effect absorption chiller has a COP that is approximately twice as high as that of a single effect system. Additionally, it also improves exergetic efficiency [39]. The double effect absorption cycle incorporates a high temperature generator that functions at increased temperature and pressure, in addition to the standard components of a single effect system. This enhancement leads to a more effective usage of the provided heat. This system has two configurations, series and parallel. In the series flow system, the solution that was pumped from the absorber reaches to the high-pressure generator through heat exchangers. The primary vapor is produced at the exit of HPG and the secondary vapor is produced in LPG from the medium-concentrated solution. On the other hand, in the parallel configuration, the solution flow gets split into two sections before entering into the first heat exchanger. One stream gets circulated through HPG and another stream directly enters into LPG after being throttled.

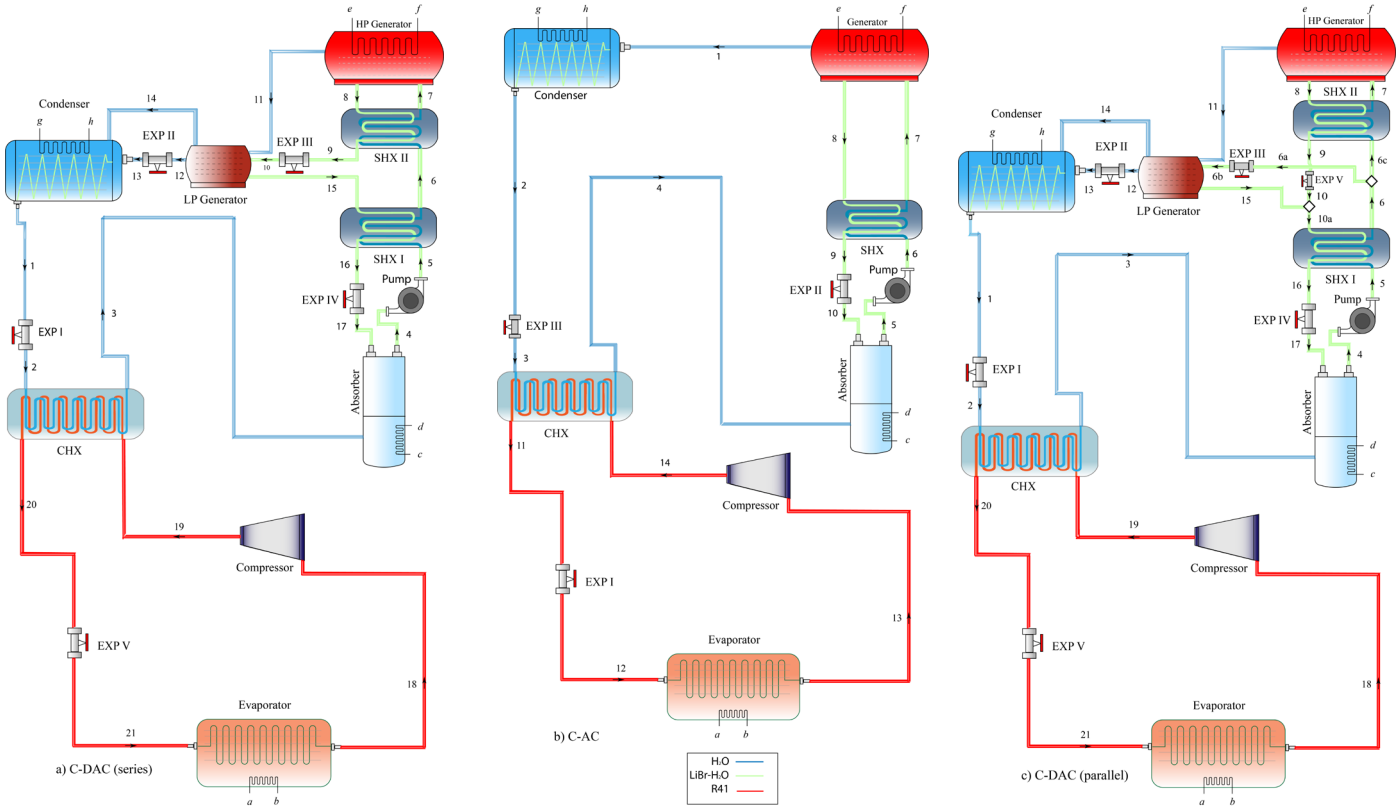

Fig. 1: Schematic illustration of the traditional Single Effect (b), Double Effect Absorption System series flow (a) and parallel flow (c) system cascaded with Vapor Compression Cycle

Additionally, there are some drawbacks with the absorption cycle as well. One significant issue associated with the LiBr-H_2O combination is the crystallization of LiBr at modest concentrations. As the water is circulated as the refrigerant, frozen-water problem below the freezing point in the evaporator comes up as a leading problem. Additional disadvantages are associated with the lithium bromide-water combination, specifically the low pressure and highly viscous solution [53]. Although the mentioned problems in latter part can be mitigated by the appropriate design of equipment. With the NH_3- H_2O pair there are major disadvantages as well. Because of the inherent volatility of the water, the ammonia vapor produced by the generator is presented with substantial amount of water vapor in it, thus reducing the efficiency. Another significant problem encountered in the functioning of these systems pertains to the potential occurrence of crystallization within them. Under realistic circumstances for the aforementioned absorption systems, the concentration of LiBr-H_2O in water at some steps of the cycles is elevated and it reaches to a borderline to the boundary of crystallization. Nevertheless, it is highly probable that crystallization will occur in the weaker solution after

entering the absorber, as this location exhibits the highest concentration and lowest temperature. It has been observed that in series flow systems, the likelihood of crystallization rises as the high-pressure generator temperature, evaporator temperature and effectiveness of the HX increases, while the condenser temperature gets reduced. Furthermore, in a parallel cycle, it has been established that the likelihood of crystallization is minimal under the examined conditions. However, in practical applications, the mechanical structure of the system and the real-life operating conditions might significantly influence this situation [28].

To overcome this problem, Xu et al. [51] proposed compression and absorption subsystem cascade which can be operated at a very low evaporator temperature. Enhancement in COP compared to the standard system is noticed in this novel system. The absorption system, acting as a higher temperature circuit (HTC), supplies low-quality cooling capacity to the low-temperature circuit (LTC) in the compression system. As a result, the evaporator temperature decreases and there is an observed increase in high-grade cooling capacity in the compression system [54]. But this system is still not fully capable to utilize the energy provided, lots of losses still occur in the cascaded system. Energy loss in the expansion process, relatively higher energy input in the compression system and provision of low-grade heat in the absorption system are some of the leading improvement scopes. [55]

3.2 Proposed novel cascade systems

The proposed novel systems incorporate the introduction of four cascaded cycles. Two ejector-based vapor compression refrigeration systems are used to combine modified double effect absorption cycles in both series and parallel configurations. **Fig. 2(a), Fig. 2(b), Fig. 3(a)** and **Fig. 3(b)** illustrates the novel systems under consideration, namely the Ejector-Double effect Absorption Cascade (E-DAC) and the Ejector Injection-Double effect Absorption Cascade (EI-DAC), which are presented in two distinct configurations. The double effect absorption cycle exhibits notable enhancements compared to the single effect cycle, mostly attributed to its enhanced heat recovery capability achieved by the utilization of two generators running at distinct pressures. This system enhances the overall performance of the cycle by recovering a greater amount of heat. In contrast, the implementation of an ejector system is proposed as an alternative to the typical VCR system, primarily in response to the significant energy dissipation occurring in the throttle valve during the isentropic process. The utilization of an ejector allows for the harnessing of energy from a high-pressure motor fluid in order to guide a low-pressure suction fluid towards an intermediate discharge pressure. In the ejector-injection

system, the utilization of multistage compression is employed to augment the separation of the liquid refrigerant into two distinct phases.

As illustrated in **Fig. 2(a)** and **Fig. 2(b)**, the $LiBr.H_2O$ solution is circulated as a fluid in the series flow circuit in HTC. The weak solution is transferred to the high-pressure generator (HPG) via two heat exchangers, where it undergoes heat transfer. Subsequently, the primary vapor is generated at the HPG outlet (point 11) and goes into the LPG, while the medium concentrated solution enters at the LPG inlet (point 10). After being subjected to further heating, secondary vapor is produced. The concentrated solution originating from the LPG outlet is directed towards the absorber, while the primary and secondary vapors are sent towards the condenser (point 13) where they undergo heat dissipation. The liquid refrigerant at high pressure is sent through the RHX and subsequently passes through the expansion valve, where a pressure drop is observed, until it reaches the pressure of the CHX. Subsequently, the fluid passes via the Cascade Heat Exchanger (CHX), where it absorbs thermal energy, before returning to the absorber. (Point 17)

The weak solution is transferred to SHX-I within the parallel flow circuit, subsequently undergoing separation into two distinct streams, denoted as point 6c and 6a that is shown in the HTC of **Fig. 3(a)** and **Fig. 3(b)**. One of the streams is directed to the High-Pressure Generator (HPG) via the SHX-II, while another stream is immediately directed to LPG after being throttled in the expansion valve (point 6b). The primary vapor is extracted from the high-pressure generator (HPG) and subsequently reaches the low-pressure generator (LPG) at point 11. The concentrated solution exiting the HPG is diluted and combines with the medium solution originating from the LPG at point 10a. After passing through SHX-I and the expansion valve (point 17), the combined flow is returned to the absorber in the form of a medium strong solution.

The ejector-based VCR is utilized in the LTC, depicted in **Fig. 2(a)** and **Fig. 2(b)**. The ejector consists of three main components: a diffuser, a nozzle, and a mixing chamber. Additionally, a flash tank is incorporated into the LTC to facilitate the separation of the mixture. Upon heat rejection at CHX, the high-pressure refrigerant undergoes saturation and then enters the ejector intake (point 22) as the motive fluid. The low-pressure refrigerant at the exit is a result of the fast area changes caused by the converging-diverging nozzle. The saturated vapor originating from the output of the evaporator is sucked through the suction side inlet of the ejector as a result of the low pressure. Then both fluids are blended at the mixing chamber (point 24), then expanded at the diffuser portion of the ejector to retain the lost energy in pressure and goes out as a double-phased refrigerant (point 25). Subsequently, the mixture is introduced into the flash

tank and subsequently separated. The vapor is introduced into the compressor, where it undergoes compression and subsequently dissipates heat at the CHX, before returning to the inlet of the ejector motive. Conversely, the liquid from the outlet of the flash tank passes through the expansion valve, where it is regulated to the pressure of the evaporator. Then the liquid converts into saturated vapor and flows back as the suction fluid in the ejector to recycle the system.

In the ejector-injection system, shown in the **Fig. 3(a)** and **Fig. 3(b),** the refrigerant mixture, consisting of two phases, is discharged from the ejector outlet (point 25) and then enters flash tank-I. Inside the flash tank, the mixture is divided into two states: saturated vapor (point 26) and saturated liquid (point 27). The saturated vapor is injected to the mixing chamber portion for the purpose of injection process, and the liquid portion moves through the TX valve -II and departs as a double-phased mixture (point 28). Then it enters in the Flash Tank- II, gets separated as saturated liquid (point 31) and saturated vapor (point 29). The suction intake of the ejector absorbs the saturated vapor as suction fluid, and the saturated liquid enters at throttle valve – I to get throttled to evaporator pressure, then it goes through evaporator to change into saturated vapor (point 33). Subsequently, the gas is compressed within a low-side compressor in order to attain an intermediate pressure. Point 34 Subsequently, the injected vapor is combined with the mixture and subsequently compressed to the high-side compressor (point 21) in order to achieve the CHX pressure. Subsequently, it undergoes heat dissipation and transforms into a saturated liquid (at point 22) before entering the ejector motive side to initiate the recirculation of the cycle. The implementation of double separation in the flow ensures an improved refrigerant flow via the heat exchanger (CHX), hence enhancing the overall efficiency of the innovative system.

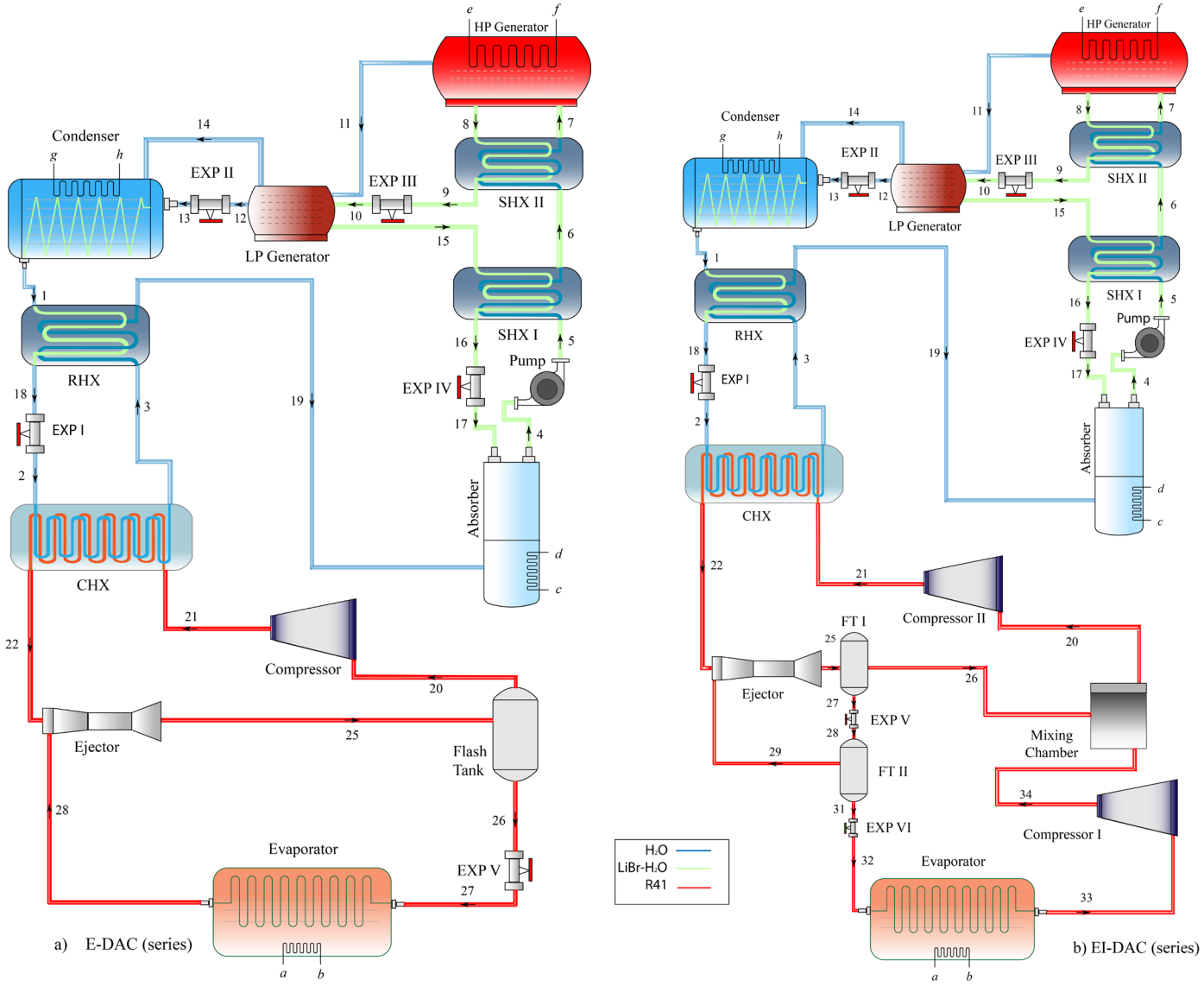

Fig. 2: Schematic illustration of the new systems a) Ejector-Double effect Cascade (E-DAC) and b) Ejector Injection-Double effect Cascade (EI-DAC) in series configuration

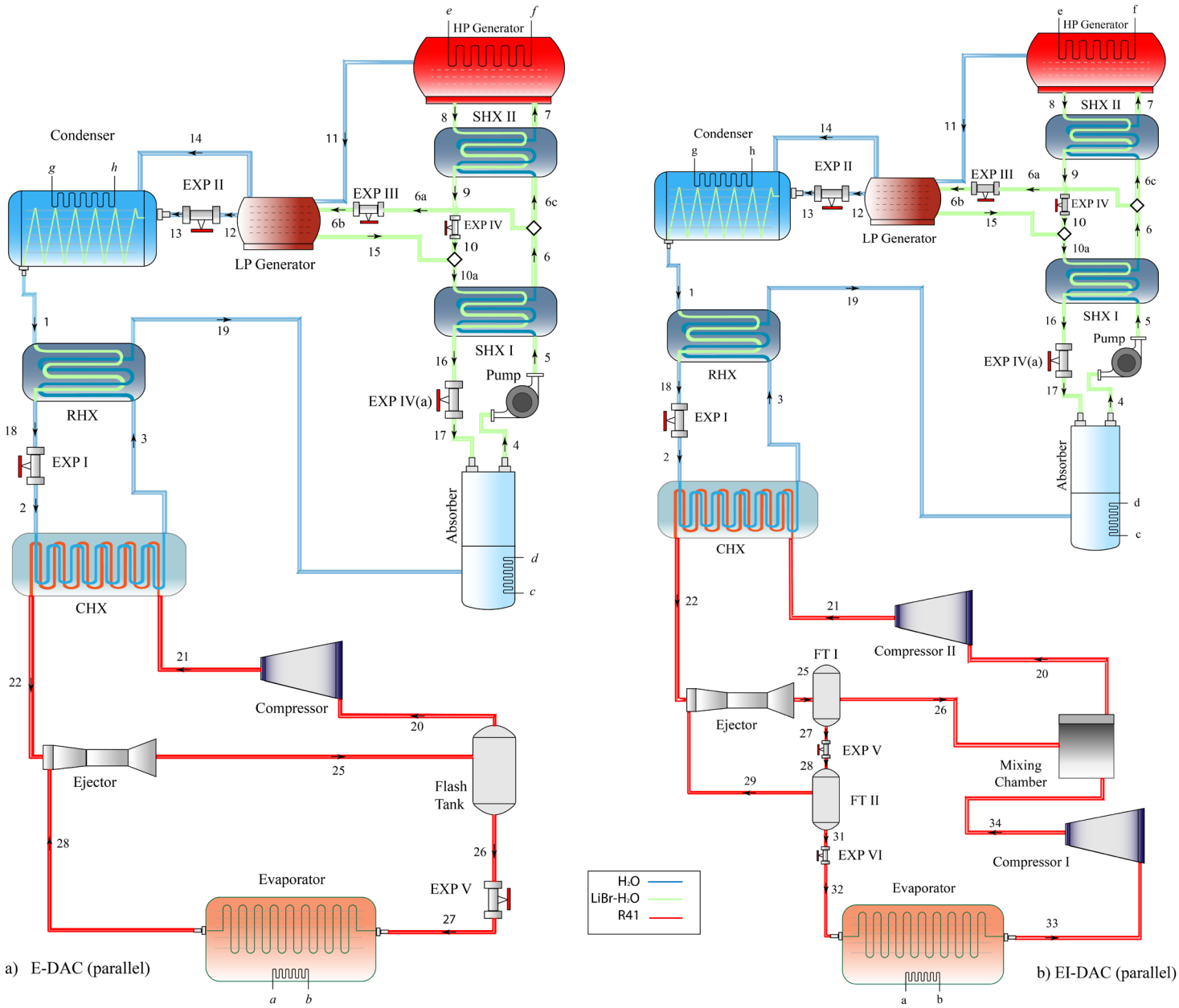

Fig. 3: Schematic illustration of the new systems a) Ejector-Double effect Cascade (E-DAC) and b) Ejector Injection-Double effect Cascade (EI-DAC) in parallel configuration

For the convenience of understanding the refrigerant and solution circulation of all the four novel systems, the P-h diagram along with solution temperature vs pressure diagram is shown in **Fig. 4(a)** and **Fig. 4(b).** The corresponding diagrams gives a vivid picture of the happenings inside the cycle. All the pressure lines are displayed with the point-to-point changes of the state of both refrigerant and the solution in the system.

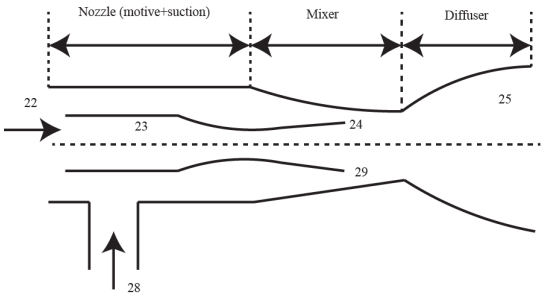

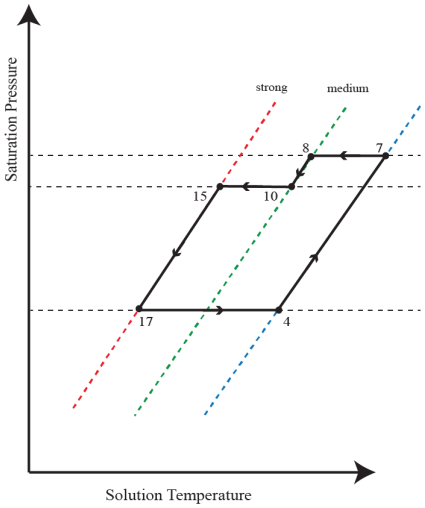

Series

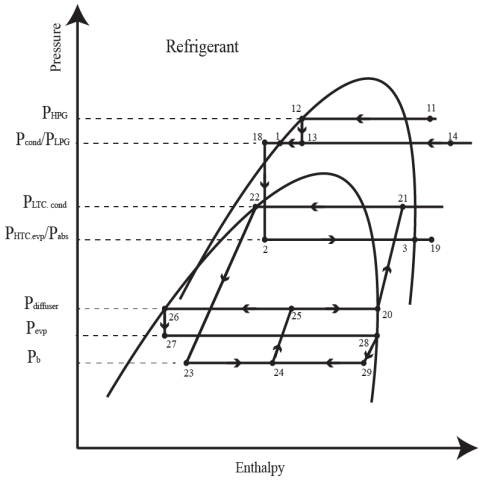

E-DAC

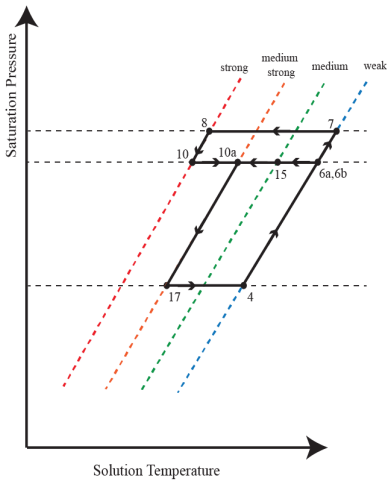

Parallel

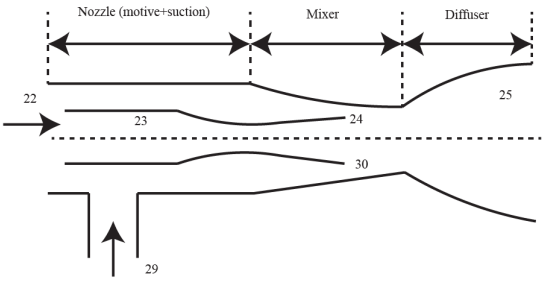

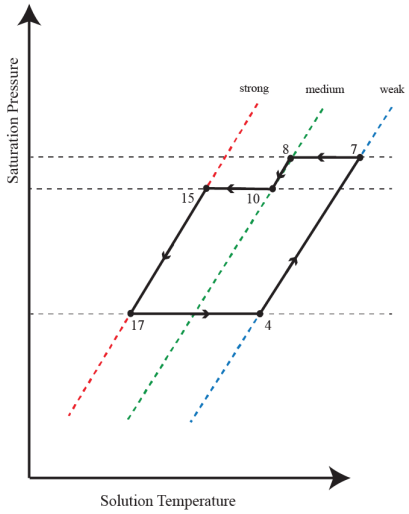

Series

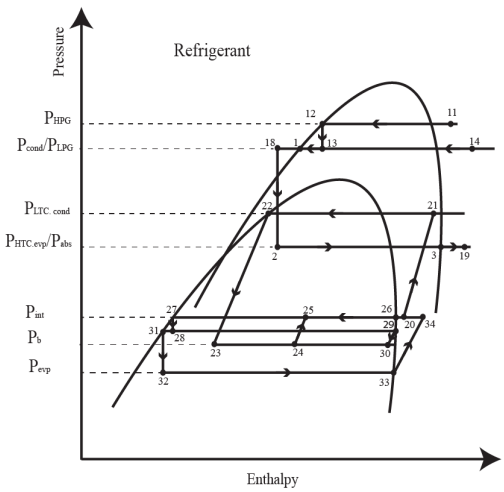

EI-DAC

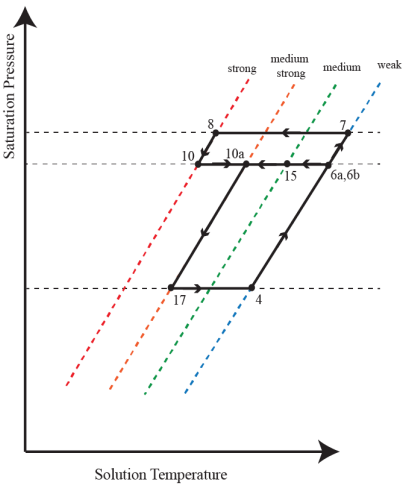

Parallel

Fig. 4: Proposed a) E-DAC and b) EI-DAC system's representation of pressure-enthalpy along with solution's pressure-temperature diagram

Chapter 4: Thermodynamic Modeling

4.1 Assumptions

In order to simplify the simulations, the following assumptions are made [[56][57], [58]]

- The simulation is performed under steady state condition
- The refrigerants at HTC (water) and LTC (R41) leaving the evaporators and condensers in saturated conditions.
- No heat transfer is considered with the environment other than stated.
- Pressure drops in the pipe and heat exchangers are negligible.
- Flow in the ejector is considered to be homogenous and One-dimensional.
- The vapor and the liquid leaving the flash tanks are in saturated conditions.
- The motive and suction steams reach the same pressure before mixing in the mixing chamber.
- Fluid properties are considered to remain constant over the entire cross-section following complete mixing at the output of the mixing chamber
- To include frictional losses in the ejector, nozzle, diffuser and mixing section efficiencies are taken into consideration.
- The solutions leaving the absorber, high-pressure generator and low-pressure generators are at an equilibrium state.
- A minimum temperature difference of 2.5 °C is maintained1 in the LPG, i.e., T_{12}-T_{14}=2.5K.

4.2 Energy Analysis

The principles of conservation dictate that mass, energy, and exergy balance equations can be used to analyze each component of the respective cycles. These equations allow for the calculation of various thermodynamic parameters at distinct state points, ultimately determining the performance of the cycle. In order to apply mass, energy, and exergy balance, it is possible to consider the components as a control volume.
Mass balance: Continuity equations can be used to analyze the flow of each component in the respective cycles. The mass balance equation is as follows:

$$\sum \dot{m}_i = \sum \dot{m}_e \tag{1}$$

For the solution concentration balance,

$$\sum \dot{m}_i X_i = \sum \dot{m}_e X_e \tag{2}$$

Where X is the mass fraction of the LiBr.

Energy Balance:

$$\sum \dot{m}_i \left(h_i + \frac{V_i^2}{2} + g z_i \right) + \dot{Q} = \sum \dot{m}_e \left(h_e + \frac{V_e^2}{2} + g z_e \right) + \dot{W} \tag{3}$$

Where, ṁ= The rate of mass transfer, Q̇=The rate of heat transfer, Ẇ=The rate of work transfer.

Disregarding the potential energy,

$$\sum \dot{m}_i h_i + \dot{Q} = \sum \dot{m}_e h_e + \dot{W} \tag{4}$$

From the definition of COP,

$$COP = \frac{Desired\ Output}{Work\ Input} \tag{5}$$

For the system COP,

$$COP_{system} = \frac{\dot{Q}_{evp}}{\dot{W}_{Compressor} + \dot{Q}_{HPG} + \dot{W}_{pump}} \tag{6}$$

$$COP_{LTC} = \frac{\dot{Q}_{evp}}{\dot{W}_{Compressor}}, COP_{HTC} = \frac{\dot{Q}_{CHX}}{\dot{Q}_{HPG} + \dot{W}_{pump}} \tag{7}$$

4.3 Exergy analysis

Exergy is a metric that quantifies the maximum amount of useful work that may be extracted from a system while it is in balance with its surroundings. The environment is considered as a dead state point.

The flow exergy equation can be defined as,

$$\dot{E}x = \dot{m}_r[(h - h_0) - T_0(s - s_0) + \frac{V^2}{2} + gz] \tag{8}$$

Disregarding the potential and kinetic energy, this equation can be written as,

$$\dot{E}x = \dot{m}_r\ [(h - h_0) - T_0(s - s_0)] \tag{9}$$

Exergy balance equation for control volume, [59]

$$\sum \dot{E}x_i + \dot{E}x_Q = \sum \dot{E}x_e + \dot{E}x_W + \dot{E}x_D \quad (10)$$

Here, $\dot{E}x_Q$ and $\dot{E}x_W$ represent exergy transfer by heat and work respectively. [59]

$$\dot{E}x_Q = \left(1 - \frac{T_0}{T_k}\right) \dot{Q}_k \quad (11)$$

$$\dot{E}x_W = \dot{W}_k \quad (12)$$

$\dot{E}x_D$ is the exergy destruction.

So, exergy destruction equation becomes for control volume,

$$\dot{E}x_D = \sum \dot{E}x_i - \sum \dot{E}x_o + \dot{E}x_W + \dot{E}x_Q \quad (13)$$

Exergy efficiency can be defined for a system, [59]

$$\eta_{exergy} = \frac{Exergy\ recovered}{Exergy\ expended} = 1 - \frac{Exergy\ destroyed}{Exergy\ expended} \quad (14)$$

Total exergy destruction can be calculated by,

$$\dot{E}x_{D\,.total} = \sum \dot{E}x_{D\,component} \quad (15)$$

Exergy efficiency can be written for the whole system, [60]

$$\eta_{exergy} = \frac{\dot{Q}_{evp} \times \left|1 - \frac{T_o}{T_{evp}}\right|}{\dot{Q}_{HPG} \times \left[1 - \frac{T_o}{T_{HPG}}\right] + \dot{W}_{comp} + \dot{W}_{pump}} \quad (16)$$

4.4 Ejector modeling

Ejector is one of the most fundamental components of our proposed system. Ejector basically has three sections, receiving section (suction and motive nozzle), mixing section and diffuser section, as shown in **Fig. 5**. From the comparative studies [12][52], constant area mixing ejectors are less efficient than the constant pressure mixing ejectors. The constant pressure mixing ejectors are selected for the numerical modeling and the assumptions are mentioned in ***4.1 Assumptions*** section.

By definition, entrainment ration can be defined as,

$$w = \frac{\dot{m}_{suction}}{\dot{m}_{motive}} \quad (17)$$

If ΔP is the pressure drop in suction nozzle, the back pressure at the suction outlet can be calculated by,

$$P_b = P_{suction} - \Delta P \tag{18}$$

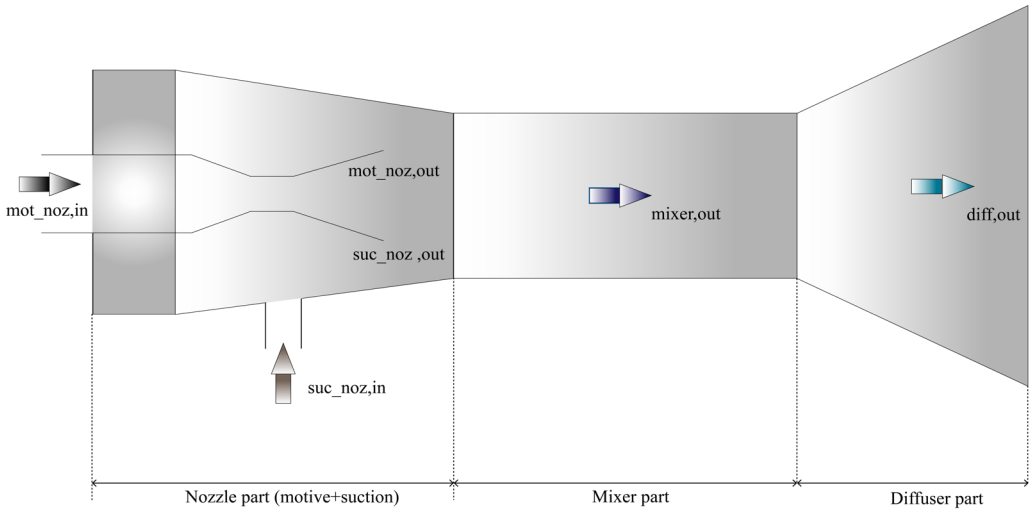

Fig. 5: Schematic illustration of ejector's working procedure

At the suction nozzle outlet (suc_noz, out):

Pressure,

$$p_{suc\_noz,out} = p_{suc\_noz,in} - \Delta p \tag{19}$$

Isentropic enthalpy,

$$h_{suc\_noz\,,out,s} = f\left(s_{suc\_noz\,,out,is}, P_{suc\_noz,out}\right) \tag{20}$$

Actual enthalpy,

$$h_{suc\_noz\,,out} = h_{suc\_noz\,,in} - \eta_{suc\_noz}(h_{suc\_noz\,,in} - h_{suc\_noz\,,out,s}) \tag{21}$$

Velocity,

$$v_{suc\_noz,out} = \sqrt{2(h_{suc\_noz\,,in} - h_{suc\_noz\,,out})} \tag{22}$$

Density,

$$\rho_{suc\_noz,out} = f(P_{suc\_noz,out}, h_{suc\_noz,out}) \tag{23}$$

Cross-sectional area,

$$A_{suc\_noz,out} = \frac{w}{v_{suc\_noz,out} * \rho_{suc\_noz,out}(1+w)} \tag{24}$$

At the outlet of motive nozzle,

Pressure,

$$p_{mot\_noz,out} = p_{mot\_noz,in} - \Delta p \tag{25}$$

Isentropic enthalpy,

$$h_{mot\_noz,out,s} = f\left(s_{mot\_noz,out,is}, P_{mot\_noz,out}\right) \tag{26}$$

Actual enthalpy,

$$h_{mot\_noz,out} = h_{mot\_noz,in} - \eta_{mot\_noz}(h_{mot\_noz,in} - h_{mot\_noz,out,s}) \tag{27}$$

Velocity,

$$v_{mot\_noz,out} = \sqrt{2(h_{mot\_noz,in} - h_{mot\_noz,out})} \tag{28}$$

Density,

$$\rho_{mot\_noz,out} = f(P_{mot\_noz,out}, h_{mot\_noz,out}) \tag{29}$$

Cross-sectional area,

$$A_{mot\_noz,out} = \frac{w}{v_{mot\_noz,out} * \rho_{mot\_noz,out}(1+w)} \tag{30}$$

At mixing section outlet,

Pressure,

$$p_{mixer} = p_{mot\_noz,out} = p_{suc\_noz,out} \tag{31}$$

Velocity,

$$v_{mixer,out} = \sqrt{\eta_{mixer}}\left(\frac{1}{1+w}\, c_{mot\_noz,out} + \frac{w}{1+w}\, c_{suc\_noz,out}\right) \tag{32}$$

Enthalpy,

$$h_{mixer,out} = \frac{1}{1+w}\left(h_{mot\_noz,out} + \frac{v^2_{mot\_noz,out}}{2}\right) + \frac{w}{1+w}\left(h_{suc\_noz,out} + \frac{v^2_{suc\_noz,out}}{2}\right) - \frac{v^2_{mixer,out}}{2} \tag{33}$$

Entropy,

$$s_{mixer,out} = s(p_{mixer}, h_{mixer,out}) \tag{34}$$

At diffuser outlet,

Actual enthalpy,

$$h_{diff,out} = h_{mixer,out} + \frac{v^2_{mixer,out}}{2} \tag{35}$$

Isentropic enthalpy,

$$h_{diff,out,s} = h_{mixer,out} + \eta_{diff}(h_{diff,out} - h_{mixer,out}) \tag{36}$$

Pressure,

$$P_{diff,out} = p(h_{diff,out,s}\ , s_{mixer,out}) \tag{37}$$

Quality,

$$x_{diff,out} = f(h_{diff,out,is}\ , P_{diff,out}) \tag{38}$$

The entrainment ratio for ejector injection modelling can be calculated by, [[61]]

$$w = \sqrt{\eta_{mot\_noz}\eta_{mixer}\eta_{diff}\ \frac{h_{mn\ ,in}\ - h_{mn\ ,out,is}}{h_{sn\ ,in}\ - h_{sn\ ,out,is}}} - 1 \tag{39}$$

4.5 Mathematical modeling

E-DAC(Series), E-DAC(Parallel), EI-DAC(Series) and EI-DAC(Parallel) have a subtle modified (HTC) Double effect absorption refrigeration cycle with RHX. The modified double effect absorption refrigeration cycle (Series configuration) has 13 components (absorber, solution pump, two solution heat exchangers, two solution expansion valves, HPG, LPG, two refrigerant expansion valves, one refrigerant heat exchanger and one cascade heat exchanger). Whereas the corresponding parallel configuration has 14 components with an additional solution expansion valve. For the parallel configuration, distribution ratio is defined as:

$$D = \frac{\dot{m}_{6c}}{\dot{m}_4} \tag{40}$$

And x_{17} can be calculated from,

$$\dot{x}_{17} = \frac{1}{\frac{D}{\dot{x}_8} + \frac{1-D}{\dot{x}_{15}}} \tag{41}$$

Similarly, for LTC with ejector has ejector in common for the proposed systems. E-DAC(Series) and E-DAC(Parallel) both have one compressor, one flash tank, one evaporator, one expansion valve, one evaporator and cascade heat exchanger. Whereas E-DAC(Series) and E-DAC(Parallel) have one additional flash tank, compressor, expansion valve and mixing chamber. The assumptions regarding the numerical modeling were mentioned in ***4.1 Assumptions***.

Table 3: Governing equations for modified double effect absorption refrigeration cycle series configuration (E-DAC(Series) and EI-DAC(Series))

Name of Components	**Equations of mass balance**	**Equations of energy balance**	**Exergy destruction equations**

Cascade heat exchanger	$\dot{m}_2$=$\dot{m}_3$ $\dot{m}_{21}$=$\dot{m}_{22}$	$\dot{Q}_{CHX}$ $= \dot{m}_{21}$ $\times (h_{21} - h_{22})$ $= \dot{m}_2 \times (h_3 - h_2)$	$\dot{E}_{D,CHX} = \dot{E}x_2 + \dot{E}x_{21} - \dot{E}x_3 - \dot{E}x_{22}$ $= \dot{m}_2((h_2 - h_3) - T_0(s_2 - s_3))$ $+ \dot{m}_{21}((h_{21} - h_{22})$ $- T_0 (s_{21} - s_{22}))$
Expansion valve I	$\dot{m}_{18}$=$\dot{m}_2$	$h_{18} = h_2$	$\dot{E}_{D,TV-I} = \dot{E}x_{18} - \dot{E}x_2$ $= \dot{m}_{18}((h_{18} - h_2) - T_0(s_{18} - s_2))$
Refrigerant heat exchanger	$\dot{m}_1$=$\dot{m}_{18}$ $\dot{m}_3$=$\dot{m}_{19}$	$\dot{Q}_{RHX}$ $= \dot{m}_1 \times (h_1 - h_{18})$ $= \dot{m}_3 \times (h_{19} - h_3)$	$\dot{E}_{D,RHX} = \dot{E}x_1 + \dot{E}x_3 - \dot{E}x_{18} - \dot{E}x_{19}$ $= \dot{m}_1\big((h_1 - h_{18}) - T_0(s_1 - s_{18}))$ $+ \dot{m}_3((h_3 - h_{19}) - T_0 (s_3$ $- s_{19})\big)$
Absorber	$\dot{m}_{19} + \dot{m}_{17}$ $= \dot{m}_4$	$\dot{Q}_{abs} = \dot{m}_{17} \times h_{17}$ $+\dot{m}_{19} \times h_{19} - \dot{m}_4$ $\times h_4$	$\dot{E}_{D,abs} = \dot{E}x_{19} + \dot{E}x_{17} - \dot{E}x_4 + (\dot{E}x_c - \dot{E}x_d)$ $= \dot{m}_{19}((h_{19} - h_0) - T_0(s_{19} - s_0))$ $+ \dot{m}_{17}((h_{17} - h_0) - T_0(s_{17}$ $- s_0))$ $- \dot{m}_4((h_4 - h_0) - T_0(s_4$ $- s_0))$ $+ \dot{m}_c((h_c - h_d) - T_0 (s_c$ $- s_d))$
Solution Pump	$\dot{m}_4 = \dot{m}_5$	$\dot{W}_{pump}$ $= \dot{m}_4 \times \frac{h_{5s} - h_4}{\eta_s}$	$\dot{E}_{D,Pump} = \dot{E}x_4 - \dot{E}x_5$ $= \dot{m}_4((h_4 - h_5) - T_0(s_4$ $- s_5))$
SHX-I	$\dot{m}_5 = \dot{m}_6$ $\dot{m}_{15} = \dot{m}_{16}$	$\dot{Q}_{SHX-I} = \dot{m}_5 \times (h_6$ $- h_5)$ $= \dot{m}_{15}$ $\times (h_{15} - h_{16})$	$\dot{E}_{D,SHX-I} = \dot{E}x_5 + \dot{E}x_{15} - \dot{E}x_6 - \dot{E}x_{16}$ $= \dot{m}_5((h_5 - h_6) - T_0(s_5 - s_6))$ $+ \dot{m}_{15}((h_{15} - h_{16}) - T_0 (s_{15}$ $- s_{16}))$
SHX-II	$\dot{m}_6 = \dot{m}_7$ $\dot{m}_8 = \dot{m}_9$	$\dot{Q}_{SHX-II} = \dot{m}_6$ $\times (h_7$ $- h_6)$ $= \dot{m}_8 \times (h_8 - h_9)$	$\dot{E}_{D,SHX-II} = \dot{E}x_6 + \dot{E}x_8 - \dot{E}x_7 - \dot{E}x_9$ $= \dot{m}_6((h_6 - h_7) - T_0(s_6 - s_7))$ $+ \dot{m}_8((h_8 - h_9) - T_0 (s_8$ $- s_9))$
HPG	$\dot{m}_7$ $= \dot{m}_8 + \dot{m}_{11}$	$\dot{Q}_{HPG} = \dot{m}_8 \times h_8$ $+\dot{m}_{11} \times h_{11} - \dot{m}_7$ $\times h_7$	$\dot{E}_{D,HPG} = \dot{E}x_7 - \dot{E}x_8 - \dot{E}x_{11} + \big(\dot{E}x_e - \dot{E}x_f\big)$

			$= \dot{m}_7((h_7 - h_0) - T_0(s_7 - s_0)) - \dot{m}_8((h_8 - h_0) - T_0(s_8 - s_0)) - \dot{m}_{11}((h_{11} - h_0) - T_0(s_{11} - s_0)) + \dot{m}_e\big((h_e - h_f) - T_0\,(s_e - s_f)\big)$
Expansion valve III	$\dot{m}_9 = \dot{m}_{10}$	$h_9 = h_{10}$	$\dot{E}_{D,TV-III} = \dot{E}x_9 - \dot{E}x_{10} = \dot{m}_9((h_9 - h_{10}) - T_0(s_9 - s_{10}))$
LPG	$\dot{m}_{10} + \dot{m}_{11} = \dot{m}_{12} + \dot{m}_{14} + \dot{m}_{15}$	$\dot{Q}_{LPG} = \dot{m}_{12} \times h_{12} + \dot{m}_{14} \times h_{14} + \dot{m}_{15} \times h_{15} - \dot{m}_{10} \times h_{10} - \dot{m}_{11} \times h_{11}$	$\dot{E}_{D,LPG} = \dot{E}x_{10} + \dot{E}x_{11} - \dot{E}x_{12} - \dot{E}x_{14} - \dot{E}x_{15} = \dot{m}_{10}((h_{10} - h_0) - T_0(s_{10} - s_0)) + \dot{m}_{11}((h_{11} - h_0) - T_0(s_{11} - s_0)) - \dot{m}_{12}((h_{12} - h_0) - T_0(s_{12} - s_0)) - \dot{m}_{14}((h_{14} - h_0) - T_0(s_{14} - s_0)) - \dot{m}_{15}((h_{15} - h_0) - T_0\,(s_{15} - s_0))$
Expansion valve II	$\dot{m}_{12} = \dot{m}_{13}$	$h_{12} = h_{13}$	$\dot{E}_{D,TV-II} = \dot{E}x_{12} - \dot{E}x_{13} = \dot{m}_{12}((h_{12} - h_{13}) - T_0(s_{12} - s_{13}))$
Expansion valve IV	$\dot{m}_{16} = \dot{m}_{17}$	$h_{16} = h_{17}$	$\dot{E}_{D,TV-IV} = \dot{E}x_{16} - \dot{E}x_{17} = \dot{m}_{16}((h_{16} - h_{17}) - T_0(s_{16} - s_{17}))$
Condenser	$\dot{m}_1 = \dot{m}_{13} + \dot{m}_{14}$	$\dot{Q}_{cond} = \dot{m}_{13} \times h_{13} + \dot{m}_{14} \times h_{14} - \dot{m}_1 \times h_1$	$\dot{E}_{D,cond} = \dot{E}x_{13} + \dot{E}x_{14} - \dot{E}x_{11} + \big(\dot{E}x_g - \dot{E}x_h\big) = \dot{m}_{13}((h_{13} - h_0) - T_0(s_{13} - s_0)) + \dot{m}_{14}((h_{14} - h_0) - T_0(s_{14} - s_0)) - \dot{m}_1((h_1 - h_0) - T_0(s_1 - s_0)) + \dot{m}_g\big((h_g - h_h) - T_0\,(s_g - s_h)\big)$

Table 4: Governing equations for modified double effect absorption refrigeration cycle

parallel configuration (E-DAC(Parallel) and EI-DAC(Parallel))

Name of Components	**Equations of mass balance**	**Equations of energy balance**	**Exergy destruction equations**
Cascade heat exchanger	$\dot{m}_2=\dot{m}_3$ $\dot{m}_{21}=\dot{m}_{22}$	$\dot{Q}_{CHX} = \dot{m}_{21} \times (h_{21} - h_{22}) = \dot{m}_2 \times (h_3 - h_2)$	$\dot{E}_{D,CHX} = \dot{E}x_2 + \dot{E}x_{21} - \dot{E}x_3 - \dot{E}x_{22} = \dot{m}_2((h_2 - h_3) - T_0(s_2 - s_3)) + \dot{m}_{21}((h_{21} - h_{22}) - T_0(s_{21} - s_{22}))$
Expansion valve I	$\dot{m}_{18}=\dot{m}_2$	$h_{18} = h_2$	$\dot{E}_{D,TV-I} = \dot{E}x_{18} - \dot{E}x_2 = \dot{m}_{18}((h_{18} - h_2) - T_0(s_{18} - s_2))$
Refrigerant heat exchanger	$\dot{m}_1=\dot{m}_{18}$ $\dot{m}_3=\dot{m}_{19}$	$\dot{Q}_{RHX} = \dot{m}_1 \times (h_1 - h_{18}) = \dot{m}_3 \times (h_{19} - h_3)$	$\dot{E}_{D,RHX} = \dot{E}x_1 + \dot{E}x_3 - \dot{E}x_{18} - \dot{E}x_{19} = \dot{m}_1\big((h_1 - h_{18}) - T_0(s_1 - s_{18})\big) + \dot{m}_3((h_3 - h_{19}) - T_0(s_3 - s_{19}))$
Absorber	$\dot{m}_{19} + \dot{m}_{17} = \dot{m}_4$	$\dot{Q}_{abs} = \dot{m}_{17} \times h_{17} + \dot{m}_{19} \times h_{19} - \dot{m}_4 \times h_4$	$\dot{E}_{D,abs} = \dot{E}x_{19} + \dot{E}x_{17} - \dot{E}x_4 + (\dot{E}x_c - \dot{E}x_d) = \dot{m}_{19}((h_{19} - h_0) - T_0(s_{19} - s_0)) + \dot{m}_{17}((h_{17} - h_0) - T_0(s_{17} - s_0)) - \dot{m}_4((h_4 - h_0) - T_0(s_4 - s_0)) + \dot{m}_c((h_c - h_d) - T_0(s_c - s_d))$
Solution Pump	$\dot{m}_4 = \dot{m}_5$	$\dot{W}_{pump} = \dot{m}_4 \times \frac{h_{5s} - h_4}{\eta_s}$	$\dot{E}_{D,Pump} = \dot{E}x_4 - \dot{E}x_5 = \dot{m}_4((h_4 - h_5) - T_0(s_4 - s_5))$
SHX-I	$\dot{m}_5 = \dot{m}_6$ $\dot{m}_{10a} = \dot{m}_{16}$	$\dot{Q}_{SHX-I} = \dot{m}_5 \times (h_6 - h_5) = \dot{m}_{15} \times (h_{15} - h_{16})$	$\dot{E}_{D,SHX-I} = \dot{E}x_5 + \dot{E}x_{10a} - \dot{E}x_6 - \dot{E}x_{16} = \dot{m}_5((h_5 - h_6) - T_0(s_5 - s_6)) + \dot{m}_{10a}((h_{10a} - h_{16}) - T_0(s_{10a} - s_{16}))$
SHX-II	$\dot{m}_{6c} = \dot{m}_7$ $\dot{m}_8 = \dot{m}_9$	$\dot{Q}_{SHX-II} = \dot{m}_{6c} \times (h_7 - h_6) = \dot{m}_8 \times (h_8 - h_9)$	$\dot{E}_{D,SHX-II} = \dot{E}x_{6c} + \dot{E}x_8 - \dot{E}x_7 - \dot{E}x_9 = \dot{m}_{6c}((h_{6c} - h_7) - T_0(s_{6c} - s_7)) + \dot{m}_8((h_8 - h_9) - T_0(s_8 - s_9))$

HPG	$\dot{m}_7 = \dot{m}_8 + \dot{m}_{11}$	$\dot{Q}_{HPG} = \dot{m}_8 \times h_8 + \dot{m}_{11} \times h_{11} - \dot{m}_7 \times h_7$	$\dot{E}_{D,HPG} = \dot{E}x_7 - \dot{E}x_8 - \dot{E}x_{11} + (\dot{E}x_e - \dot{E}x_f) = \dot{m}_7((h_7 - h_0) - T_0(s_7 - s_0)) - \dot{m}_8((h_8 - h_0) - T_0(s_8 - s_0)) - \dot{m}_{11}((h_{11} - h_0) - T_0(s_{11} - s_0)) + \dot{m}_e((h_e - h_f) - T_0(s_e - s_f))$
Expansion valve III	$\dot{m}_{6a}=\dot{m}_{6b}$	$h_{6a} = h_{6b}$	$\dot{E}_{D,TV-III} = \dot{E}x_{6a} - \dot{E}x_{6b} = \dot{m}_{6a}((h_{6a} - h_{6b}) - T_0(s_{6a} - s_{6b}))$
LPG	$\dot{m}_{6b} + \dot{m}_{11} = \dot{m}_{12} + \dot{m}_{14} + \dot{m}_{15}$	$\dot{Q}_{LPG} = \dot{m}_{12} \times h_{12} + \dot{m}_{14} \times h_{14} + \dot{m}_{15} \times h_{15} - \dot{m}_{6b} \times h_{6b} - \dot{m}_{11} \times h_{11}$	$\dot{E}_{D,LPG} = \dot{E}x_{6b} + \dot{E}x_{11} - \dot{E}x_{12} - \dot{E}x_{14} - \dot{E}x_{15} = \dot{m}_{6b}((h_{6b} - h_0) - T_0(s_{6b} - s_0)) + \dot{m}_{11}((h_{11} - h_0) - T_0(s_{11} - s_0)) - \dot{m}_{12}((h_{12} - h_0) - T_0(s_{12} - s_0)) - \dot{m}_{14}((h_{14} - h_0) - T_0(s_{14} - s_0)) - \dot{m}_{15}((h_{15} - h_0) - T_0(s_{15} - s_0))$
Expansion valve II	$\dot{m}_{12}=\dot{m}_{13}$	$h_{12} = h_{13}$	$\dot{E}_{D,TV-II} = \dot{E}x_{12} - \dot{E}x_{13} = \dot{m}_{12}((h_{12} - h_{13}) - T_0(s_{12} - s_{13}))$
Expansion valve IV	$\dot{m}_9=\dot{m}_{10}$	$h_9 = h_{10}$	$\dot{E}_{D,TV-IV} = \dot{E}x_9 - \dot{E}x_{10} = \dot{m}_9((h_9 - h_{10}) - T_0(s_9 - s_{10}))$
Expansion valve IV(a)	$\dot{m}_{16}=\dot{m}_{17}$	$h_{16} = h_{17}$	$\dot{E}_{D,TV-IV(a)} = \dot{E}x_{16} - \dot{E}x_{17} = \dot{m}_{16}((h_{16} - h_{17}) - T_0(s_{16} - s_{17}))$
Condenser	$\dot{m}_1=\dot{m}_{13} + \dot{m}_{14}$	$\dot{Q}_{cond} = \dot{m}_{13} \times h_{13} + \dot{m}_{14} \times h_{14} - \dot{m}_1 \times h_1$	$\dot{E}_{D,cond} = \dot{E}x_{13} + \dot{E}x_{14} - \dot{E}x_{11} + (\dot{E}x_g - \dot{E}x_h)$

			$= \dot{m}_{13}((h_{13} - h_0) - T_0(s_{13} - s_0)) + \dot{m}_{14}((h_{14} - h_0) - T_0(s_{14} - s_0)) - \dot{m}_1((h_1 - h_0) - T_0(s_1 - s_0)) + \dot{m}_g((h_g - h_h) - T_0(s_g - s_h))$

Table 5: Governing equations for ejector expansion VCR cycle (E-DAC(Series) and E-DAC(Parallel))

Component	**Mass balance equations**	**Energy balance equations**	**Exergy destruction equations**
Evaporator	$\dot{m}_{27}=\dot{m}_{28}$	$\dot{Q}_{evp} = \dot{m}_{27} \times (h_{28} - h_{27})$	$\dot{E}_{D,Evp} = \dot{E}x_{27} - \dot{E}x_{28} + (\dot{E}x_a - \dot{E}x_b) = \dot{m}_{27}((h_{27} - h_{28}) - T_0(s_{27} - s_{28})) + \dot{m}_a((h_a - h_b) - T_0(s_a - s_b))$
Ejector	$\dot{m}_{22} + \dot{m}_{28} = \dot{m}_{25} = \dot{m}_{24}$		$\dot{E}_{D,ejector} = \dot{E}x_{22} + \dot{E}x_{28} - \dot{E}x_{25} = \dot{m}_{22}((h_{22} - h_0) - T_0(s_{22} - s_0)) + \dot{m}_{28}((h_{28} - h_0) - T_0(s_{28} - s_0)) - \dot{m}_{25}((h_{25} - h_0) - T_0(s_{25} - s_0))$
Flash Tank	$\dot{m}_{20} + \dot{m}_{26} = \dot{m}_{25}$ $\dot{m}_{26}=\dot{m}_{25}(1 - x_{25})$ $\dot{m}_{20}= \dot{m}_{25}\, x_{25}$	$\dot{m}_{25}\, h_{25} = \dot{m}_{20}\, h_{20} + \dot{m}_{26}\, h_{26}$	$\dot{E}_{D,FT} = \dot{E}x_{25} - \dot{E}x_{20} - \dot{E}x_{26} = \dot{m}_{25}((h_{25} - h_0) - T_0(s_{25} - s_0)) - \dot{m}_{20}((h_{20} - h_0) - T_0(s_{20} - s_0)) - \dot{m}_{26}((h_{26} - h_0) - T_0(s_{26} - s_0))$
Expansion valve V	$\dot{m}_{26}=\dot{m}_{27}$	$h_{26} = h_{27}$	$\dot{E}_{D,TV-\mathrm{V}} = \dot{E}x_{26} - \dot{E}x_{27} = \dot{m}_{26}((h_{26} - h_{27}) - T_0(s_{26} - s_{27}))$

Compressor	$\dot{m}_{20} = \dot{m}_{21}$	$\dot{W}_{comp} = \dot{m}_{20} \times \frac{h_{21s} - h_{20}}{\eta_s}$	$\dot{E}_{D,comp} = \dot{E}x_{20} - \dot{E}x_{21} = \dot{m}_1((h_{20} - h_{21}) - T_0(s_{20} - s_{20})$

Table 6: Governing equations for ejector expansion VCR cycle (EI-DAC(Series) and EI-DAC(Parallel))

Component	**Mass balance equations**	**Energy balance equations**	**Exergy destruction equations**
Evaporator	$\dot{m}_{32}=\dot{m}_{33}$	$\dot{Q}_{evp} = \dot{m}_{32} \times (h_{33} - h_{32})$	$\dot{E}_{D,evp} = \dot{E}x_{32} - \dot{E}x_{33} + (\dot{E}x_a - \dot{E}x_b) = \dot{m}_{32}((h_{32} - h_{33}) - T_0(s_{32} - s_{33}) + \dot{m}_a((h_a - h_b) - T_0 (s_a - s_b))$
Ejector	$\dot{m}_{22} + \dot{m}_{29} = \dot{m}_{25}$ $\dot{m}_{24} = \dot{m}_{25}$		$\dot{E}_{D,ejector} = \dot{E}x_{22} + \dot{E}x_{29} - \dot{E}x_{25} = \dot{m}_{22}((h_{22} - h_0) - T_0(s_{22} - s_0)) + \dot{m}_{29}((h_{29} - h_0) - T_0(s_{29} - s_0)) - \dot{m}_{25}((h_{25} - h_0) - T_0(s_{25} - s_0))$
Flash Tank I	$\dot{m}_{26} + \dot{m}_{27} = \dot{m}_{25}$ $\dot{m}_{27}=\dot{m}_{25} (1 - x_{25})$ $\dot{m}_{26}= \dot{m}_{25} x_{25}$	$\dot{m}_{25} h_{25} = \dot{m}_{26} h_{26} + \dot{m}_{27} h_{27}$	$\dot{E}_{D,FT-I} = \dot{E}x_{25} - \dot{E}x_{26} - \dot{E}x_{27} = \dot{m}_{25}((h_{25} - h_0) - T_0(s_{25} - s_0)) - \dot{m}_{26}((h_{26} - h_0) - T_0(s_{26} - s_0)) - \dot{m}_{27}((h_{27} - h_0) - T_0(s_{27} - s_0))$
Flash Tank II	$\dot{m}_{29} + \dot{m}_{31} = \dot{m}_{28}$	$\dot{m}_{28} h_{28} = \dot{m}_{29} h_{29} + \dot{m}_{31} h_{31}$	$\dot{E}_{D,FT-II} = \dot{E}x_{28} - \dot{E}x_{29} - \dot{E}x_{31} = \dot{m}_{28}((h_{28} - h_0) - T_0(s_{28} - s_0)) - \dot{m}_{29}((h_{29} - h_0) - T_0(s_{29} - s_0)) - \dot{m}_{31}((h_{31} - h_0) - T_0(s_{31} - s_0))$
Expansion valve V	$\dot{m}_{27}=\dot{m}_{28}$	$h_{27} = h_{28}$	$\dot{E}_{D,TV-V} = \dot{E}x_{27} - \dot{E}x_{28} = \dot{m}_{27}((h_{27} - h_{28}) - T_0(s_{27} - s_{28})$
Expansion valve VI	$\dot{m}_{31}=\dot{m}_{32}$	$h_{31} = h_{32}$	$\dot{E}_{D,TV-VI} = \dot{E}x_{31} - \dot{E}x_{32} = \dot{m}_{31}((h_{31} - h_{32}) - T_0(s_{31} - s_{32})$

Compressor I	$\dot{m}_{33} = \dot{m}_{34}$	$\dot{W}_{comp-I} = \dot{m}_{33} \times \frac{h_{34s} - h_{33}}{\eta_s}$	$\dot{E}_{D,comp-I} = \dot{E}x_{33} - \dot{E}x_{34} = \dot{m}_{33}((h_{33} - h_{34}) - T_0(s_{33} - s_{34})$
Compressor II	$\dot{m}_{20} = \dot{m}_{21}$	$\dot{W}_{comp-II} = \dot{m}_{20} \times \frac{h_{21s} - h_{20}}{\eta_s}$	$\dot{E}_{D,comp-II} = \dot{E}x_{20} - \dot{E}x_{21} = \dot{m}_{20}((h_{20} - h_{21}) - T_0(s_{20} - s_{21})$
Mixing chamber	$\dot{m}_{26} + \dot{m}_{34} = \dot{m}_{20}$	$\dot{m}_{26}\, h_{26} + \dot{m}_{34}\, h_{34} = \dot{m}_{20}\, h_{20}$	$\dot{E}_{D,mixing\ chamber} = \dot{E}x_{26} + \dot{E}x_{34} - \dot{E}x_{20} = \dot{m}_{26}\big((h_{26} - h_{0)} - T_0(s_{26} - s_0)\big) + \dot{m}_{34}\big((h_{34} - h_{0)} - T_0(s_{34} - s_0)\big) - \dot{m}_{20}\big((h_{20} - h_{0)} - T_0(s_{20} - s_0)\big)$

4.6 Fixed Parameters and System flow-chart

A mathematical model has been developed in EES by integrating mass, energy, and exergy balance equations described in section *4.2 Energy Analysis4.3 Exergy analysis*. analysis refers to the study and evaluation of the efficiency and potential of a system or process in terms of its ability to perform useful work *4.4 Ejector modeling 4.5 Mathematical modeling*. The characteristics of both the refrigerant and solutions are gathered from EES's integrated library. The simulation begins by initializing with a predetermined set of operating settings specified in Table 7.

Table 7: Fixed data used in the simulation [57][56]

Parameters	**Values**
Evaporator temperature, T_{evp}	-30 ℃
Evaporator temperature of HTC, T_{evpHTC}	4 ℃
Absorber temperature, T_{abs}	35 ℃
Condenser temperature, T_{cond}	35 ℃
High pressure generator temperature, T_{HPG}	130 ℃
Load of the Refrigeration, Q_{evp}	300 kW
Temperature of the ambient, T_0	25 ℃

Pressure of the ambient, P_0	101.325 kPa
SHX effectiveness (solution heat exchanger), ε_{SHX}	0.7
Difference in cascade temperature, ΔT	5
RHX effectiveness (refrigerant heat exchanger), ε_{RHX}	0.7
Temperature of the outside air entering the Evaporator	T_{evp} + 8
Temperature of the outside air leaving the Evaporator	T_{evp} + 3
Temperature of the cooling water entering the Absorber	T_{Abs} - 8
Temperature of the cooling water leaving the Absorber	T_{Abs} -3
Temperature of the heat source water entering the HPG	T_{HPG} + 18
Temperature of the heat source water leaving the HPG	T_{HPG} + 8
Temperature of the cooling water entering the Condenser	T_{Cond} - 8
Temperature of the cooling water leaving the Condenser	T_{Cond} - 3
Efficiency of the Diffuser, η_{diff}	0.85
Efficiency of the Nozzle, η_n	0.85
Efficiency of the Compressor, η_{comp}	0.95
Efficiency of the Mixer, η_{mixer}	0.95

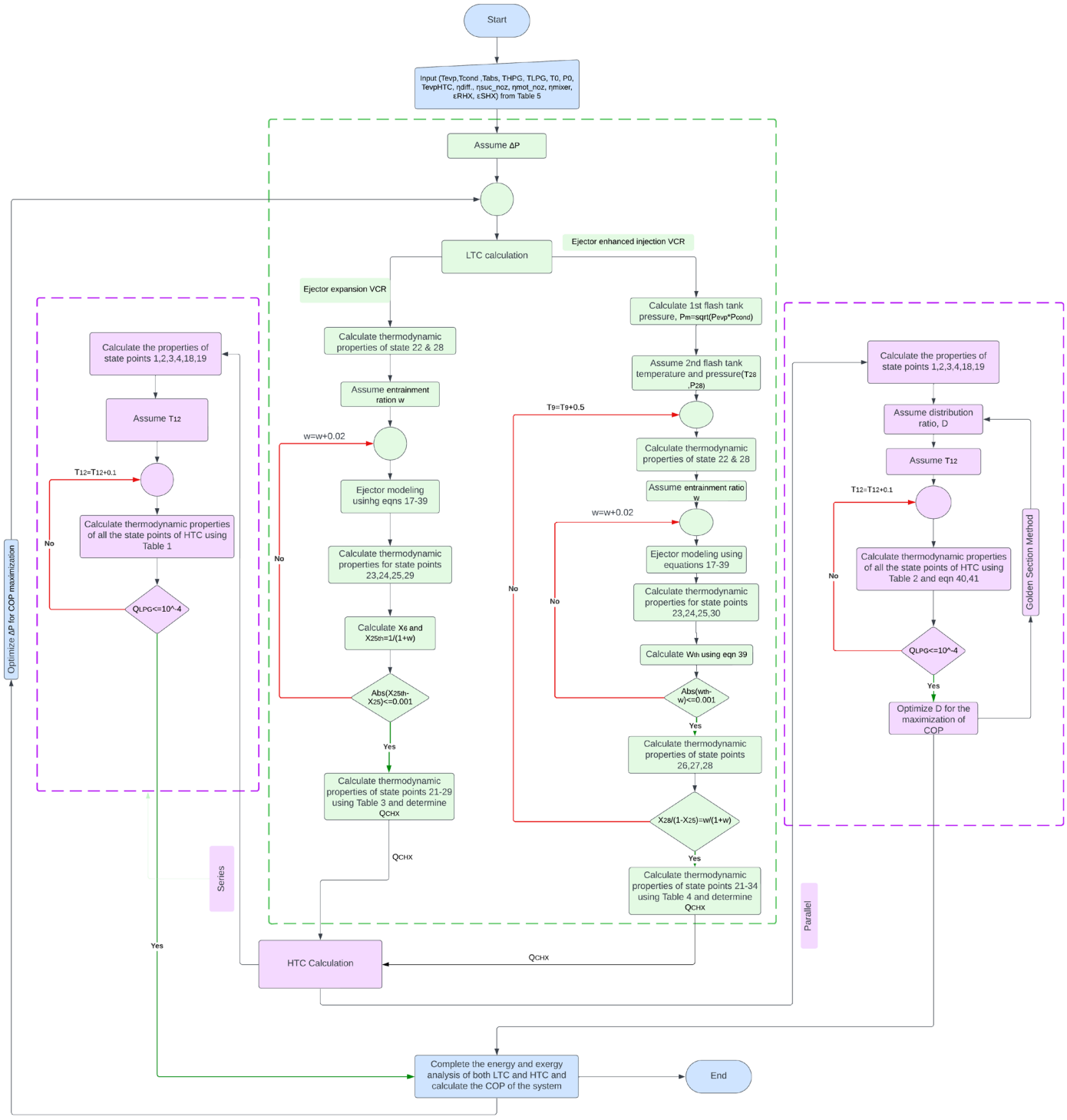

Fig. 6: Flow chart with the numerical framework illustrating the modelling of the proposed system ((E-DAC (series and parallel) and EI-DAC (series and parallel))

Chapter 5: Model Validation

As our proposed systems are novel in nature, these cannot be validated against any other existing papers. However, as our systems are cascaded with the conventional refrigeration cycles, the conventional stand-alone cycles can be validated with the existing works. In our approach to validation, double effect absorption refrigeration cycle (series and parallel), ejector expansion VCR cycle and ejector injection VCR cycle will be validated against the existing works.

Double effect Absorption Refrigeration cycle (series configuration) has been validated against Gomri et al. [57]. The parametric validation of the different components is shown in ***Table 8***. The fixed parameters for the Table 8 are $T_{cond}=T_{abs}=35°C$, $T_{evp}=4°C$, $T_{HPG}=130°C$, $\varepsilon_I=\varepsilon_{II}=0.7$, $\eta_{pump}=0.95$

Table 8: Table for the validation of double effect absorption refrigeration cycle (Series)

Parameters	**LiBr-H_2O**		**Relative Difference (%)**
	Present Work	**Ref (Gomri)**	
High-Pressure Generator, $\dot{Q}_{HPG}$(kW)	245	252.407	2.934
Condenser Load, $\dot{Q}_{cond}$(kW)	168.4	167.205	0.714
Evaporator Load, $\dot{Q}_{evp}$(kW)	300	300	0
Absorber Load, $\dot{Q}$abs(kW)	384.7	385.236	0.139
Pump Input, $\dot{W}_{pump}$(kW)	0.05754	0	0
COP	1.225	1.189	3.027

In Table 8**,** it can be seen that the errors are approximately below 3% for the different. Error occurred due to using different libraries for numerical simulation. FORTAN program was used for our reference study where different empirical equations were used for the calculation of different state points for LiBr-H2O solution. For our case, EES integrated library is used for LiBr-H2O solution.

Table 9: Validation for double effect absorption refrigeration cycle (Parallel)

Parameters	**LiBr-H_2O**		**Relative Difference (%)**
	Present	**Ref**	

	Work	(Bagheri)	
High-Pressure Generator, $\dot{Q}_{HPG}$(kW)	259.7	265.5	2.18
Condenser Load, $\dot{Q}_{cond}$(kW)	144.9	145.3	0.28
Evaporator Load, $\dot{Q}_{evp}$(kW)	300	300	0
Absorber Load, $\dot{Q}$abs(kW)	414.7	420.3	1.3
Pump Input, $\dot{W}_{pump}$(kW)	0.1156	0.1162	0.005
COP	1.155	1.129	2.3

Parametric validation for different components of double effect absorption cycle (DAC) parallel configuration has been shown in **Table 9**. The fixed parameters for Table 9 are T_{cond}=T_{abs}=35°C, T_{evp}=4°C, T_{HPG}=134°C, ε_I= ε_{II}=0.7, η_{pump}=0.95. There is a subtle deviation between the present work and reference work of Bagheri et al.[58]. There error is almost close to 2% which can be neglected in numerical simulations.

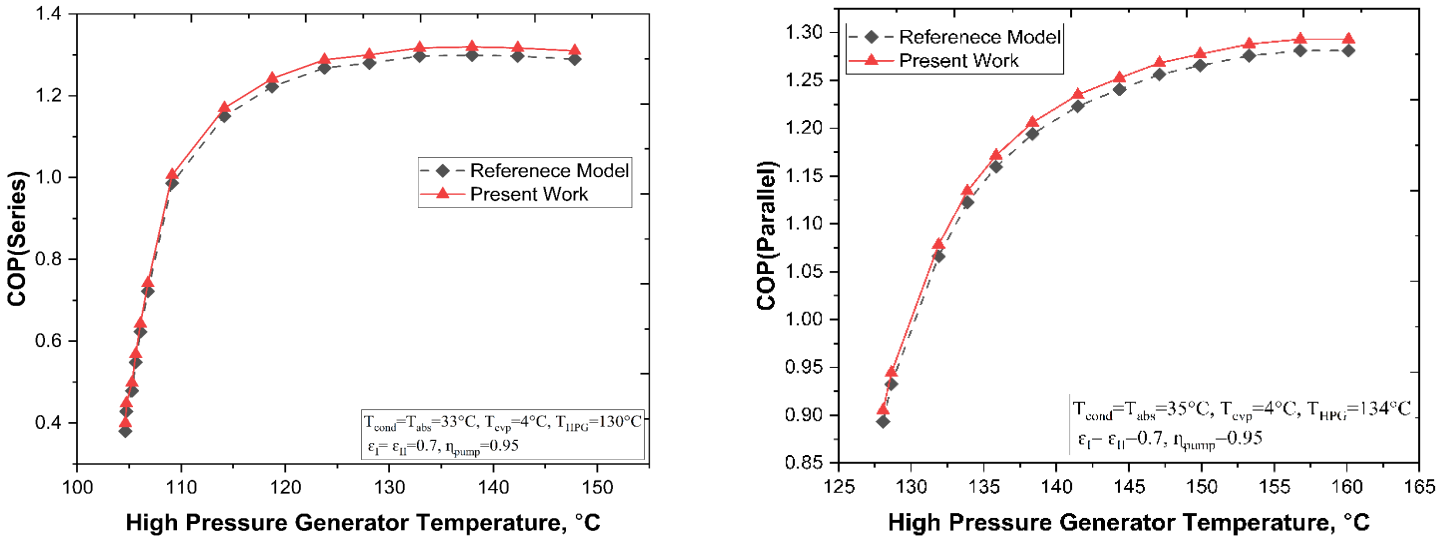

(a) (b)

Fig. 7: Validation for Double Effect Absorption Cycle (DAC) a) series and b) parallel

Fig. 7 show the graphical validation for DAC series and parallel configuration respectively. It is basically the comparisons of COP between the present work and reference study. The comparisons show that the refrigeration cycle is modeled with high accuracy irrespective of subtle deviations between the two works in each configuration due to using thermodynamic

library packages and softwares.

According to the study conducted by Li et al. [62], **Fig. 8** illustrates the validation of the Ejector expansion VCR cycle using R1234yf as the working fluid. The operational parameters for this comparison are as follows: T_{cond} = 50 °C, T_{evap} = 5 °C, $\eta_{mn} = \eta_{sn} = \eta_d = 0.85$, and $\eta_{ms} = 0.95$. The presented representation demonstrates a high level of accuracy in the modeling of the ejector-enhanced compression refrigeration cycle.

Validation of the injector improved vapor injection refrigeration system was done according to the research by Wang et al. [61], with R22, R290, and R32 used as coolants. In **Fig. 9**, the coefficient of performance (COP) between the standard model and the current model is shown next to each other. For this study, the following settings were used: It's 50 °C outside, 5 to -35 °C inside, $\Delta T_{sub\text{-}cool}$ = 5 °C, the tip is 0.9 °C, the mixer is 0.85 °C, the diffuser is 0.8 °C, and the s is 0.75 °C. During the confirmation process, the biggest mistake that was seen was less than 1%. Researchers have found that using different thermodynamic library packages is what is causing the error.

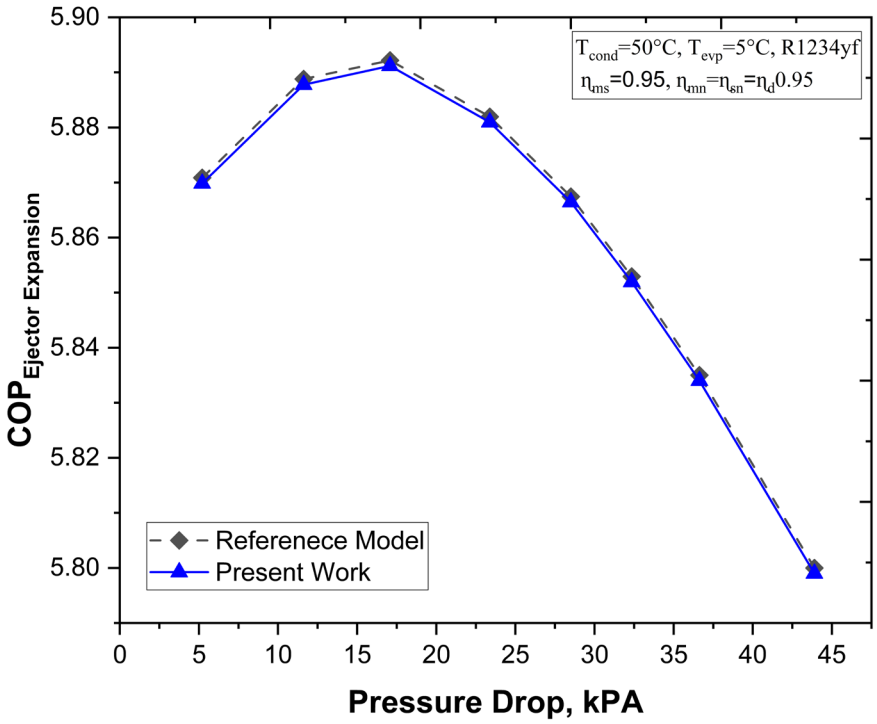

Fig. 8: Validation and evaluation of the ejector refrigeration cycle utilized in the ECAC with regard to [62]

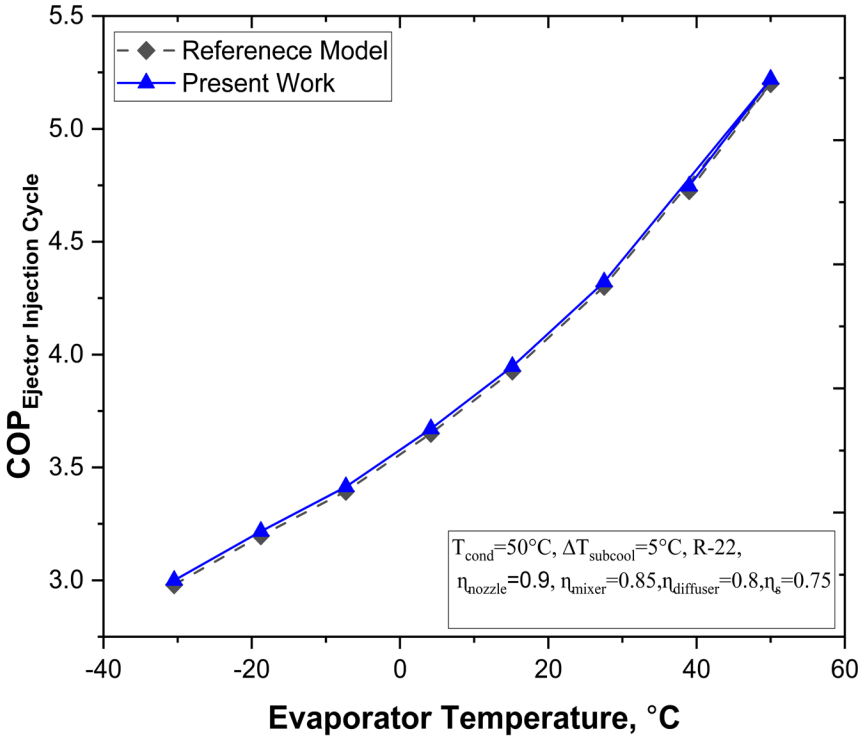

Fig. 9: : Validation and evaluation of the ejector refrigeration cycle utilized in the ECAC with regard to [61]

The ejector plays a crucial role in the proposed models, as it serves the vital purpose of recuperating energy losses that occur during the expansion process, thereby enhancing the efficiency of the system. To assure the accuracy and reliability of the provided models, it is imperative to validate the performance of the ejector using experimental data. The benchmark for this purpose is derived from a study done by Elbel et al. [63], and the findings are displayed in **Table 10**. This study aims to examine the influence of geometric parameters on the performance of ejectors, with R744 being employed as the working fluid. In this study, we compare the entrainment ratio derived from different experimental input conditions with our numerical ejector model, which is based on Li et al.'s technique. The findings suggest that the numerical model provides a more precise representation of the experimental model of the ejector, specifically when considering a diffuser angle of 5°.

Table 10: Validation of the ejector model through an experiment [63]

Diffuser Angle, α_{diff}	**P_{mn} (MPa)**	**T_{mn}, (°C)**	**P_{sn}, (MPa)**	**x_{sn}, in**	**Entrainment ratio, $w = \frac{m_{suction}}{m_{motive}}$**		**Suction pressure ratio, $\pi = \frac{P_{diffuser}}{P_{suction}}$**	
					Reference work [63]	**Numerical model**	**Reference work** [63]	**Numerical model**
5°	9.33	37.2	3.68	0.98	0.50	0.54	1.095	1.174
	9.66	35.2	3.57	0.95	0.54	0.57	1.072	1.155
10°	9.38	37.2	3.73	0.99	0.47	0.56	1.094	1.169
	9.52	37.2	3.65	0.95	0.50	0.57	1.078	1.156
15°	9.38	37.6	3.77	0.98	0.46	0.55	1.071	1.176
	9.72	36.1	3.73	0.96	0.54	0.62	1.021	1.47

Chapter 6: Results and Discussions

The proposed E-DAC(Series), E-DAC(Parallel), EI-DAC(Series), and EI-DAC(Parallel) systems were subjected to a comparative thermal analysis with the standard C-DAC(Series) and C-DAC(Parallel) systems, following the verification of the thermodynamic model. The analyses are based on various performance parameters, such as *COP*, High pressure generator load ($\dot{Q}_{HPG}$), compressor load ($\dot{W}_{comp}$), exergetic efficiency (η_{II}), and total exergy destruction ($\dot{E}_{D,total}$). Four controllable variables are considered as working parameters: High pressure generator temperature (T_{HPG}), evaporator temperature (T_{evp}), condenser temperature (T_{cond}), and absorber temperature (T_{abs}).

6.1 Thermodynamic Performance Analysis

An internal EES program is used to simulate the proposed models. The refrigerant pair R41-LiBr/H2O has been selected for the purpose of evaluating and comparing thermal performance. The rationale for the choice is rooted in its environmentally sustainable characteristics and widespread accessibility. According to reference[64] , R41 exhibits a zero ODP, an extremely low GWP (97), and a lower boiling point temperature of -78.1 ℃. This feature enhances its compatibility for use in lower temperature circuit (LTC). Previous studies have also suggested the utilization of this refrigerant due to its superior performance in low-temperature applications [65][64]. The thermodynamic state parameters of the proposed novel systems are provided in ***Table 11***, ***Table 12***, ***Table 13*** and ***Table 14*** considering the boundary conditions mentioned in corresponding tables.

Table 11: The attributes of the thermodynamic state point of the E-DAC (series) for R41-LiBr/H₂O solution at T_{evp} = -30℃, T_{HPG} = 130℃, T_{abs} = 35℃, T_{cond} = 35℃, and ΔT_{CHX} = 5℃

State Point	T (℃)	x (%)	$\dot{m}$ (kg s^{-1})	h (kJ kg^{-1})	s (kJ kg^{-1} K^{-1})	P (kPa)	Point Exergy(kW)
1	35	-	0.1498	146	0.5031	5.583	0.08838
2	4	-	0.1498	55.23	0.1998	0.805	0.02952
3	4	-	0.1498	2508	9.054	0.805	-27.83
4	35	0.5588	2.029	87.36	0.2072	0.805	61.1
5	35	0.5588	2.029	87.36	0.2072	52.32	61.1
6	66.6	0.5588	2.029	151.2	0.4048	52.32	71.19

7	111	0.5588	2.029	244.1	0.6605	52.32	105
8	130	0.58	1.955	288.1	0.7365	52.32	143
9	85.6	0.58	1.955	197.1	0.4984	52.32	103.7
10	85.6	0.58	1.955	197.1	0.4984	5.583	103.7
11	130	-	0.07402	2741	7.825	52.32	30.6
12	82.6	-	0.07402	345.3	1.105	52.32	1.528
13	35	-	0.07402	345.3	1.15	5.583	0.5226
14	80.1	-	0.07578	2643	8.614	5.583	6.092
15	80.1	0.6034	1.879	196	0.4503	5.583	124.7
16	48.5	0.6034	1.879	135.7	0.2711	5.583	111.6
17	48.5	0.6034	1.879	135.7	0.2711	0.805	111.6
18	13.3	-	0.1498	55.23	0.1975	5.583	0.1336
19	52.4	-	0.1498	2599	9.356	0.805	-27.71
20	-27.1	-	0.9633	535.7	2.385	897.9	155.6
21	48.5	-	0.9633	605.3	2.418	2589	213.2
22	9	-	0.9633	223.9	1.082	2589	229.2
23	-31.3	-	0.9633	215.3	1.089	779.2	219.2
24	241.7	-	1.712	355.2	1.667	779.2	333.7
25	245.9	-	1.712	360	1.67	897.9	340.4
26	245.9	-	0.7485	134.4	0.7525	897.9	184.7
27	243	-	0.7485	134.4	0.7532	814.2	184.5
28	243	-	0.7485	535.2	2.403	814.2	116.5
29	241.7	-	0.7485	533.3	2.404	779.2	114.8

Table 12: The attributes of the thermodynamic state point of the E-DAC (Parallel) for R41-LiBr/H_2O solution at T_{evp} = -30℃, T_{HPG} = 130℃, T_{abs} = 35℃, T_{cond} = 35℃, D=0.3658 and ΔT_{CHX} = 5℃

State Point	**T (℃)**	**x (%)**	$\dot{m}$ **(kg s^{-1})**	**h (kJ kg^{-1})**	**s (kJ kg^{-1} K^{-1})**	**P (kPa)**	**Point Exergy(kW)**
1	35	-	0.1498	146	0.5031	5.583	0.08838
2	4	-	0.1498	55.23	0.1998	0.805	0.02952

3	4	-	0.1498	2508	9.054	0.805	-27.83
4	35	0.5588	2.967	87.36	0.2072	0.805	89.34
5	35	0.5588	2.967	87.36	0.2072	42.2	89.34
6	67.2	0.5588	2.967	152.6	0.4088	42.2	104.6
6a	340.2	0.5588	1.881	152.6	0.4088	42.2	66.32
6b	340.2	0.5588	1.881	152.6	0.4088	5.583	66.32
6c	340.2	0.5588	1.085	152.6	0.4088	42.2	38.25
7	111.8	0.5588	1.085	245.8	0.6651	42.2	56.61
8	130	0.6059	1.001	295.3	0.7074	42.2	89.04
9	81.7	0.6059	1.001	200.3	0.4572	42.2	68.62
10	81.7	0.6059	1.001	200.3	0.4572	5.583	68.62
10a	349.9	0.5885	2.817	182.9	0.4425	5.583	156.5
11	130	-	0.08432	2720	7.926	42.2	30.57
12	77.3	-	0.08432	323.1	1.042	42.2	1.447
13	35	-	0.08432	323.1	1.078	5.583	0.5344
14	74.8	-	0.06548	2634	8.586	5.583	5.239
15	74.8	0.579	1.816	174.9	0.4377	5.583	88.97
16	44.6	0.5885	2.817	120	0.2538	5.583	137.8
17	44.6	0.5885	2.817	120	0.2538	0.805	137.8
18	13.3	-	0.1498	55.23	0.1975	5.583	0.1336
19	52.4	-	0.1498	2599	9.356	0.805	-27.71
20	-27.1	-	0.9633	535.7	2.385	897.9	155.6
21	48.5	-	0.9633	605.3	2.418	2589	213.2
22	9	-	0.9633	223.9	1.082	2589	229.2
23	-31.3	-	0.9633	215.3	1.089	779.2	219.2
24	-31.3	-	1.712	355.2	1.667	779.2	333.7
25	-27.1	-	1.712	360	1.67	897.9	340.4
26	-27.1	-	0.7485	134.4	0.7525	897.9	184.7
27	-30	-	0.7485	134.4	0.7532	814.2	184.5
28	-30	-	0.7485	535.2	2.403	814.2	116.5
29	-31.3	-	0.7485	533.3	2.404	779.2	114.8

Table 13: The attributes of the thermodynamic state point of the EI-DAC (series) for R41-LiBr/H_2O solution at T_{evp} = -30℃, T_{HPG} = 130℃, T_{abs} = 35℃, T_{cond} = 35℃, and ΔT_{CHX} = 5℃

State Point	T (℃)	x (%)	$\dot{m}$ (kg s^{-1})	h (kJ kg^{-1})	s (kJ kg^{-1} K^{-1})	P (kPa)	Point Exergy(kW)
1	35	-	0.1476	146	0.5031	5.583	0.0871
2	4	-	0.1476	55.23	0.1998	0.805	0.02909
3	4	-	0.1476	2508	9.054	0.805	-27.42
4	35	0.5588	2	87.36	0.2072	0.805	60.22
5	35	0.5588	2	87.36	0.2072	52.32	60.22
6	66.6	0.5588	2	155.9	0.4184	52.32	71.33
7	111	0.5588	2	252	0.6809	52.32	107.2
8	130	0.58	1.927	288.1	0.7365	52.32	140.9
9	85.6	0.58	1.927	194.1	0.49	52.32	101.2
10	85.6	0.58	1.927	194.1	0.49	5.583	101.2
11	130	-	0.07294	2741	7.825	52.32	30.16
12	82.6	-	0.07294	345.3	1.105	52.32	1.505
13	35	-	0.07294	345.3	1.15	5.583	0.515
14	80.1	-	0.07467	2643	8.614	5.583	6.003
15	80.1	0.6034	1.852	196	0.4503	5.583	122.9
16	48.5	0.6034	1.852	131.4	0.2579	5.583	109.5
17	48.5	0.6034	1.852	131.4	0.2579	0.805	109.5
18	13.3	-	0.1476	55.23	0.1975	5.583	0.1316
19	52.4	-	0.1476	2599	9.356	0.805	-27.31
20	3.9	-	0.957	564.1	2.396	1452	178.6
21	46.6	-	0.957	602.2	2.408	2589	211.6
22	9	-	0.957	223.9	1.082	2589	227.7
23	-15.8	-	0.957	219.1	1.082	1291	223.2
24	-14.9	-	0.9729	225.1	1.105	1291	226
25	-11.9	-	0.9729	227	1.108	1452	227
26	-11.9	-	0.1513	536.1	2.292	1452	28.7
27	-11.9	-	0.8216	170	0.8903	1452	198.3

28	-14.9	-	0.8216	170	0.8911	1326	198.1
29	-14.9	-	0.02431	536.4	2.31	1326	4.485
30	-15.8	-	0.8216	535.1	2.31	1291	150.5
31	-14.9	-	0.8057	162.8	0.8632	1326	195.2
32	-30	-	0.8057	162.8	0.8703	814.2	193.4
33	-30	-	0.8057	535.2	2.403	814.2	125.4
34	7.2	-	0.8057	569.4	2.415	1452	150.1

Table 14: The attributes of the thermodynamic state point of the EI-DAC(Parallel)for R41-LiBr/H_2O solution at T_{evp} = -30℃, T_{HPG} = 130℃, T_{abs} = 35℃, T_{cond} = 35℃, D=0.3658 and ΔT_{CHX} = 5℃

State Point	**T (℃)**	**x (%)**	$\dot{m}$ **(kg s^{-1})**	**h (kJ kg^{-1})**	**s (kJ kg^{-1} K^{-1})**	**P (kPa)**	**Point Exergy(kW)**
1	35	-	0.1476	146	0.5031	5.583	0.0871
2	4	-	0.1476	55.23	0.1998	0.805	0.02909
3	4	-	0.1476	2508	9.054	0.805	-27.42
4	35	0.5588	2.898	87.36	0.2072	0.805	87.27
5	35	0.5588	2.898	87.36	0.2072	42.55	87.27
6	67.2	0.5588	2.898	157	0.4217	42.55	103.8
6a	340.2	0.5588	1.838	157	0.4217	42.55	65.83
6b	340.2	0.5588	1.838	157	0.4217	5.583	65.83
6c	340.2	0.5588	1.06	157	0.4217	42.55	37.97
7	111.8	0.5588	1.06	253.3	0.6841	42.55	57.14

8	130	0.6049	0.9793	294.9	0.7084	42.55	86.5
9	81.7	0.6049	0.9793	197.1	0.4503	42.55	66.07
10	81.7	0.6049	0.9793	197.1	0.4503	5.583	66.07
10a	349.9	0.5888	2.75	183.2	0.4426	5.583	153.4
11	130	-	0.0808	2720	7.922	42.55	29.38
12	77.3	-	0.0808	323.9	1.044	42.55	1.397
13	35	-	0.0808	323.9	1.081	5.583	0.5143
14	74.8	-	0.06682	2634	8.587	5.583	5.347
15	74.8	0.5799	1.771	175.7	0.4382	5.583	87.89
16	44.6	0.5888	2.75	116.2	0.241	5.583	134.4
17	44.6	0.5888	2.75	116.2	0.241	0.805	134.4
18	13.3	-	0.1476	55.23	0.1975	5.583	0.1316
19	52.4	-	0.1476	2599	9.356	0.805	-27.31
20	3.9	-	0.957	564.1	2.396	1452	178.6
21	46.6	-	0.957	602.2	2.408	2589	211.6
22	9	-	0.957	223.9	1.082	2589	227.7
23	-15.8	-	0.957	219.1	1.082	1291	223.2
24	-14.9	-	0.9729	225.1	1.105	1291	226
25	-11.9	-	0.9729	227	1.108	1452	227
26	-11.9	-	0.1513	536.1	2.292	1452	28.7
27	-11.9	-	0.8216	170	0.8903	1452	198.3
28	-14.9	-	0.8216	170	0.8911	1326	198.1
29	-14.9	-	0.02431	536.4	2.31	1326	4.485
30	-15.8	-	0.8216	535.1	2.31	1291	150.5
31	-14.9	-	0.8057	162.8	0.8632	1326	195.2
32	-30	-	0.8057	162.8	0.8703	814.2	193.4

33	-30	-	0.8057	535.2	2.403	814.2	125.4
34	7.2	-	0.8057	569.4	2.415	1452	150.1

6.1.1 Comparison Between Proposed and Conventional System

A comparative performance study has been carried out to compare between the proposed systems (E-DAC(Series), E-DAC (parallel), EI-DAC (Series) and EI-DAC (parallel)) and the conventional systems (C-AC), C-DAC(Series), C-DAC(Parallel)). For the working conditions, the input parameters are taken from **Table 7.** For the C-AC the input conditions are T_{gen} = *80℃,* T_{evp} = *-30℃,* T_{abs} = *35℃,* T_{cond} = *35℃,* and ΔT_{CHX} = *5℃.* The energy and exergy analysis of the corresponding components of the respective cycles are provided in **Table 15. Fig. 10** shows the comparison among the proposed systems as well as against the conventional systems.

Table 15: Comparison between proposed systems and conventional systems

Component	**Conventional System**			**Proposed systems**			
	C-AC	**C-DAC(Series)**	**C-DAC(Parallel)**	**E-DAC(Series)**	**E-DAC(Parallel)**	**EI-DAC(Series)**	**EI-DAC(Parallel)**
Generator, $\dot{Q}_{HPG/gen}$ (kW)	502.2	286.4	279	270.9	258	251.1	240.1
Condenser, $\dot{Q}_{cond}$ (kW)	396.5	215.6	187.3	204	177.8	201	180.6
Evaporator, $\dot{Q}_{evp}$ (kW)	300	300	300	300	300	300	300
Absorber, $\dot{Q}_{abs}$ (kW)	479.7	479.4	483.2	467	468.2	452.4	450

Compressor, $\dot{W}_{comp}$ (kW)	74.07	74.07	74.07	67.01	67.01	64.01	64.01
Exergy destruction, $\dot{E}_{D,total}$ (kW)	86.39	85.73	78.95	74.6	70.25	67.77	64.38
Coefficient of performance, COP	0.5206	0.8321	0.8595	0.8876	0.9127	0.9518	0.9822
η_{II}	0.2706	0.4564	0.4624	0.4932	0.5055	0.5243	0.5361

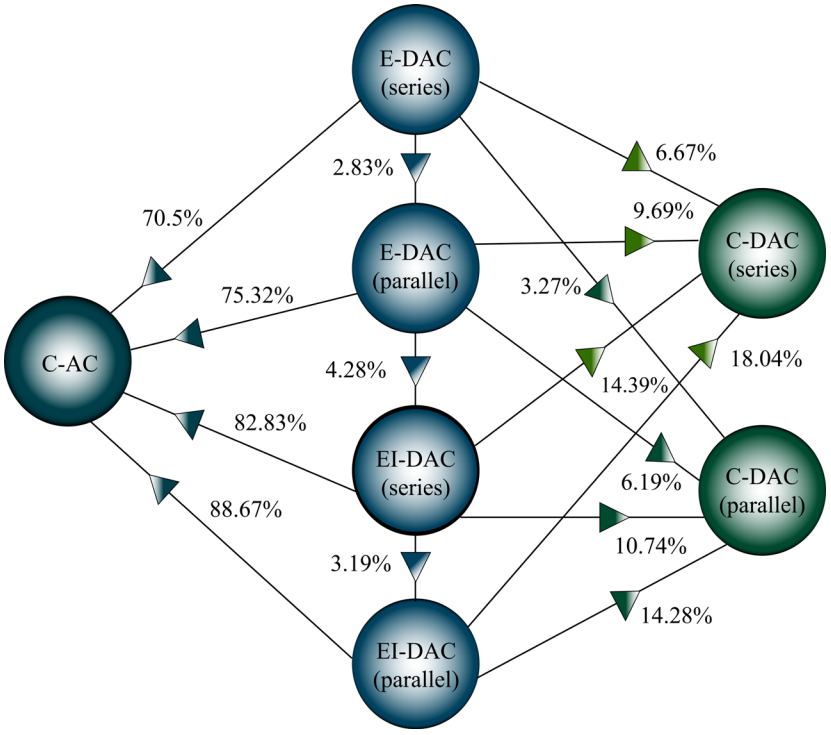

Fig. 10: Comparison of the COP improvements with the conventional systems

6.1.2 System sub-cycles performance analysis

Prior to undertaking a thorough investigation of the performance of the proposed systems, the influence of input conditions on the subsystems is investigated initially. In the proposed refrigeration systems, COP_{LTC} is related to the compressor load whereas COP_{HTC} is associated with the generator load neglecting the pump work. From **Fig. 11(a)** it can be seen that, with the increase of High-Pressure Generator Temperature, for the LTC, pressure ration remains same as T_{evp}=30°C doesn't change with T_{HPG}, so COP_{LTC} remains constant but COP_{HTC} increases as the High-Pressure Generator Load decreases. The modified HTC DE-ARC (with RHX) achieves an enhancement of 3-4% is achieved from the conventional DE-ARC (without RHX) for both the series and parallel configurations.

From **Fig. 11(b),** as the T_{evp} increases, the pressure ratio increases but compressor load decreases so eventually, COP_{LTC} increases. But as T_{evpHTC}= 4°C remains same in the HTC, so COP_{HTC} remains constant. The ejector injection model for the LTC exhibits a consistent enhancement of around 7-8.5% when compared to the ejector expansion model.

The performance of the single effect ARC is notably inferior when compared to both the DE-ARC conventional and modified configurations. For the sake of a more thorough analysis, we have excluded the integration of a Single effect ARC cascaded with VCR.

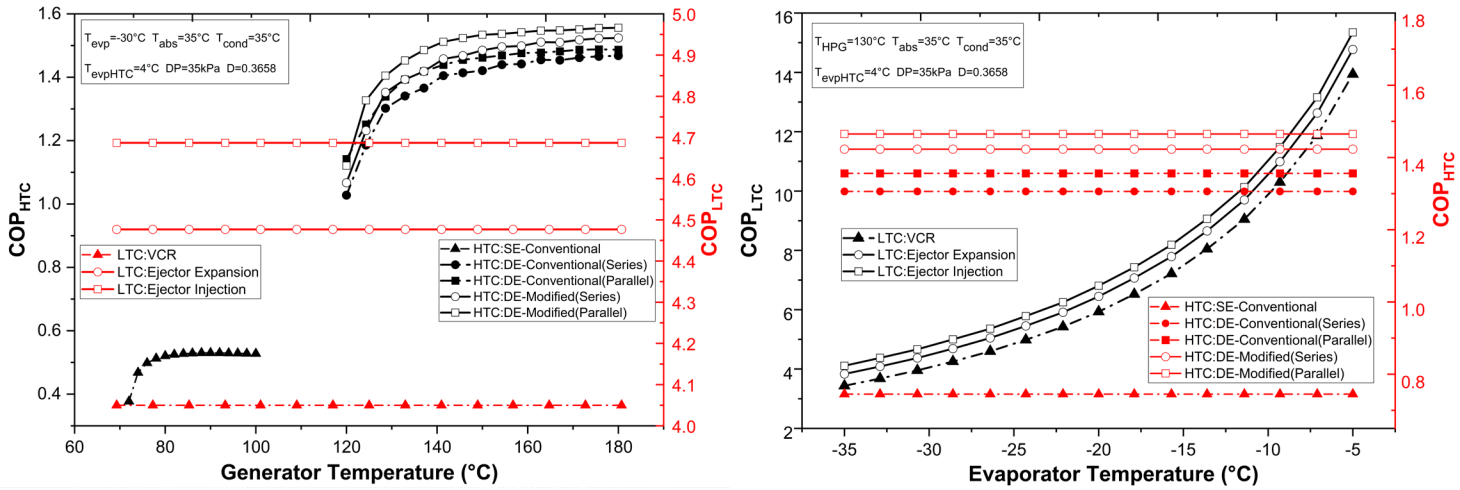

(a) (b)

Fig. 11: The impact of (a) High Pressure Generator Temperature and (b) Evaporator Temperature on COP_{LTC} and COP_{HTC} at T_{cond} = 35°C, T_{abs} = 35°C, D=0.3658

6.1.3 Impact of Pressure Drop on the System Performance of the Ejector Nozzle

The inclusion of an ejector in the LTC significantly impacts the pressure drop, hence drastically affecting the COPs our proposed novel systems. The optimum value is attained by iteratively

adjusting the operating conditions of the proposed systems using the EES software. In the E-DAC (Series and Parallel) systems, the coefficient of performance (COP) varies by a factor of 0.002, however in the EI-DAC (Series and Parallel) systems, the COP changes by a factor of 0.01, which is five times greater than that of the aforementioned systems. E-DAC (Series and Parallel) systems are significantly impacted by pressure drop. The optimal coefficient of performance (COP) for E-DAC (Series and Parallel) systems is achieved at a pressure drop of around 35kPa, after which it steadily falls. However, in the case of EI-DAC (Series and Parallel) systems, the highest efficiency may be obtained when the pressure drop is approximately 80kPa. Beyond this point, the impact of pressure drop becomes negligible.

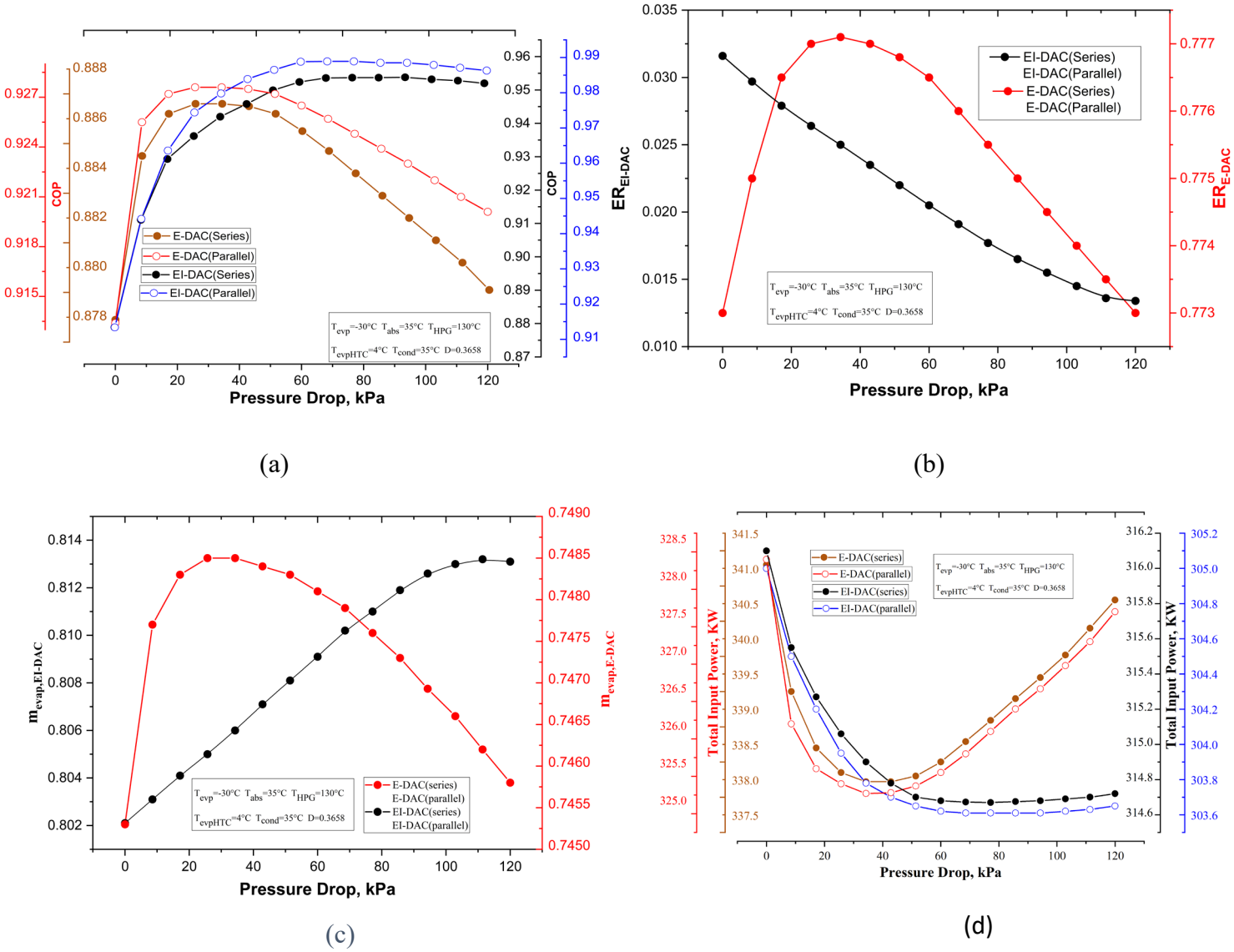

Fig. 12: Impact of ΔP on (a) COP of the proposed system, (b) Entrainment ratio (c) $\dot{m}_{evp}$ and (d) Total power input at Thpg=130℃, Tcond = 35℃, Tabs = 35℃, Tevp = -30℃, D=0.3658

For further inspection on the LTC's configurations, to demonstrate the change of COP with pressure drop, it can be seen that for E-DAC (series and parallel), Entrainment ratio (ER) increases in the same manner as COP, as shown in **Fig. 12(a)** and **Fig. 12(b)**. For these configurations, $ER = \frac{\dot{m}_{suction}}{\dot{m}_{motive}}$ and $\dot{m}_{suction}$=$\dot{m}_{evp}$ and $\dot{m}_{evp}$ has linear relationship with COP. So, COP increases in similar pattern as ER. But for the EI-DAC (series and parallel), ER decreases with pressure drop. The decrement in ER, results in decrement in $\dot{m}_{suction}$. And $\dot{m}_{suction} = \frac{1-x_{28}}{x_{28}}\dot{m}_{evp}$. To satisfy this equation, $\dot{m}_{evp}$ increases which eventually results in the increment of COP. Figure shows the $\dot{m}_{evp}$ vs Pressure Drop graph which satisfies the pattern found in the COP vs Pressure Drop. These phenomena can further be explained from **Fig. 12(c)** and **Fig. 12(d) ,** Pressure drop vs Total input which follows an inverse trend than that of Pressure drop vs COP graph which is expected as COP and Total input have inverse relation. The highest COP can be achieved from EI-DAC (Parallel) configuration while consisting of the lowest input work.

6.1.4 Effect of High Pressure Generator- Evaporator Temperature

To compare the performances of the proposed systems with respect to T_{HPG} (HP generator temperature) vs T_{evp} (Evaporator temperature), COP is optimized against pressure drop and distribution ratio, D in the simulation. The effectiveness of the new systems relies heavily on the T_{HPG} and T_{evp} being the refrigeration cycles.

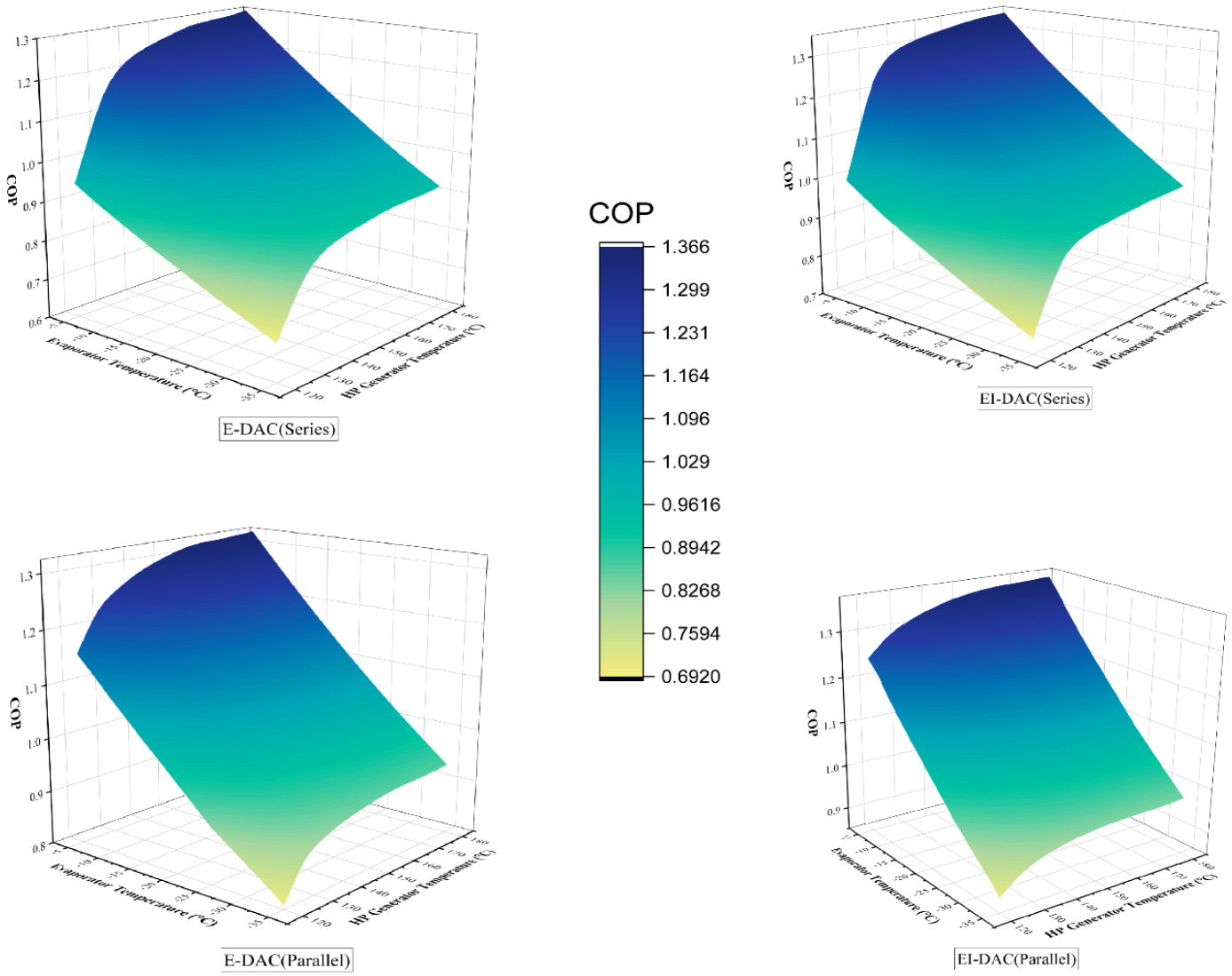

Fig. 13: The effect of T_{HPG} and T_{evp} on COP at at T_{cond} = 35°C, T_{abs} = 35°C, D=0.3658

From **Fig. 13**, in the proposed four systems, increasing the T_{HPG} and T_{evp} shows the similar pattern regarding the COP of the novel systems. Increasing the T_{evp} results in the higher COP and it increases almost in linear pattern whereas increasing the T_{HPG}, system COP increases very rapidly within the initial range of the HP generator temperature (125°C to 140°C) and then becomes flat. The optimal COP has reached for the novel systems is around at 140°C. Among the four proposed systems, EI-DAC(Parallel) shows the highest COP within the operating range. For EI-DAC(Parallel) highest COP can be achieved at T_{evp}=-5°C and T_{HPG}=140°C.

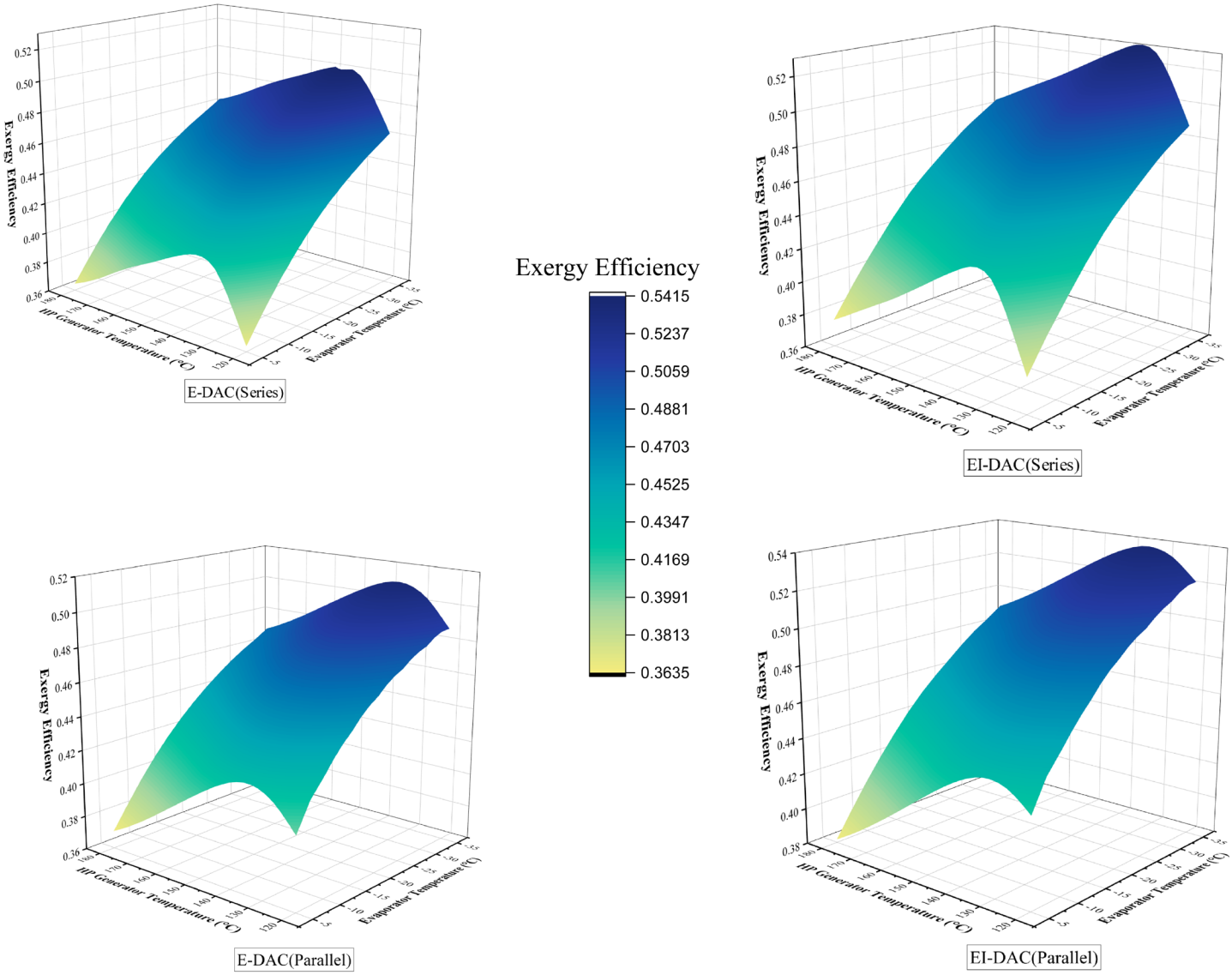

Fig. 14: The effect of T_{HPG} and T_{evp} on Exergy Efficiency at at T_{cond} = 35℃, T_{abs} = 35℃, D=0.3658

Fig. 14 shows the impact of T_{HPG} and T_{evp} on the 2nd law efficiency. It can be seen that exergy efficiency increases with a steeper slope at a fixed T_{evp} temperature with the increment of T_{HPG} and as the system approaches its optimal value, there is a progressive decline in exergy efficiency. Likewise, for the T_{evp}, as it increases corresponding to a fixed T_{HPG}, the increase in exergy efficiency follows a similar pattern to that of COP. The systems approach to the highest exergy efficiency is approximately at T_{HPG}=135°C. When comparing the four systems from

fig2, it is evident that EI-DAC(Parallel) has a notably superior exergy efficiency in comparison to the remaining systems.

6.1.5 Effect of High Pressure Generator- Condenser Temperature

Similar to the T_{HPG} and T_{evp}, our proposed systems have significant dependency on the condenser temperature (T_{cond}) as well. So similar analysis is carried out in **Fig. 15** and **Fig. 16.**

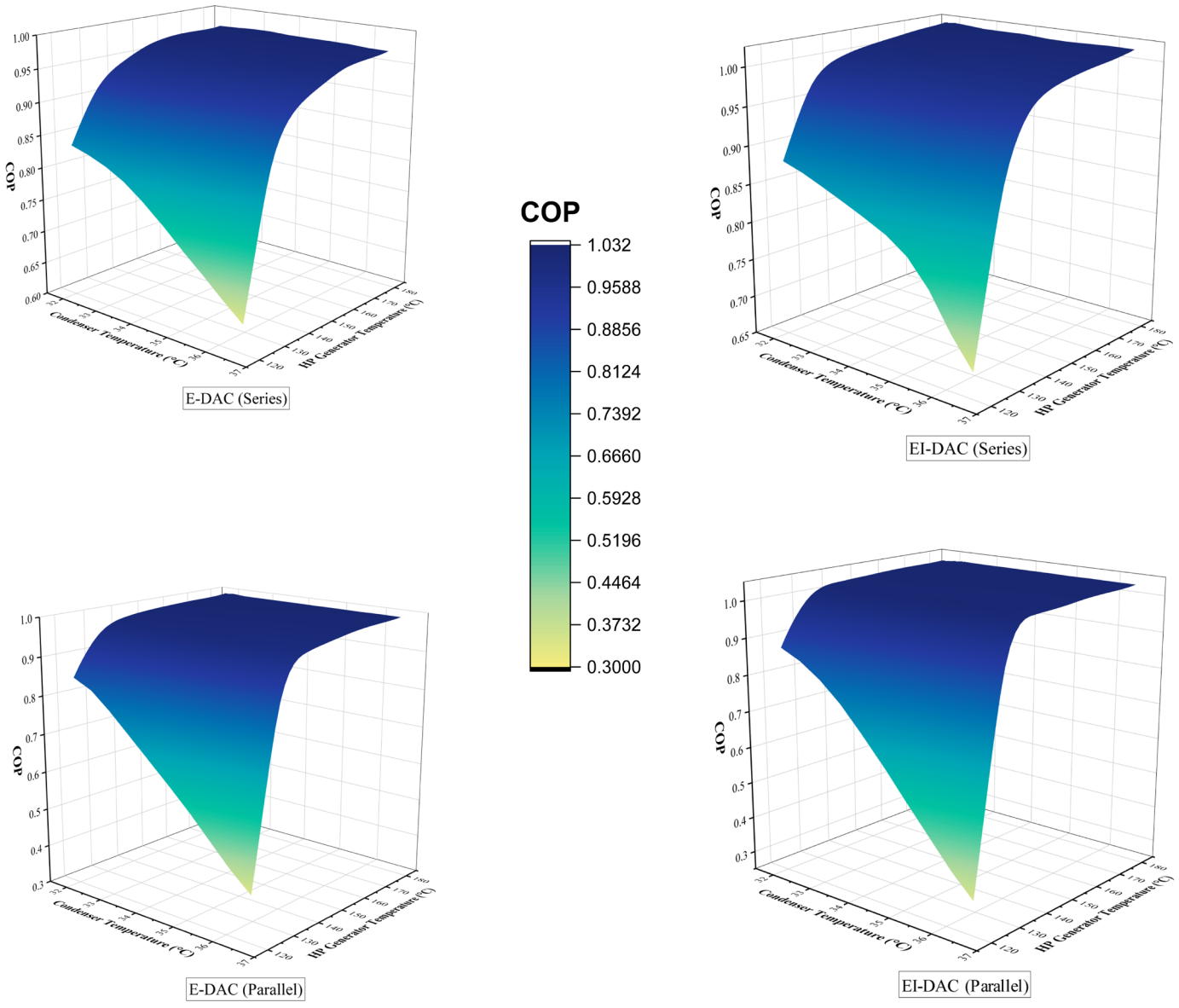

Fig. 15: The impact of T_{HPG} and T_{cond} on COP at at T_{evp} = -30℃, Tabs = 35℃, D=0.3658

From **Fig. 13**, from the (T_{HPG} vs T_{evp}) vs COP analysis, T_{HPG} increases similarly with higher steep in the lower range of the T_{HPG}. T_{cond} range is taken from 32°C to 37°C and each rise in T_{cond}, results in a decrease in COP gradually. So, from the figure, higher COP can be obtained at lower T_{cond}. Among the four configurations, E-DAC(Parallel) shows the highest achievable COP within the range of T_{HPG} vs T_{cond}.

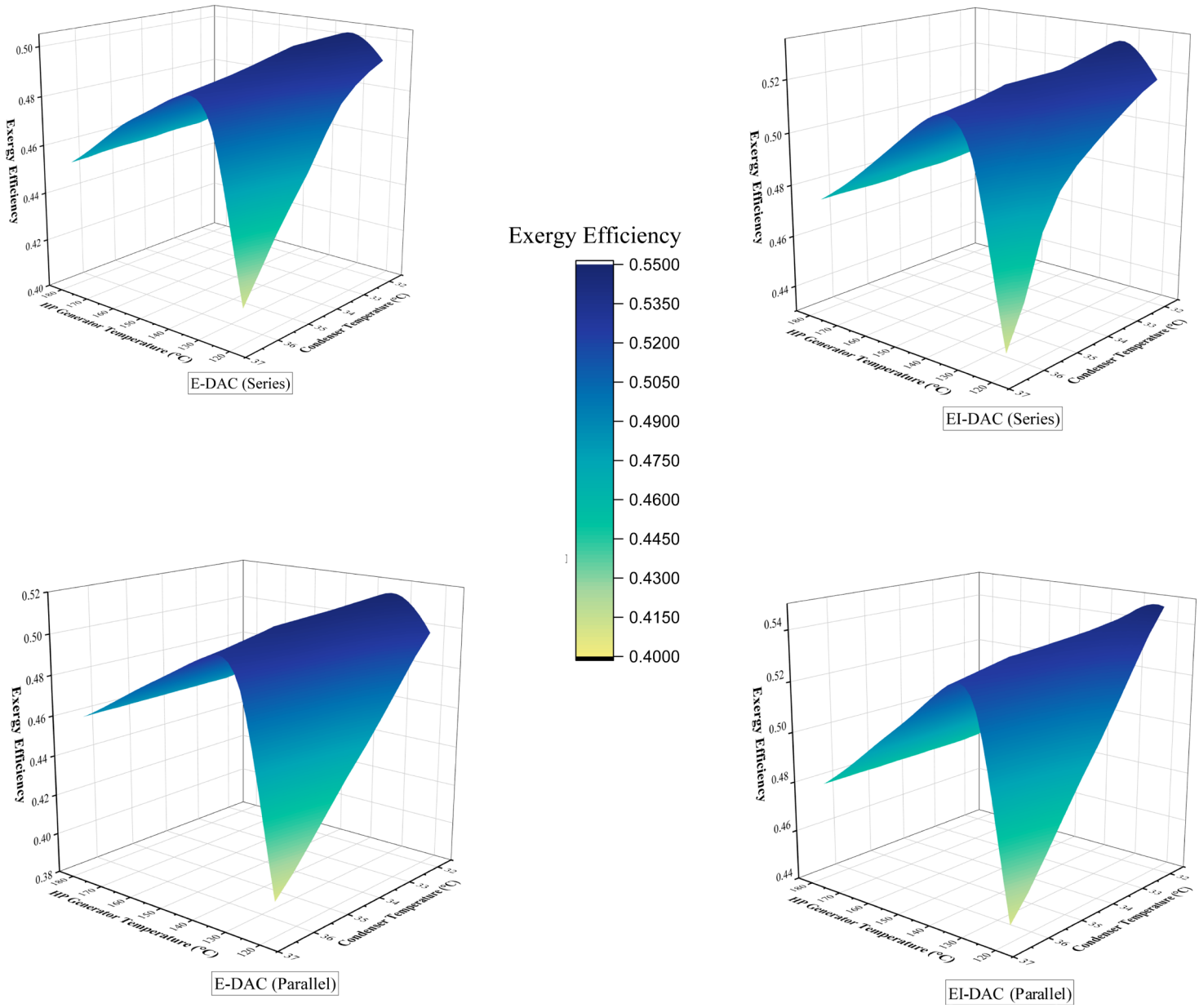

Fig. 16 :The impact of T_{HPG} and T_{cond} on Exergy Efficiency at at T_{evp} = -30°C, Tabs = 35°C, D=0.3658

In second law efficiency analysis, T_{HPG} shows the similar trend to that of (T_{HPG} vs T_{evp}) vs Exergy Efficiency, The T_{HPG} exhibits a significant increase in the lower range, followed by a progressive drop. The E-DAC(Parallel) system has superior exergy efficiency compared to the other three proposed systems. The optimal exergy efficiency is attained when T_{cond} is set to 32°C and T_{HPG} is set at 140°C for E-DAC(Parallel).

6.1.6 Effect of High Pressure Generator Temperature

To facilitate a comprehensive examination, the impact of each operational parameter is assessed individually, while holding all remaining variables constant. This study offers a comprehensive examination of the system's reasonable working range and limiting variables, aiming to facilitate efficient operation.

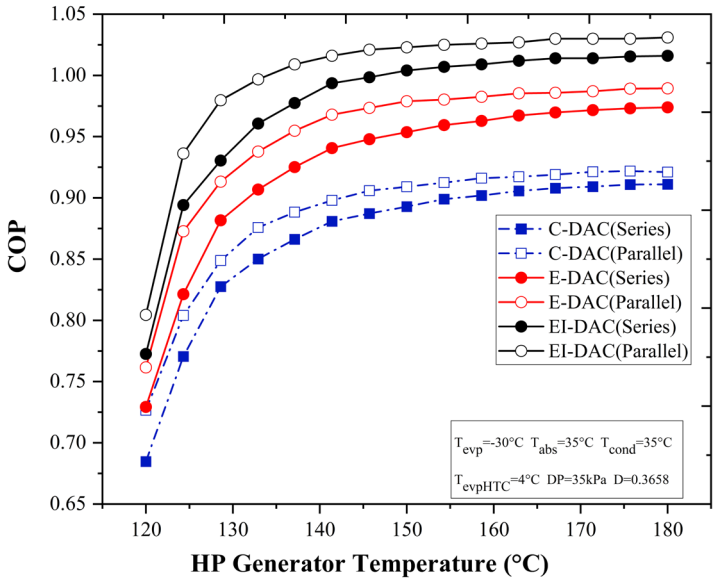

(a)

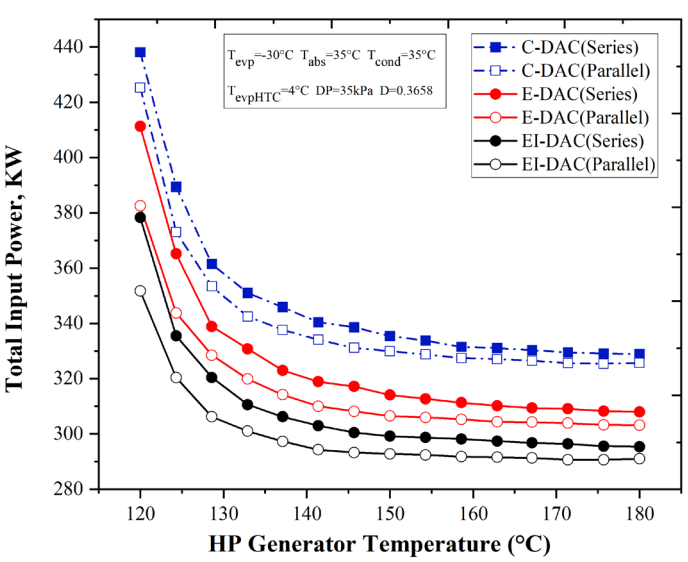

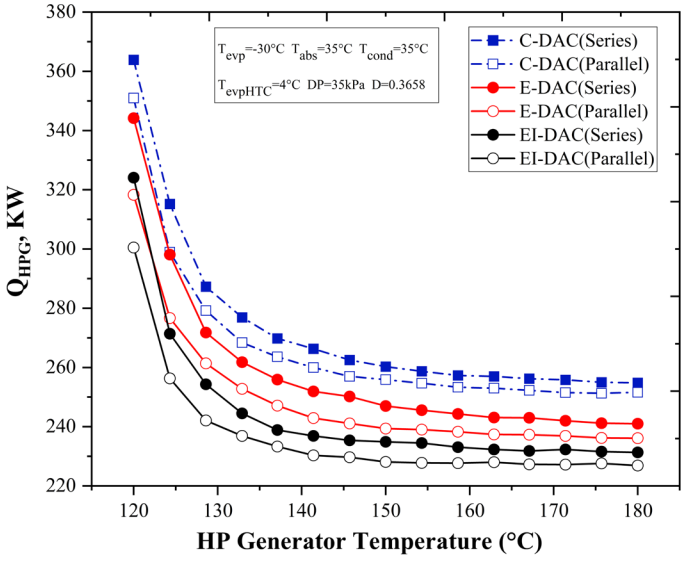

(b) (c)

Fig. 17*: Impact of T_{HPG} on (a) COP of the novel systems, (b)Total power input (c)Q_{HPG} at T_{cond} = 35℃, T_{abs} = 35℃, T_{evp} = -30℃, D=0.3658*

Fig. 17 shows the impact of T_{HPG} on the performance of the cascaded novel systems. For further in-depth analysis, four proposed systems are compared against the two conventional C-DAC(Series) and C-DAC(Parallel) systems. Based on the results presented in **Fig. 17(a),** it can be observed that the coefficient of performance (COP) exhibits a significant increase within the lower temperature range of the HP generator. Furthermore, it is noted that an optimality is attained after a specific temperature range. For all the proposed systems, it can be said that the optimal condition is reached after T_{HPG}=140°C. For EI-DAC(Parallel) configuration, optimality is achieved slightly later than T_{HPG}=142°C resulting in the highest achieved COP among the other 3 novel systems. This behavior can further be explained from Fig. 17**(b)** which depicts basically Total Input Power Vs $T_{HPG.}$ From Fig. 17(b)**,** it is clear that the total input power declines with the increase of T_{HPG}. For a further look on Fig. 17(b)**,** this represents a total opposite trend of the COP graph. Between the two LTC models of the ejector, Injection model rejects less heat than the ejector expansion model in the cascade heat exchanger which results in lower mass flow rate in the HTC which eventually decreases the High-pressure generator load, $Q_{HPG.}$ This phenomenon is also clear from **Fig. 17(c).** Moreover, between the two HTC models, the parallel configuration of the double effect absorption refrigeration cycle performs better (more or less 3%) than the series configuration because in the parallel configuration, the mass flow rate directed towards the HPG is divided, with one piece being allocated to the HPG and the other component being allocated to the LPG resulting the lower Q_{HPG} for the parallel configuration and which is clearly depicted in Fig 17(c). Besides, High Pressure generator load is defined as, $\dot{Q}_{HPG} = \dot{m}_{11} \times h_{11} + \dot{m}_8 \times h_8 - \dot{m}_7 \times h_7$. As the T_{HPG} increases, concentration of LiBr/H_2O increases resulting in the increase of specific enthalpy of the state 8 but enthalpy of the vapor of state 11 decreases. On the contrary, with the increase of concentration, mass flow rate of state 8 decreases which results in the overall decline of Q_{HPG}. So, the COP of the system increases. But after reaching the optimal value of the T_{HPG}, the increment of the concentration of the solution and decrement of the mass flow rate of state 8 becomes near constant and so the system COP also becomes flat.

So overall, injection model of the LTC and parallel configuration of the HTC combinedly perform better than the other 3 combinations of the proposed systems resulting in EI-DAC(Parallel) being the novel system with the highest achievable COP.

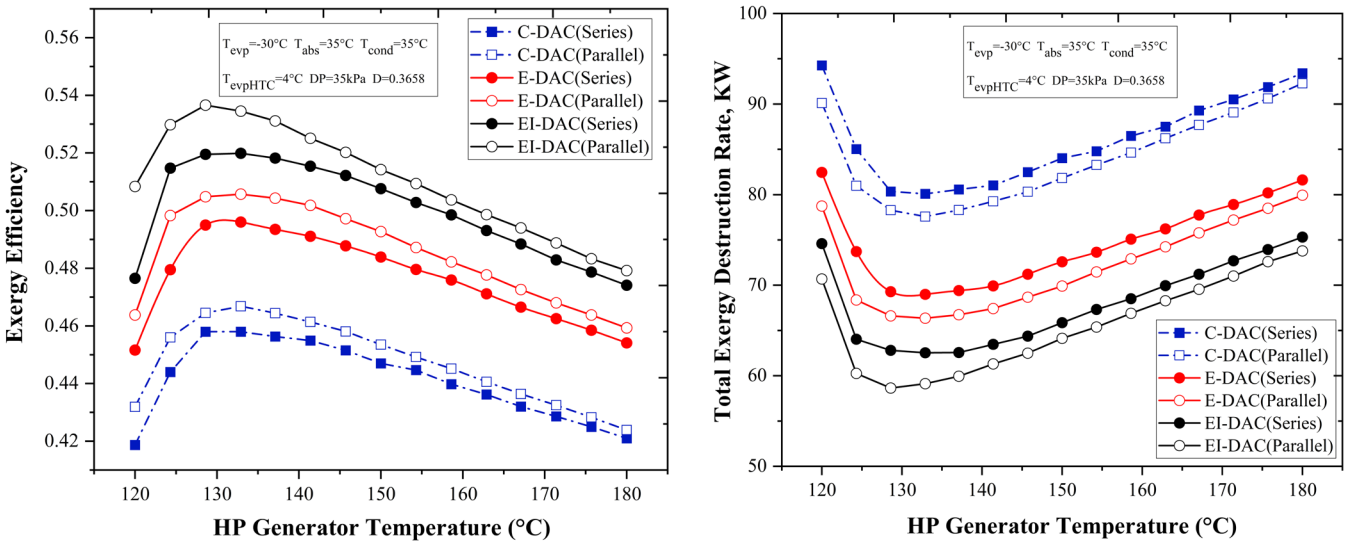

Fig. 18 : Impact of T_{HPG} on (a) exegetic efficiency and (b) Total Exergy Destruction rate of the proposed systems at T_{cond} = 35°C, T_{abs} = 35°C, T_{evp} = -30°C, D=0.3658

Fig. 18(a) demonstrates the performance of the proposed systems from the exegetic perspective. Although the energy performance of the systems may show small alterations once optimality is achieved, the exegetic efficiency experiences a substantial fall beyond the optimum state. From Fig 18(a), it is clear that exergy efficiency increases with higher steep before the optimality is reached and then declines gradually. This phenomenon can be demonstrated from the **Fig. 18(b).** The rise in T_{HPG} leads to an improvement in refrigeration capacity, hence resulting in an immediate spike in exergy efficiency. Following the attainment of the optimal T_{HPG}, the vapor generated at the HPG exerts a significant impact on the performance of the system, resulting in a higher percentage of exergy destruction in the HPG, condenser, and absorber visualized in Fig 18(b**)**. Consequently, this ultimately leads to a reduction in the overall exergy efficiency of the system. To get the optimal performance from the exegetic perspective, T_{HPG} must be kept in the range of 130 to 140°C. According to Figure 18(a), the EI-DAC(Parallel) model outperforms the other models that are considered. The performance of EI-DAC(Parallel) is roughly 16.7% higher than that of C-DAC(Parallel) and 17.5% higher than that of C-DAC(Series).

6.1.7 Effect of Evaporator Temperature

Fig. 19(a) depicts the influence of T_{evp} on the system performance of the proposed novel systems. As the evaporator temperature rises, the coefficient of performance (COP) of the system also increases. The observed effect can be elucidated by referring to **Fig. 19(b),** wherein the total input load of the system exhibits a decrease as the evaporator temperature increases, so ultimately enhancing the coefficient of performance (COP) of the system. This can be further explained from the **Fig. 19(c).** For the injection ejector model in the LTC (EI-DAC (Series & Parallel)), as the evaporator temperature increases, $\dot{m}_{evp}$ also increases but $\dot{m}_{suction}$ decreases, resulting in the lower ER which is also depicted in Fig 19(c). Whereas for the ejector expansion model in LTC (E-DAC (Series & Parallel)), $\dot{m}_{evp} = \dot{m}_{suction}$. So, ER increases with the increase of evaporator temperature. Due to the proportional relationship between $\dot{m}_{evp}$ and COP, eventually COP of the system increases.

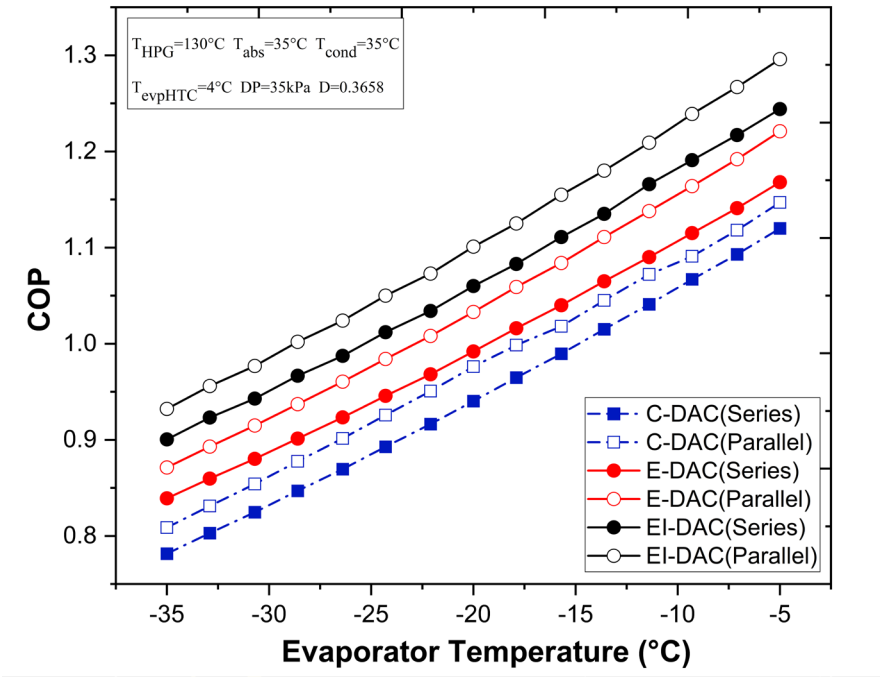

(a)

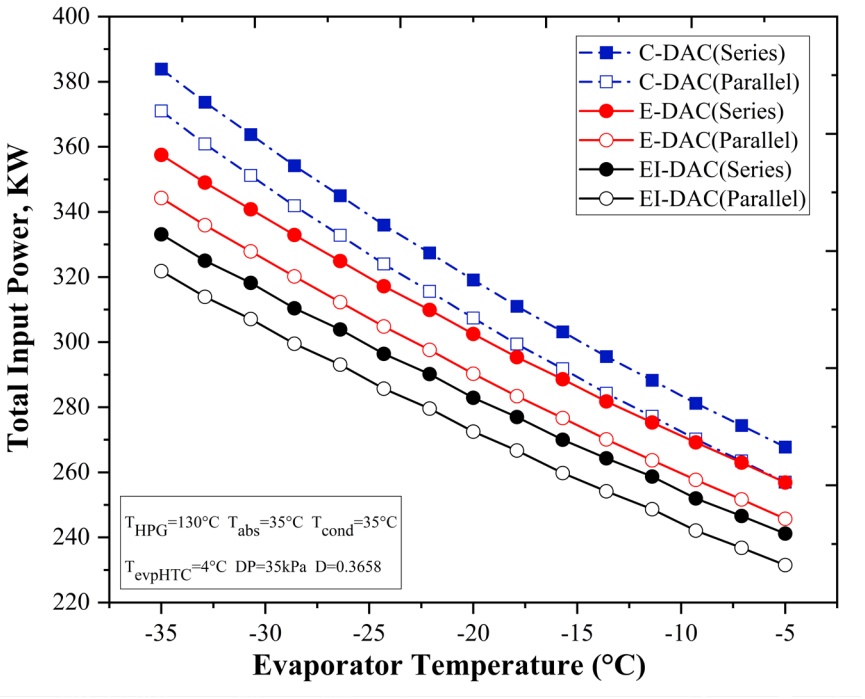

(b)

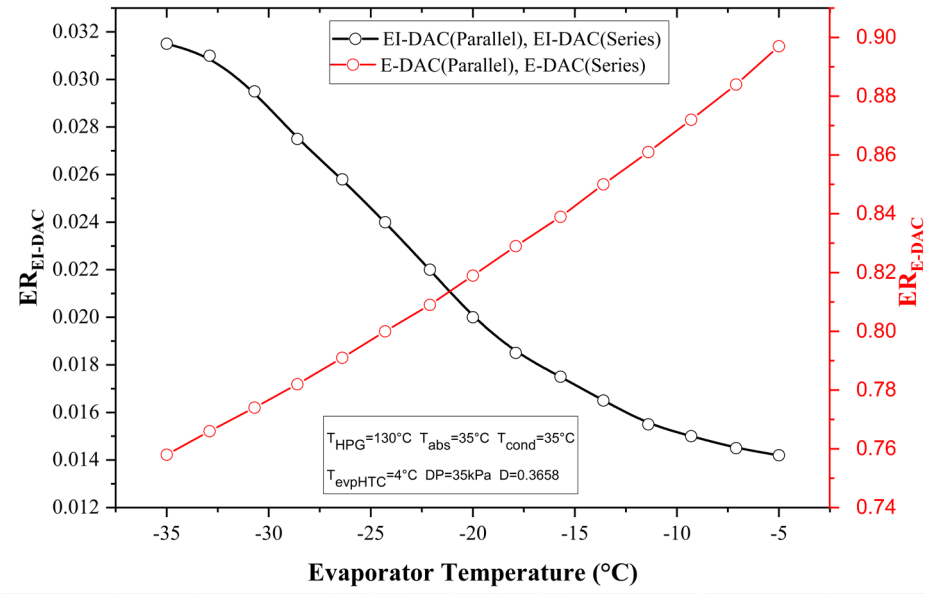

(c)

Fig. 19: Impact of T_{evp} on (a) COP (b) Total Input Power and (c) Entrainment ratio (ER) of the proposed systems at T_{cond} = 35℃, T_{abs} = 35℃, T_{HPG} = 130℃, D=0.3658

Among the four proposed systems, EI-DAC(Parallel) performs significantly better than the conventional C-DAC(Parallel) and C-DAC(Series) with an improvement of approximately 14.5% and 17% respectively.

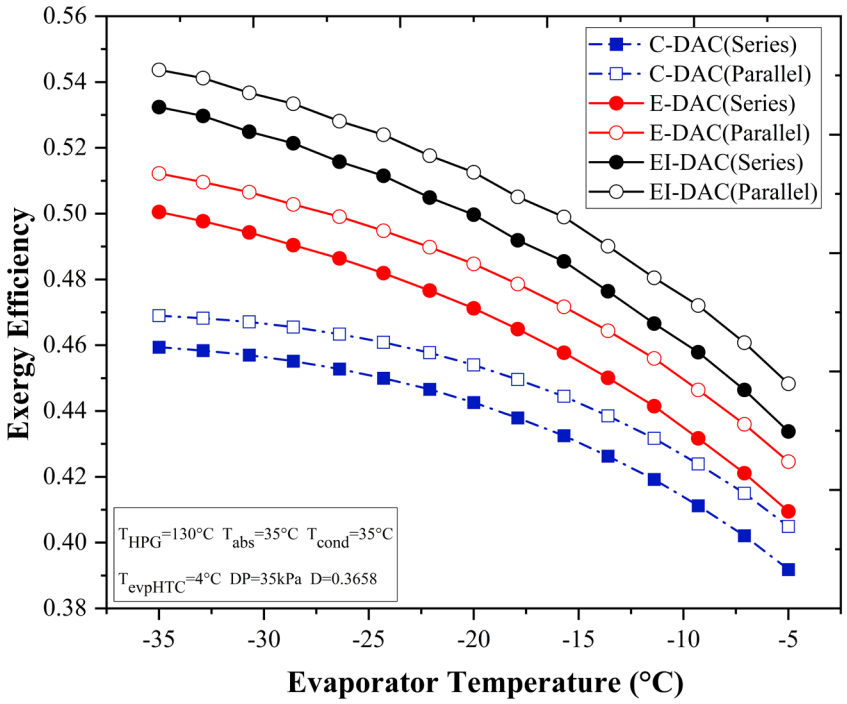
Exergy Efficiency
Evaporator Temperature (°C)
C-DAC(Series)
C-DAC(Parallel)
E-DAC(Series)
E-DAC(Parallel)
EI-DAC(Series)
EI-DAC(Parallel)
T_HPG=130°C T_abs=35°C T_cond=35°C
T_evpHTC=4°C DP=35kPa D=0.3658

(a)

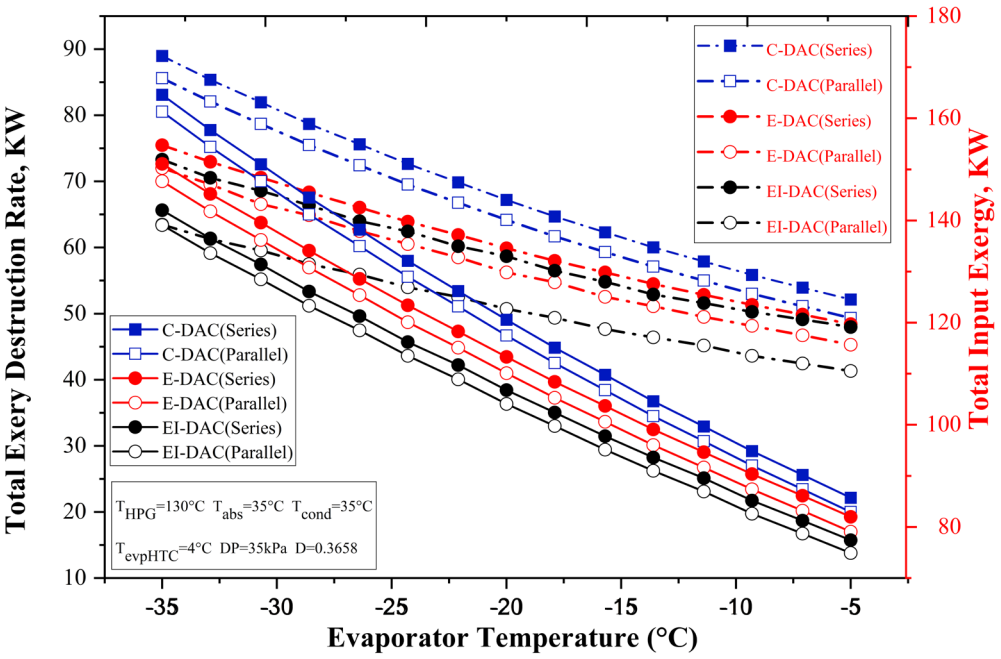
Total Exery Destruction Rate, KW
Total Input Exergy, KW
Evaporator Temperature (°C)
C-DAC(Series)
C-DAC(Parallel)
E-DAC(Series)
E-DAC(Parallel)
EI-DAC(Series)
EI-DAC(Parallel)
T_HPG=130°C T_abs=35°C T_cond=35°C
T_evpHTC=4°C DP=35kPa D=0.3658

(b)

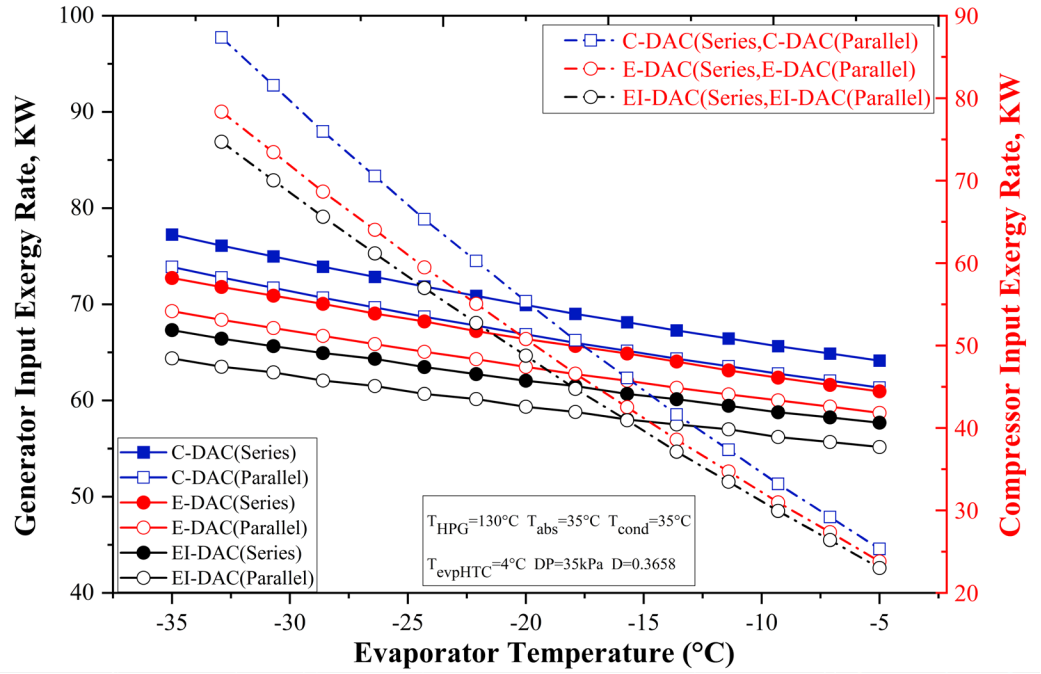

(c)

Fig. 20: Impact of T_{evp} on (a) Exergy Efficiency (b) $\dot{E}_{D,total}$ and (c) $\dot{E}_{x,in}$ of the proposed systems at T_{cond} = 35℃, T_{abs} = 35℃, T_{HPG} = 130℃, D=0.3658

The exergy efficiency has a negative correlation with the evaporator temperature, as illustrated in **Fig. 20(a)**. According to **Fig. 20(b),** there is a decrease in total exergy destruction as the evaporator temperature increases. As the temperature of the evaporator rises, there is a corresponding drop in the refrigeration capacity or heat extraction potential of the system. This leads to a reduction in the utilization of the available energy, ultimately resulting in a decrease in the overall rate of exergy destruction. Moreover, the reduced heat extraction potential in the evaporator leads to a decrease in Q_{CHX}, thus resulting in a reduction in Q_{HPG}. According to **Fig. 20(c),** the exergy of the generator decreases in a linear manner as the refrigeration capacity is less utilized. However, the exergy of the compressor decreases with a greater gradient compared to the generator input exergy. This is attributed to the decrease in pressure ratio in the low-temperature compressor (LTC), which leads to a decline in exergy efficiency as the evaporator temperature increases, as shown in Fig. 20(a).

Deep down in further investigation, it becomes evident that the decremental rate varies across different temperatures. The EI-DAC(Parallel) exhibits a notable enhancement in exergy efficiency compared to the conventional C-DAC(Series) and C-DAC(Parallel) configurations, with improvements of approximately 14% and 17.5% respectively, at a temperature of T_{evp}=-

35°C. Similarly, at a temperature of T_{evp}=-5°C, the EI-DAC(Parallel) demonstrates an improvement of approximately 11% and 13.5% over the conventional series and parallel configurations, respectively. The difference in exergy destruction, exergy input, and exergy efficiency is caused by the higher-pressure ratio in LTC at lower evaporator temperature. In contrast, when the evaporator temperature is increased, the pressure ratio decreases, leading to a reduced disparity in the corresponding analysis. Based on the examination of the influence of evaporator temperature, it can be concluded that the coefficient of performance (COP) of the system exhibits a nearly linear trend, while the rate of exergy decrement demonstrates variation.

6.1.7 Effect of Condenser Temperature

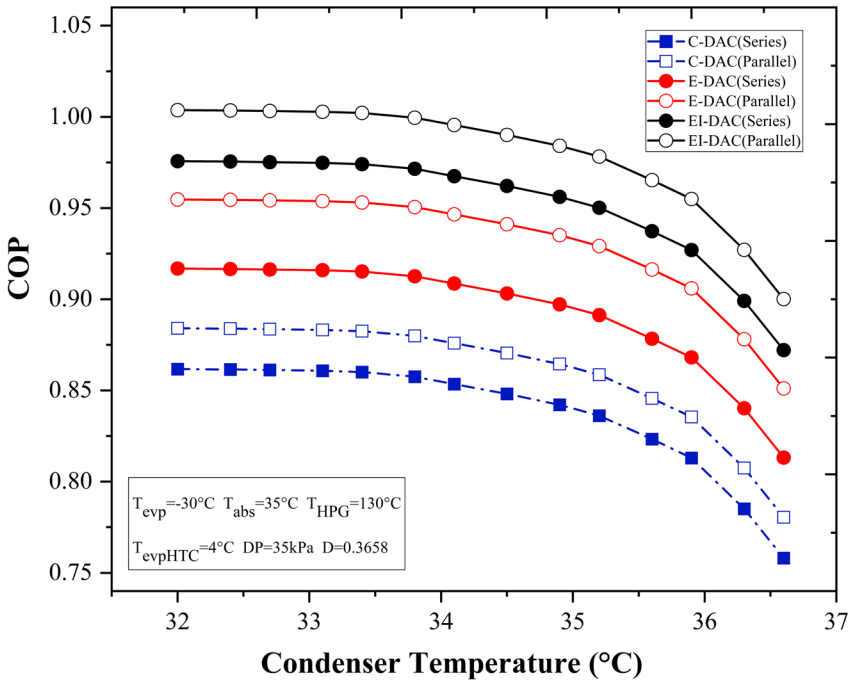

(a)

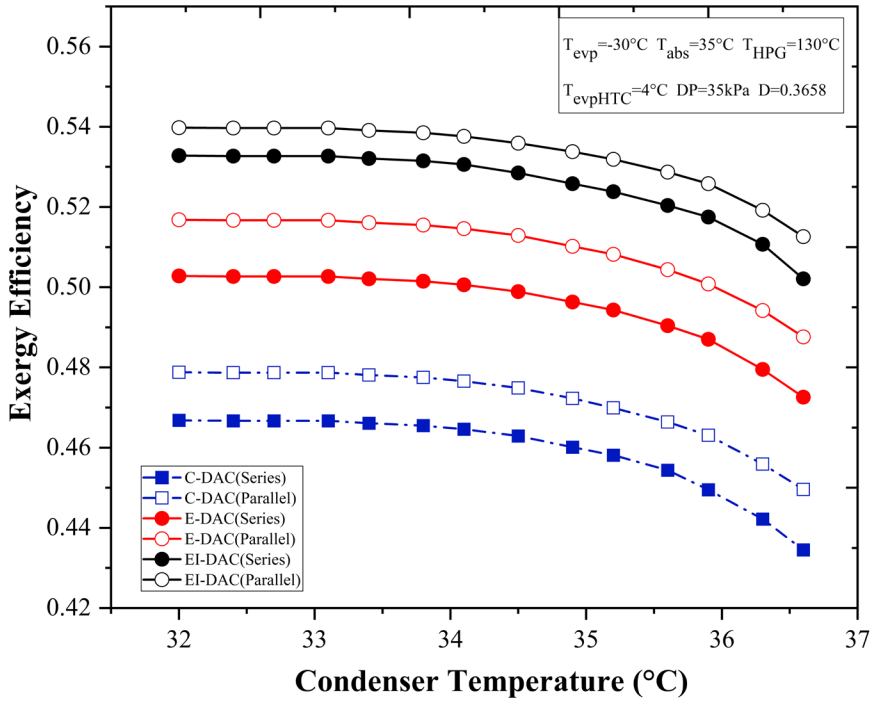

(b)

Fig. 21: Impact of T_{cond} on a) COP and b) exergy efficiency of the proposed systems at T_{evp} = -30°C, T_{abs} = 35°C, T_{HPG} = 130°C, D=0.3658

Fig. 21(a) and Fig. 21(b) demonstrate that the system's coefficient of performance (COP) and exergy efficiency decline as the condenser temperature increases. The elevation of the condenser temperature leads to a reduction in heat rejection, hence reducing the utilization of available energy. Consequently, this leads to an increase in exergy destruction, ultimately resulting in a fall in exergy efficiency. Both coefficient of performance (COP) and exergy efficiency exhibit a linear decline until T_{cond}=35°C, beyond which they both fall with a more pronounced gradient. While maintaining the condenser temperature within the acceptable range, Among the four proposed systems, the EI-DAC(Parallel) configuration demonstrates superior performance compared to the other three configurations. It achieves an enhancement of around 15% and 17.5% in the coefficient of performance (COP) when compared to the standard parallel and series configurations, respectively.

6.2 Exergetic Analysis of the Proposed Systems

The exergy analysis is conducted according to the data obtained. The exergy flow diagram, depicted in **Fig. 22** , illustrates the exergy destruction rate and percentage. Based on the data presented in Figure 10, it can be observed that the absorber experiences the greatest amount of exergy destruction across all four combinations. This may be attributed to the irreversible nature of the absorber, which arises from the simultaneous presence of both strong and weak solutions. In contrast, the expansion valve in E-DAC(Series) and E-DAC(Parallel) design experiences the least amount of exergy destruction. Conversely, in EI-DAC(Series) and EI-DAC(Parallel) configuration, the mixing chamber has the lowest level of exergy destruction. The exergy destruction rate at expansion valves is less than 2% for E-DAC(Series) and E-DAC(Parallel) configurations, while the exergy destruction rate at the mixing chamber is below 1% for EI-DAC(Series) and EI-DAC(Parallel) configurations. Ejection expansion LTC models lack a mixing chamber, while ejector injection LTC models incorporate two additional expansion valves. Irrespective of the variations, it can be observed from Figure 10 that the condenser exhibits the lowest exergy destruction, a characteristic shared by all four proposed models. The exergy destruction rates of both ejector expansion LTC and ejector injection LTC models are nearly identical.

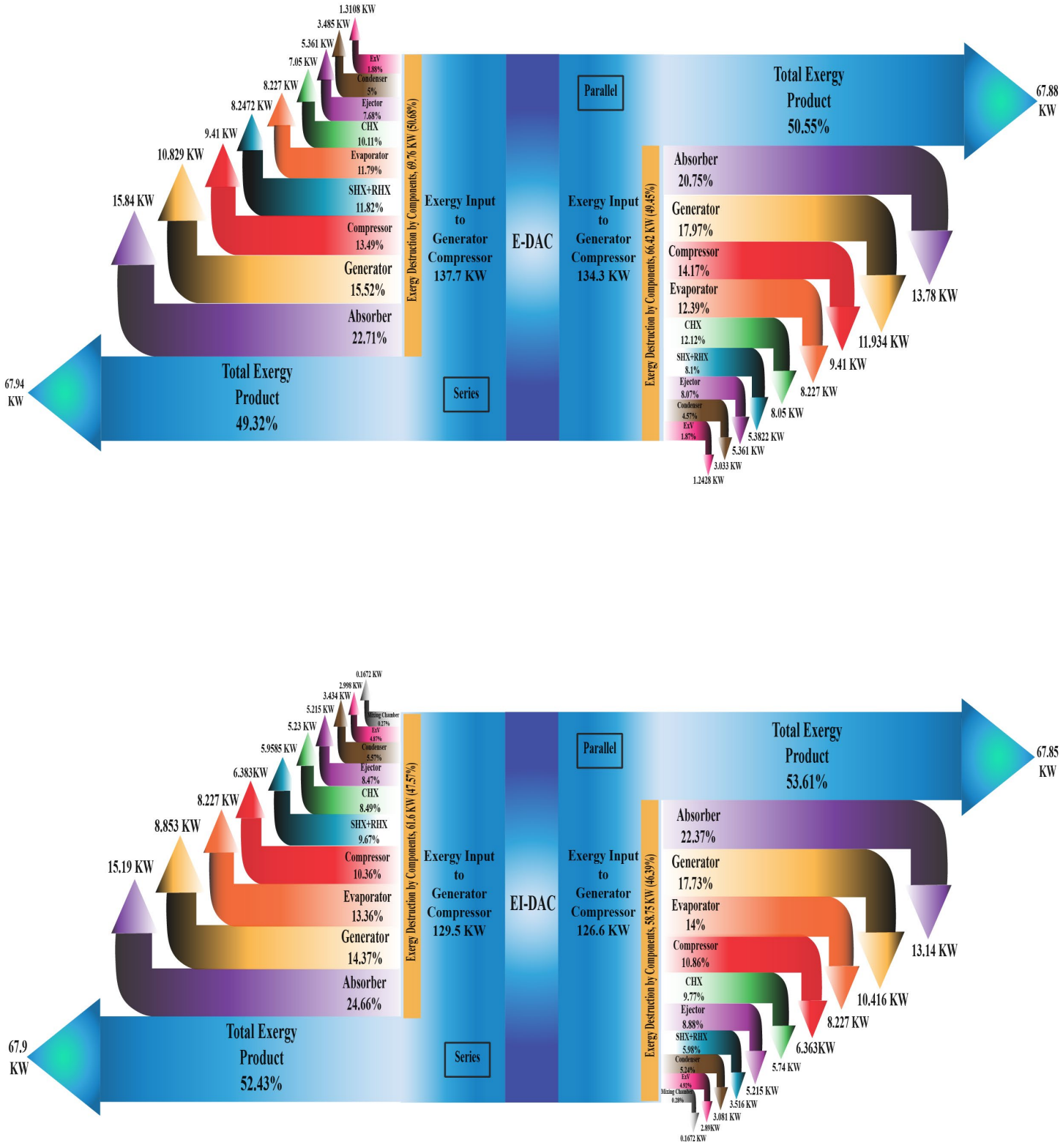

Fig. 22: *The proposed systems' exergy transit rate and the destruction of exergy rate of their associated components at T_{HPG} = 130℃, T_{evp} = -30℃, T_{abs} = 35℃, T_{cond} = 35℃, and ΔT_{CHX} = 5℃*

Chapter 7: Conclusion

The present work shows a comprehensive analysis on the performance of the four novel refrigeration systems E-DAC (Series and Parallel) and EI-DAC (Series and Parallel) compared against the conventional C-DAC (Series and Parallel). The analysis is performed from the perspective of both the first and second law of thermodynamics on different operating parameters like high pressure generator temperature, evaporator temperature and condenser temperature. The proposed systems have great potential to achieve effective and sustainable cooling solutions at lower temperatures, with greater industrial applicability. This is achieved by strategically using waste heat to enhance generator efficiency and optimize compressor operation. The comprehensive thermodynamic analysis yields the following conclusions:

- From the analysis of the two operating parameters, high pressure generator temperature and evaporator temperature, the four proposed systems exhibit a significant improvement over the two conventional systems while the EI-DAC (Parallel) configuration outperforms the rest three novel systems as well as the conventional systems showing an improvement of around 16.5% and 14% against the C-DAC (Series) and C-DAC (Parallel) respectively.
- Exergy efficiency with the change of high-pressure generator temperature shows more sensitivity than the COP. After reaching the optimum condition, the energetic efficiency decreases and before reaching the optimal value it increases with a steeper slope. To get the optimal performance from the exegetic perspective, T_{HPG} must be kept in the range of 130 to 140°C. The performance of EI-DAC(Parallel) is roughly 16.7% higher than that of C-DAC(Parallel) and 17.5% higher than that of C-DAC(Series).
- COPs of the proposed systems increase linearly with the evaporator temperature but exergy efficiencies increase at different rates and fall drastically after a certain evaporator temperature which makes our systems suitable in operating at a very lower temperature application.
- Pressure drops influences the performance of our proposed systems. By performing a comprehensive analysis on the performance of our systems by pressure drops shows that ejector expansion cycle as the LTC (E-DAC (Series and Parallel)) are more sensitive to pressure drops than ejector injection cycle as the LTC (EI-DAC (Series and Parallel)).
- The parallel configurations for the HTC (E-DAC (Parallel), EI-DAC (Parallel)) are sensitive to the distribution ratio and for the simplicity, the optimum distribution was

determined using Golden Ratio method and then the rest of the analysis are carried out.

- At a fixed operating condition, the absorber is responsible for the highest rate of exergy destruction among the four suggested systems. In the case of the EI-DAC (Parallel) system, the destruction percentage amounts to around 22% of the total exergy produced. Out of the four systems that were presented, EI-DAC offers superior performance compared to the other proposed systems based on energetic analysis. The overall exergy destruction rate is approximately 58.75kW, resulting in an enhanced exergy efficiency compared to conventional systems.

Chapter 8: Limitations and Future Recommendations

Although the four proposed systems come with numerous scopes and novelty, it is essential to comprehend the fact that there are still shortcomings in this research. Further improvements can be employed by overcoming these limitations mentioned below.

8.1 Limitations

- Thermodynamic modelling assumption: As for the simplification of the numerical study, many required assumptions were implemented to develop the system. All those assumptions may not be in-line with the real-world circumstances. There are potential avenues for further development of this project in the future, which involve considering factors with more details such as heat losses, pressure drop, and component efficiency.
- Implementation scope: The developed model mainly investigates on a few operational parameters, whereas there are many more aspects of employment in real-world scenario such as long-term viability, environmental impact, economic expenses and so on.
- Experimental research: To understand the full potential of these novel systems in practical world, it is essential to perform experimental validation that will incorporate prototype evaluation.

8.2 Future recommendations

To facilitate the scopes of improvements of this study, here are few recommendations that will assist for further comprehension by enriching this specific research area.

- Advanced Exergy analysis: To understand the component's all-inclusive contribution to the exergy destruction, an advanced exergy analysis can be employed to investigate to which limit exergy destruction can be excluded. Furthermore, exergonomic analysis can be carried out to integrate the economic aspect.

- Optimization: Multi-objective optimization can be a feasible way to maximize the output parameters considering the co-relation with one another. Optimization helps to determine the most suitable values of a certain parameter in a particular range that will generate the most efficient result. Subsequent research can investigate the potentialities of this undertaking.
- Empirical Evaluation: Conducting real-world testing and validation is crucial in order to design systems that are suitable for practical use. Empirical experiments should be aimed as one of the most necessary steps for the expansion of this research sector.
- Potential incorporation with green energy sources: All of the proposed novel systems have the capability to adapt renewable energy resources as the primary heat input, which opens the door of a realistic opportunity of an integration of cascaded refrigeration systems with sustainable energy sources. This optimistic collaboration can significantly advance this sector towards a more viable and effective cooling processes.

References

[1] X. Sun *et al.*, "Multi-objective optimization and thermo-economic analysis of an enhanced compression-absorption cascade refrigeration system and ORC integrated system for cooling and power cogeneration," *Energy Convers Manag*, vol. 236, May 2021, doi: 10.1016/j.enconman.2021.114068.

[2] A. Mota-Babiloni *et al.*, "Ultralow-temperature refrigeration systems: Configurations and refrigerants to reduce the environmental impact," *International Journal of Refrigeration*, vol. 111. Elsevier Ltd, pp. 147–158, Mar. 01, 2020. doi: 10.1016/j.ijrefrig.2019.11.016.

[3] A. Gupta, Y. Anand, S. K. Tyagi, and S. Anand, "Economic and thermodynamic study of different cooling options: A review," *Renewable and Sustainable Energy Reviews*, vol. 62. Elsevier Ltd, pp. 164–194, 2016. doi: 10.1016/j.rser.2016.04.035.

[4] A. Mota-Babiloni, J. Navarro-Esbrí, Á. Barragán-Cervera, F. Molés, B. Peris, and G. Verdú, "Commercial refrigeration - An overview of current status," *International Journal of Refrigeration*, vol. 57. Elsevier Ltd, pp. 186–196, Jul. 16, 2015. doi: 10.1016/j.ijrefrig.2015.04.013.

[5] J. Zhang, H. Meerman, R. Benders, and A. Faaij, "Comprehensive review of current natural gas liquefaction processes on technical and economic performance," *Applied Thermal Engineering*, vol. 166. Elsevier Ltd, Feb. 05, 2020. doi: 10.1016/j.applthermaleng.2019.114736.

[6] X. She *et al.*, "Energy-efficient and -economic technologies for air conditioning with vapor compression refrigeration: A comprehensive review," *Applied Energy*, vol. 232. Elsevier Ltd, pp. 157–186, Dec. 15, 2018. doi: 10.1016/j.apenergy.2018.09.067.

[7] C. Park, H. Lee, Y. Hwang, and R. Radermacher, "Recent advances in vapor compression cycle technologies," *International Journal of Refrigeration*, vol. 60. Elsevier Ltd, pp. 118–134, Dec. 01, 2015. doi: 10.1016/j.ijrefrig.2015.08.005.

[8] K. A. AIKINS, S.-H. LEE, and J. M. CHOI, "TECHNOLOGY REVIEW OF TWO-STAGE VAPOR COMPRESSION HEAT PUMP SYSTEM," *International Journal of Air-Conditioning and Refrigeration*, vol. 21, no. 03, p. 1330002, Sep. 2013, doi: 10.1142/S2010132513300024.

[9] Z. Sun and Y. Wang, "Comprehensive performance analysis of cascade refrigeration system with two-stage compression for industrial refrigeration," *Case Studies in Thermal Engineering*, vol. 39, Nov. 2022, doi: 10.1016/j.csite.2022.102400.

[10] V. Jain, S. S. Kachhwaha, and G. Sachdeva, "Thermodynamic performance analysis of a vapor compression-absorption cascaded refrigeration system," *Energy Convers Manag*, vol. 75, pp. 685–700, 2013, doi: 10.1016/j.enconman.2013.08.024.

[11] S. Garimella, A. M. Brown, and A. K. Nagavarapu, "Waste heat driven absorption/vapor-compression cascade refrigeration system for megawatt scale, high-flux, low-temperature cooling," *International Journal of Refrigeration*, vol. 34, no. 8, pp. 1776–1785, Dec. 2011, doi: 10.1016/j.ijrefrig.2011.05.017.

[12] K. Sumeru, H. Nasution, and F. N. Ani, “A review on two-phase ejector as an expansion device in vapor compression refrigeration cycle,” *Renewable and Sustainable Energy Reviews*, vol. 16, no. 7. pp. 4927–4937, Sep. 2012. doi: 10.1016/j.rser.2012.04.058.

[13] R. Sirwan, M. A. Alghoul, K. Sopian, Y. Ali, and J. Abdulateef, “Evaluation of adding flash tank to solar combined ejector–absorption refrigeration system,” *Solar Energy*, vol. 91, pp. 283–296, May 2013, doi: 10.1016/j.solener.2013.01.018.

[14] K. Megdouli, B. M. Tashtoush, E. Nahdi, M. Elakhdar, A. Mhimid, and L. Kairouani, “Performance analysis of a combined vapor compression cycle and ejector cycle for refrigeration cogeneration,” *International Journal of Refrigeration*, vol. 74, pp. 517–527, Feb. 2017, doi: 10.1016/j.ijrefrig.2016.12.003.

[15] S. Sanaye, M. Emadi, and A. Refahi, “Thermal and economic modeling and optimization of a novel combined ejector refrigeration cycle,” *International Journal of Refrigeration*, vol. 98, pp. 480–493, Feb. 2019, doi: 10.1016/j.ijrefrig.2018.11.007.

[16] J. Navarro-Esbrí, F. Molés, and Á. Barragán-Cervera, “Experimental analysis of the internal heat exchanger influence on a vapour compression system performance working with R1234yf as a drop-in replacement for R134a,” *Appl Therm Eng*, vol. 59, no. 1–2, pp. 153–161, 2013, doi: 10.1016/j.applthermaleng.2013.05.028.

[17] R. Ahmed Mahmood, “Case study of liquid suction heat exchanger in a mechanical refrigeration system using alternative refrigerants.” [Online]. Available: www.sciencepubco.com/index.php/IJET

[18] F. M. Tello-Oquendo, E. Navarro-Peris, and J. Gonzálvez-Maciá, “A comprehensive study of two-stage vapor compression cycles with vapor-injection for heating applications, taking into account heat sink of finite capacity,” *International Journal of Refrigeration*, vol. 93, pp. 52–64, Sep. 2018, doi: 10.1016/j.ijrefrig.2018.05.039.

[19] J. Wang, D. Qv, Y. Yao, and L. Ni, “The difference between vapor injection cycle with flash tank and intermediate heat exchanger for air source heat pump: An experimental and theoretical study,” *Energy*, vol. 221, Apr. 2021, doi: 10.1016/j.energy.2021.119796.

[20] F. Wang, D. Y. Li, and Y. Zhou, “Analysis for the ejector used as expansion valve in vapor compression refrigeration cycle,” *Appl Therm Eng*, vol. 96, pp. 576–582, Mar. 2016, doi: 10.1016/j.applthermaleng.2015.11.095.

[21] X. Cao, X. Liang, L. Shao, and C. Zhang, “Performance analysis of an ejector-assisted two-stage evaporation single-stage vapor-compression cycle,” *Appl Therm Eng*, vol. 205, p. 118005, Mar. 2022, doi: 10.1016/j.applthermaleng.2021.118005.

[22] R. Shi, T. Bai, and J. Wan, “Performance analysis of a dual-ejector enhanced two-stage auto-cascade refrigeration cycle for ultra-low temperature refrigeration,” *Appl Therm Eng*, vol. 240, p. 122152, Mar. 2024, doi: 10.1016/j.applthermaleng.2023.122152.

[23] T. Bai, G. Yan, and J. Yu, “Thermodynamic analyses on an ejector enhanced CO2 transcritical heat pump cycle with vapor-injection,” *International Journal of Refrigeration*, vol. 58, pp. 22–34, Oct. 2015, doi: 10.1016/j.ijrefrig.2015.04.010.

[24] M. Walid Faruque, Y. Khan, M. Hafiz Nabil, M. Monjurul Ehsan, and A. Karim, "Thermal Performance Evaluation of a Novel Ejector-Injection Cascade Refrigeration System," *Thermal Science and Engineering Progress*, vol. 39, Mar. 2023, doi: 10.1016/j.tsep.2023.101745.

[25] S. Jing, Q. Chen, and J. Yu, "Analysis of an ejector-assisted flash tank vapor injection heat pump cycle with dual evaporators for dryer application," *Energy*, vol. 286, p. 129531, Jan. 2024, doi: 10.1016/j.energy.2023.129531.

[26] V. Boopathi Raja and V. Shanmugam, "A review and new approach to minimize the cost of solar assisted absorption cooling system," *Renewable and Sustainable Energy Reviews*, vol. 16, no. 9. pp. 6725–6731, Dec. 2012. doi: 10.1016/j.rser.2012.08.004.

[27] C. Amaris, M. Vallès, and M. Bourouis, "Vapour absorption enhancement using passive techniques for absorption cooling/heating technologies: A review," *Applied Energy*, vol. 231. Elsevier Ltd, pp. 826–853, Dec. 01, 2018. doi: 10.1016/j.apenergy.2018.09.071.

[28] L. Garousi Farshi, S. M. Seyed Mahmoudi, and M. A. Rosen, "Analysis of crystallization risk in double effect absorption refrigeration systems," *Appl Therm Eng*, vol. 31, no. 10, pp. 1712–1717, Jul. 2011, doi: 10.1016/j.applthermaleng.2011.02.013.

[29] K. Wang, O. Abdelaziz, P. Kisari, and E. A. Vineyard, "State-of-the-art review on crystallization control technologies for water/LiBr absorption heat pumps," in *International Journal of Refrigeration*, Sep. 2011, pp. 1325–1337. doi: 10.1016/j.ijrefrig.2011.04.006.

[30] R. Nikbakhti, X. Wang, A. K. Hussein, and A. Iranmanesh, "Absorption cooling systems – Review of various techniques for energy performance enhancement," *Alexandria Engineering Journal*, vol. 59, no. 2. Elsevier B.V., pp. 707–738, Mar. 01, 2020. doi: 10.1016/j.aej.2020.01.036.

[31] M. Chahartaghi, H. Golmohammadi, and A. F. Shojaei, "Performance analysis and optimization of new double effect lithium bromide–water absorption chiller with series and parallel flows," *International Journal of Refrigeration*, vol. 97, pp. 73–87, Jan. 2019, doi: 10.1016/j.ijrefrig.2018.08.011.

[32] A. Verma, S. C. Kaushik, and S. K. Tyagi, "Performance enhancement of absorption refrigeration systems: An overview," *Journal of Thermal Engineering*, vol. 9, no. 4, pp. 1100–1113, 2023, doi: 10.18186/thermal.1334225.

[33] P. S. Arshi Banu and N. M. Sudharsan, "Review of water based vapour absorption cooling systems using thermodynamic analysis," *Renewable and Sustainable Energy Reviews*, vol. 82. Elsevier Ltd, pp. 3750–3761, Feb. 01, 2018. doi: 10.1016/j.rser.2017.10.092.

[34] G. P. Xu and Y. Q. Dait, "THEORETICAL ANALYSIS AND OPTIMIZATION OF A DOUBLE-EFFECT PARALLEL-FLOW-TYPE ABSORPTION CHILLER," 1996.

[35] R. Ventas, A. Lecuona, A. Zacarías, and M. Venegas, "Ammonia-lithium nitrate absorption chiller with an integrated low-pressure compression booster cycle for low driving temperatures," *Appl Therm Eng*, vol. 30, no. 11–12, pp. 1351–1359, Aug. 2010, doi: 10.1016/j.applthermaleng.2010.02.022.

[36] D. S. Ayou, J. C. Bruno, and A. Coronas, “Integration of a mechanical and thermal compressor booster in combined absorption power and refrigeration cycles,” *Energy*, vol. 135, pp. 327–341, 2017, doi: 10.1016/j.energy.2017.06.148.

[37] L. Garousi Farshi, A. H. Mosaffa, C. A. Infante Ferreira, and M. A. Rosen, “Thermodynamic analysis and comparison of combined ejector-absorption and single effect absorption refrigeration systems,” *Appl Energy*, vol. 133, pp. 335–346, Nov. 2014, doi: 10.1016/j.apenergy.2014.07.102.

[38] A. Khaliq, R. Kumar, and E. M. A. Mokheimer, “Investigation on a solar thermal power and ejector-absorption refrigeration system based on first and second law analyses,” *Energy*, vol. 164, pp. 1030–1043, Dec. 2018, doi: 10.1016/j.energy.2018.09.049.

[39] R. Gomri, “Second law comparison of single effect and double effect vapour absorption refrigeration systems,” *Energy Convers Manag*, vol. 50, no. 5, pp. 1279–1287, May 2009, doi: 10.1016/j.enconman.2009.01.019.

[40] O. Kaynakli, K. Saka, and F. Kaynakli, “Energy and exergy analysis of a double effect absorption refrigeration system based on different heat sources,” *Energy Convers Manag*, vol. 106, pp. 21–30, Dec. 2015, doi: 10.1016/j.enconman.2015.09.010.

[41] L. A. Domínguez-Inzunza, J. A. Hernández-Magallanes, M. Sandoval-Reyes, and W. Rivera, “Comparison of the performance of single-effect, half-effect, double-effect in series and inverse and triple-effect absorption cooling systems operating with the NH3-LiNO3 mixture,” *Appl Therm Eng*, vol. 66, no. 1–2, pp. 612–620, 2014, doi: 10.1016/j.applthermaleng.2014.02.061.

[42] J. M. Asensio-Delgado, S. Asensio-Delgado, G. Zarca, and A. Urtiaga, “Analysis of hybrid compression absorption refrigeration using low-GWP HFC or HFO/ionic liquid working pairs,” *International Journal of Refrigeration*, vol. 134, pp. 232–241, Feb. 2022, doi: 10.1016/j.ijrefrig.2021.11.013.

[43] L. Kairouani and E. Nehdi, “Cooling performance and energy saving of a compression-absorption refrigeration system assisted by geothermal energy,” *Appl Therm Eng*, vol. 26, no. 2–3, pp. 288–294, Feb. 2006, doi: 10.1016/j.applthermaleng.2005.05.001.

[44] C. Cimsit and I. T. Ozturk, “Analysis of compression-absorption cascade refrigeration cycles,” *Appl Therm Eng*, vol. 40, pp. 311–317, Jul. 2012, doi: 10.1016/j.applthermaleng.2012.02.035.

[45] M. Yu, P. Cui, Y. Wang, Z. Liu, Z. Zhu, and S. Yang, “Advanced Exergy and Exergoeconomic Analysis of Cascade Absorption Refrigeration System Driven by Low-Grade Waste Heat,” *ACS Sustain Chem Eng*, vol. 7, no. 19, pp. 16843–16857, Oct. 2019, doi: 10.1021/acssuschemeng.9b04396.

[46] J. Fernández-Seara, J. Sieres, and M. Vázquez, “Compression-absorption cascade refrigeration system,” *Appl Therm Eng*, vol. 26, no. 5–6, pp. 502–512, Apr. 2006, doi: 10.1016/j.applthermaleng.2005.07.015.

[47] J. Sieres and J. Fernández-Seara, “Simulation of compression refrigeration systems,” *Computer Applications in Engineering Education*, vol. 14, no. 3, pp. 188–197, Oct. 2006, doi: 10.1002/cae.20075.

[48] Z. Sun, C. Wang, Y. Liang, H. Sun, S. Liu, and B. Dai, "Theoretical study on a novel CO2 Two-stage compression refrigeration system with parallel compression and solar absorption partial cascade refrigeration system," *Energy Convers Manag*, vol. 204, Jan. 2020, doi: 10.1016/j.enconman.2019.112278.

[49] A. Razmi, M. Soltani, and M. Torabi, "Investigation of an efficient and environmentally-friendly CCHP system based on CAES, ORC and compression-absorption refrigeration cycle: Energy and exergy analysis," *Energy Convers Manag*, vol. 195, pp. 1199–1211, Sep. 2019, doi: 10.1016/j.enconman.2019.05.065.

[50] M. W. Faruque, Y. Khan, M. H. Nabil, and M. M. Ehsan, "Parametric analysis and optimization of a novel cascade compression-absorption refrigeration system integrated with a flash tank and a reheater," *Results in Engineering*, vol. 17, Mar. 2023, doi: 10.1016/j.rineng.2023.101008.

[51] Y. Xu, F. S. Chen, Q. Wang, X. Han, D. Li, and G. Chen, "A novel low-temperature absorption-compression cascade refrigeration system," *Appl Therm Eng*, vol. 75, pp. 504–512, Jan. 2015, doi: 10.1016/j.applthermaleng.2014.10.043.

[52] J. Sarkar, "Ejector enhanced vapor compression refrigeration and heat pump systems - A review," *Renewable and Sustainable Energy Reviews*, vol. 16, no. 9. pp. 6647–6659, Dec. 2012. doi: 10.1016/j.rser.2012.08.007.

[53] E. Kurem, I. Horuz, J. P. Hartnett, and W. J. Minkowycz, "A COMPARISON BETWEEN AMMONIA-WATER ANB WATER-LITHIUM BROMIDE SOLUTIONS IN ABSORPTION HEAT TRANSFORMERS," 2001.

[54] C. Cimsit, I. T. Ozturk, and O. Kincay, "Thermoeconomic optimization of LiBr/H2O-R134a compression-absorption cascade refrigeration cycle," *Appl Therm Eng*, vol. 76, pp. 105–115, Feb. 2015, doi: 10.1016/j.applthermaleng.2014.10.094.

[55] Y. Xu, G. Chen, Q. Wang, X. Han, N. Jiang, and S. Deng, "Performance study on a low-temperature absorption-compression cascade refrigeration system driven by low-grade heat," *Energy Convers Manag*, vol. 119, pp. 379–388, Jul. 2016, doi: 10.1016/j.enconman.2016.04.061.

[56] Y. Khan, M. W. Faruque, M. H. Nabil, and M. M. Ehsan, "Ejector and Vapor Injection Enhanced Novel Compression-Absorption Cascade Refrigeration Systems: A Thermodynamic Parametric and Refrigerant Analysis," *Energy Convers Manag*, vol. 289, Aug. 2023, doi: 10.1016/j.enconman.2023.117190.

[57] R. Gomri and R. Hakimi, "Second law analysis of double effect vapour absorption cooler system," *Energy Convers Manag*, vol. 49, no. 11, pp. 3343–3348, Nov. 2008, doi: 10.1016/j.enconman.2007.09.033.

[58] B. S. Bagheri, R. Shirmohammadi, S. M. S. Mahmoudi, and M. A. Rosen, "Optimization and comprehensive exergy-based analyses of a parallel flow double-effect water-lithium bromide absorption refrigeration system," *Appl Therm Eng*, vol. 152, pp. 643–653, Apr. 2019, doi: 10.1016/j.applthermaleng.2019.02.105.

[59] Cengel and Boles, *Thermodynamics: An Engineering Approach*, 8th ed. 2014.

[60] D. Colorado-Garrido, “Advanced Exergy Analysis of a Compression-Absorption Cascade Refrigeration System,” *Journal of Energy Resources Technology, Transactions of the ASME*, vol. 141, no. 4, Apr. 2019, doi: 10.1115/1.4042003.

[61] X. Wang, J. Yu, and M. Xing, “Performance analysis of a new ejector enhanced vapor injection heat pump cycle,” *Energy Convers Manag*, vol. 100, pp. 242–248, Aug. 2015, doi: 10.1016/j.enconman.2015.05.017.

[62] H. Li, F. Cao, X. Bu, L. Wang, and X. Wang, “Performance characteristics of R1234yf ejector-expansion refrigeration cycle,” *Appl Energy*, vol. 121, pp. 96–103, May 2014, doi: 10.1016/j.apenergy.2014.01.079.

[63] S. Elbel and P. Hrnjak, “Experimental validation of a prototype ejector designed to reduce throttling losses encountered in transcritical R744 system operation,” *International Journal of Refrigeration*, vol. 31, no. 3, pp. 411–422, May 2008, doi: 10.1016/j.ijrefrig.2007.07.013.

[64] C. Aktemur, I. T. Ozturk, and C. Cimsit, “Comparative energy and exergy analysis of a subcritical cascade refrigeration system using low global warming potential refrigerants,” *Appl Therm Eng*, vol. 184, p. 116254, Feb. 2021, doi: 10.1016/j.applthermaleng.2020.116254.

[65] Z. Sun, Q. Wang, Z. Xie, S. Liu, D. Su, and Q. Cui, “Energy and exergy analysis of low GWP refrigerants in cascade refrigeration system,” *Energy*, vol. 170, pp. 1170–1180, Mar. 2019, doi: 10.1016/j.energy.2018.12.055.